DESIGN OF A CARDIOVASCULAR FLOW MIMICKING PUMP

by

Christopher F. Brake

Submitted in partial fulfillment of the
requirements for the degree of
Master of Applied Science

at

Dalhousie University
Halifax, Nova Scotia
August 2015

© Copyright by Christopher F. Brake, 2015

A good thesis is a done thesis.

-Ancient Grad Student Proverb

Table of Contents

List of Tables . . . . . **v**

List of Figures . . . . . **vi**

Abstract . . . . . **ix**

List of Abbreviations Used . . . . . **x**

Chapter 1 Introduction **1**

1.1 Commercial Alternatives 2

1.2 Desired Waveforms 3

1.3 Contributions 4

1.4 Literature Review 6

Chapter 2 Custom Voice Coil Based Pump System **20**

2.1 Introduction 20

2.2 Electrical Design 21

2.3 Mechanical Design 25

2.4 Seal Design 29

2.5 Testing 34

2.6 Summary 35

Chapter 3 Commercial Voice Coil Based Pump System **37**

3.1 Introduction 37

3.2 Hardware Setup 37

3.3 Simplified System Model 39

3.4 Simulation Results of LQR Controller 43

3.5 Control Hardware 44

3.6 Voice Coil Linear Actuator 45

3.7 Valve 47
3.8 Summary 49
Chapter 4 Control 50
4.1 Introduction 50
4.2 Control with Friction Compensation 51
4.3 Identification of Parameters 54
4.4 Parameter Tuning 57
4.5 Summary 60
Chapter 5 Validation 61
5.1 Introduction 61
5.2 Particle Image Velocimetry Results 61
5.3 Summary 73
Chapter 6 Conclusions & Recommendations 74
6.1 Conclusions 74
6.2 Recommendations 75
References 77
Appendix A Drawings 84

List of Tables

2.1 Material properties used in LS-DYNA model 30

2.2 Convergence study results 33

4.1 NEA Parameter identification results 56

4.2 Ramp Input NEA Results 57

4.3 Friction and control parameters used for iterative testing 58

List of Figures

1.1 Pressure and velocity pulse waveforms in the aorta and arterial branches of a dog [24] 2

1.2 Flow waveform in the descending aorta of a dog [24] 3

1.3 Flow waveform the the femoral artery of a dog [24] 4

1.4 Elastic model of the heart [21] 7

1.5 Schematic diagram of experimental setup [44] 8

1.6 Schematic diagram of pulsatile flow simulator[17] 9

1.7 Progressive cavity pump with arbitrary flow generator setup[11] 11

1.8 Modified roller pump side view[26] 12

1.9 Schematic of the flow system with centrifugal and piston pump [41] 14

1.10 Diagram of flow system with gear pump and piston pump in series [51] 15

1.11 Basic Maxwell Slip model structure [42] 16

1.12 Stribeck curve example [53] 17

2.1 Labeled cross section of the prototype voice coil with integrated pistons 20

2.2 Sterile position feedback method 22

2.3 *Right hand rule for a current-carrying wire in a magnetic field B* by Quibik is licensed under CC BY-SA 3.0 22

2.4 Magnetic field visualization for D8Z0 bar magnet from K & J Magnetics [31] 23

2.5 Results of finite element model of the flux density for a 3 inch long 0.5 inch diameter N42 bar magnet 24

2.6 3 inch magnet with piston heads (no seals) 26

2.7 Second manufactured cylinder spool 27

2.8 Axisymmetric model of bar magnet flux density in the radial direction 28

2.9 Simple hydraulic circuit diagram of prototype pump 28
2.10 Axisymmetric model of piston cup seal 29
2.11 Model mesh with 0.007 inch element size 31
2.12 Node sets highlighted in red, 0.007 inch element size 32
2.13 Convergence study results 34

3.1 Pump setup with major parts labeled 38
3.2 Block diagram of pump setup 39
3.3 Pump system 40
3.4 Matlab simulation results for LQR controller with FBI reference tracking 43
3.5 Control structure for PWM generation from the FPGA main virtual interface 46
3.6 Actuator force 47
3.7 Exploded view of switching valve 48
3.8 Example flow without switching valve is on left. Example flow with the switching valve on the right. 48

4.1 Identification results for friction curve 55
4.2 Average of 10 pulses produced using the parameter values from set 4 in Table 4.3 59

5.1 Pair of images taken at 4000fps 62
5.2 PIV Flow measurement results of water flowing in a 10mm tube. Color scale is m/s, with directional arrows scaled by magnitude of velocity 62
5.3 Single waveform with labeled points for cross section fluid velocity seen in Figure 5.4 63
5.4 Fluid velocity across tube diameter 64
5.5 Flow measurement # 1 65
5.6 PIV measurement 10 cycle average 66
5.7 Flow measurement compared with encoder data 67

5.8 Encoder measurement 10 cycle average 68
5.9 PIV and encoder measurement comparison 69
5.10 PIV measurement of femoral waveform [7] 70
5.11 Encoder measurement of femoral waveform [7] 71
5.12 PIV and encoder measurement comparison for femoral waveform [7] 72

6.1 Waveforms produced by the pump for testing 75

Abstract

In vitro testing is an important part of the development of new cardiovascular prosthesis designs. One important aspect of simulating the cardiovascular system is properly modeling the pulsatile flow created by the heart. To test prosthesis' effect on the blood flow and the vessels themselves, it must be possible to reproduce the complex, time varying flow generated by the heart. Therefore, there is a need for a pump that is capable of delivering complex, time varying flows that can be easily adapted to mimick waveforms in a range of vessels.

A novel pump has been developed that can output a wide variety of complex pulsatile waveforms at physiologically relevant flows. The design uses a linear actuator to drive a piston pump. With closed loop velocity reference tracking of a piston head, the flow can be accurately controlled. A prototype pump was constructed as a proof of concept for the design. The prototype showed that basic linear control theory is insufficient to achieve accurate velocity control. The friction characteristics of the pump are the main source of nonlinearity in the system. The next step was to apply a LuGre model based friction compensator. Since the pulsatile flow in cardiovascular systems frequently oscillates around the zero velocity point, adequate friction compensation is critical to achieve accurate flow control. The pump has been used to output two waveforms so far. For a first attempt the results are encouraging, but the control system needs improvement to better track reference waveforms. The continued development of this novel cardiovascular mimicking pump has potential to provide a pump that fills the current gap in the available products.

List of Abbreviations Used

BPM	Beats per minute
CRIO	Compact real-time input output
DAQ	Data acquisition
DC	Direct current
FBI	Francis-Byrnes-Isidori
FE	Finite element
FPGA	Field programmable gate array
GUI	Graphical user interface
LQR	Linear-quadratic regulator
MR	Magnetic resonance
NEA	Novel evolutionary algorithm
PC	Piston cup
PD	Proportional Derivative
PI	Proportional Integral
PID	Proportional Integral Derivative
PIV	Particle image velocimetry
PTFE	Polytetrafluoroethylene
PIV	Pulse width modulation

Chapter 1

Introduction

This project started with the goal of creating a pump that could reproduce pulsatile waveforms from the cardiovascular system. Such a pump would be used for *In vitro* testing during the development of new cardiovascular prosthesis designs. One important aspect of simulating the cardiovascular system for this testing is properly mimicking the pulsatile flow created by the heart. To test prosthesis' effect on the blood flow and on the vessels themselves, it must be possible to reproduce the complex, time varying flow generated by the heart. Therefore, there is a need for a pump that is capable of delivering complex, time varying flows that can be easily adapted to waveforms from a range of vessels. For example, Figure 1.1 illustrates a variety of waveforms from the aorta and arterial branches of a dog[24].

There are a wide variety of pumps discussed in literature that can produce waveforms from the cardiovascular system. These pumps are used for researching heart valves[21], cerebral aneurysms[44], atherosclerosis[23], and more. The most common type of pump used is a piston type pump. However gear, centrifugal, roller, and diaphragm type pumps have also been used. These different types of pumps and their uses will be discussed in the literature review section of this thesis.

For this project the design of the pump stated with the specific idea to use a voice coil linear actuator to drive a piston pump to generate the pulsatile waveforms. A commercial voice coil was available for use, but some preliminary research and an innovative idea lead to the design of a custom voice coil actuator. Since the flow out of a piston pump is piston velocity multiplied by piston area, all the pump should need is accurate velocity reference tracking to output the desired waveform. Through the course of developing the pump, it was discovered that friction would make accurate velocity reference tracking difficult. Friction compensation was implemented for the controller to better track the reference waveform. Particle image velocimetry was used to verify that the fluid flow matched what was being calculated based on encoder

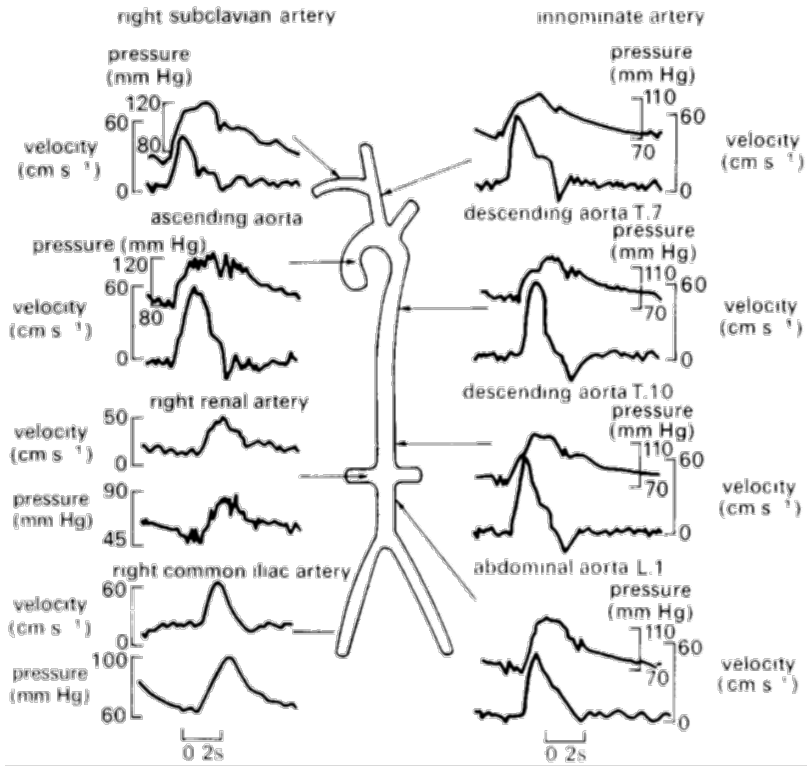

Figure 1.1: Pressure and velocity pulse waveforms in the aorta and arterial branches of a dog [24]

velocity feedback and matched the desired waveform. Each section will discuss in detail the stages of the development of the pump and the control system associated with it.

1.1 Commercial Alternatives

There are several commercially available cardiovascular pumps used in similar applications. Examples are the Shelly Compuflo, the Harvard blood pump, and a syringe pump. These pumps have a variety of capabilities and deficits. The major requirements for a comprehensive pump include:

- Sterility for working with live tissues
- Large flow range
- Programmability

What the programmability requirement means is that a wide variety of waveforms can be created using the pumps control software. Often the commercially available pumps will meet two of the three requirements. For example the Harvard pump is not programmable, nor can it maintain sterility when in use, nor can it output negative flow. The Shelly Compuflo pump has good programmability but only has a maximum flow rate of $35mL/s$. Sterility is often an overlooked capability, but can be critical for experiments conducted with biological tissue over a long period of time (24 hours) at body temperatures (37C). The goal for this project will be to develop a prototype that could have all the desired requirements in one unit.

1.2 Desired Waveforms

The first waveform used as a reference comes from Ku [24]. This profile was chosen for its large flow range, the negative flow section, and because detailed data for the profile was readily available. Figure 1.2 shows the waveform from the descending aorta referenced in Figure 1.1.

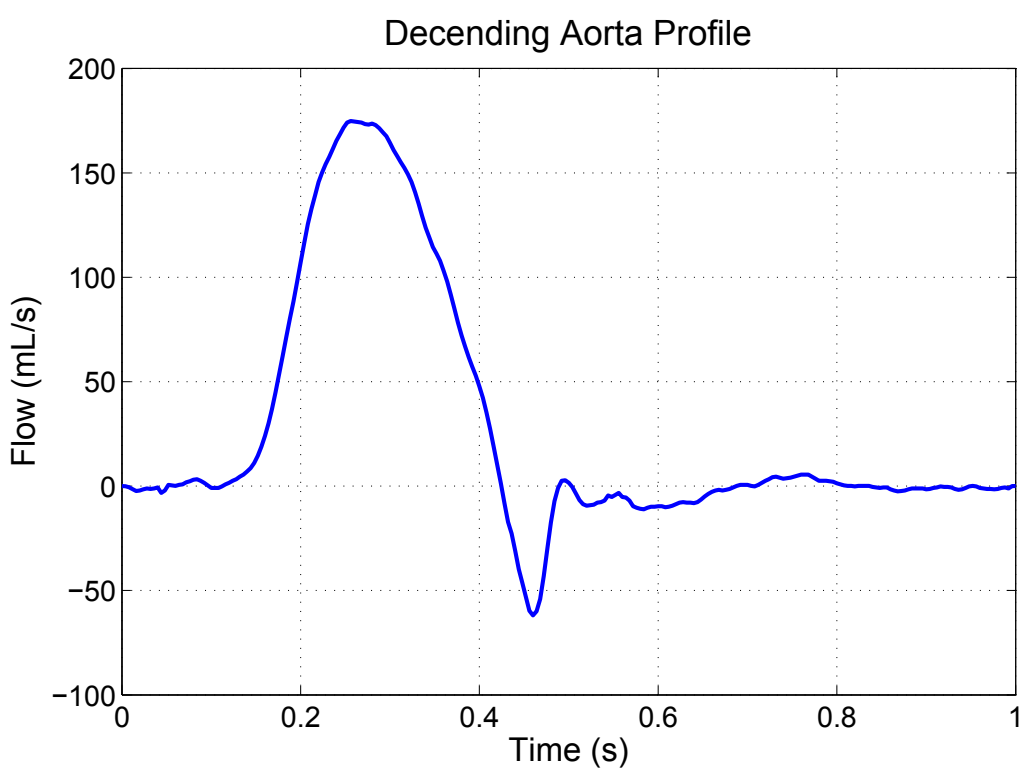

Figure 1.2: Flow waveform in the descending aorta of a dog [24]

This is the main waveform of interest for tuning the pump as it is near the peak flow rate the pump was designed for. Unfortunately due to size and power limits in the mechanical design of the first pump, the aorta waveform was scaled down by a factor of 4 when testing the pumps capabilities. The pistons used simply didn't have enough volume to produce a full scale aortic waveform in one stroke.

The second waveform from the femoral artery was tested. Figure 1.3 shows the reference waveform taken from the artery of a dog [24]. Other waveforms of interest are the carotid artery and the radial artery, although they have yet to be tested.

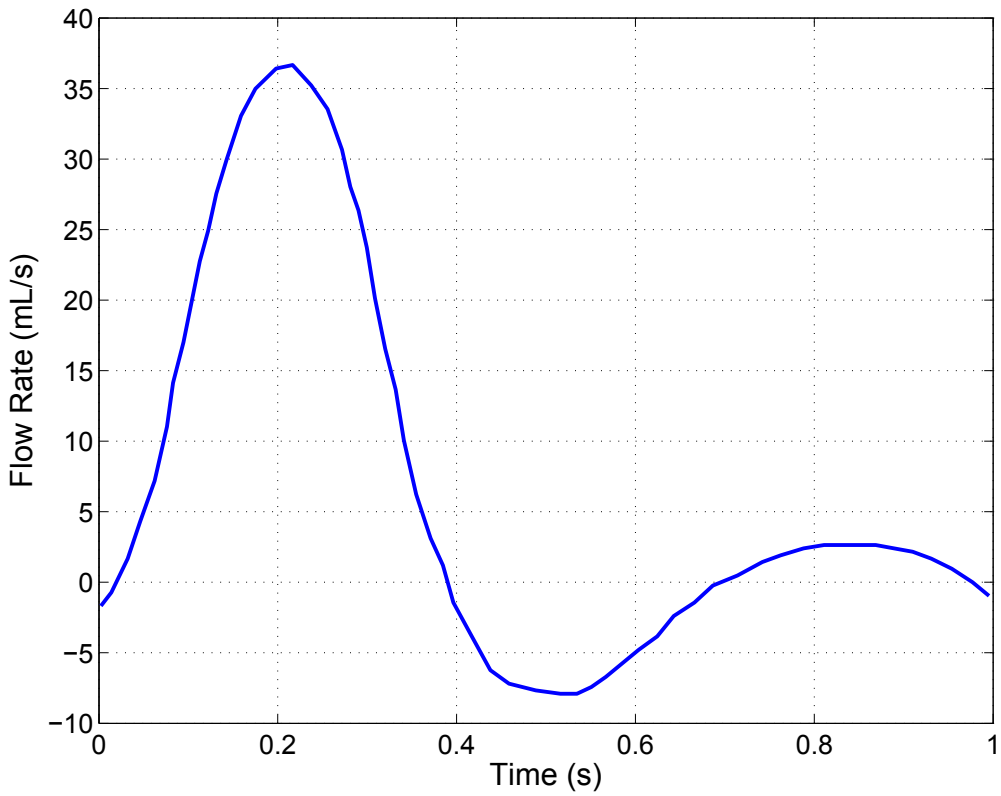

Figure 1.3: Flow waveform the the femoral artery of a dog [24]

.

1.3 Contributions

The goal of this project was to design, build, and test a novel cardiovascular flow mimicking pump that fills a gap in the capabilities of what is commercially available.

As mentioned earlier the three main capabilities a pump like this are.

- Sterility for working with live tissues
- Scalable
- Programmability

The pump should be scalable in the sense that a physically bigger unit could be built following the same general shape and operation as a small version. This scalability would allow this pump design to cover a wide range of flow rates. The programmability aspect of the pump means that the pump can produced different waveforms using only the control software without having to make changes in the pumps hardware.

The novel design of making a pump by integrating pistons into a voice coil type actuator in a major contribution of this work. The novel design for this pump is a good first step towards a pump that can meet these three requirements. Two different waveforms were produced using the pump to show that it is programmable. Two different piston sizes were used to show that it could be scaled to larger or smaller diameters. The first iteration of the pump design was not able to keep the working fluid sterile. However, a possible solution to that problem is proposed in this thesis and will be addressed in future work with the pump.

In addition to the novel design of the pump, a pump using commercially available components was built and tested. This version of the pump was required to develop the control system for the pump. The first prototype using the novel design was under powered and made the control design difficult. A friction compensation algorithm was implemented with this pump to improve the pumps capabilities in tracking an arbitrary waveform.

There is a use for the pump in other researchers work. The pump has already been used by other researchers within our group for their work. Continued development and improvements to the pump will make it more useful to other researchers outside our group. Continued development could also lead to the pump being turned into a commercial product.

1.4 Literature Review

An important aspect of testing in regards to the cardiovascular system is properly simulating the waveforms created by the heart throughout the body. To test prosthesis' effect on the blood flow and the vessels themselves, it must be possible to accurately reproduce the complex, time varying flow generated by the heart are various points throughout the cardiovascular system. Data on these waveforms is available from magnetic resonance imaging and Doppler ultrasound measurements [51].

There are many different ways a physiological flow pump have been made. A piston type positive displacement pump is often used for this application. A commercially available pump from ViVitro Systems uses a piston pump to generate a waveform through a compliant elastic model of the heart [51]. Figure 1.4 shows the elastic heart model used by Kheradvar and Gharib. The paper by Kheradvar and Gharib [21] looks at the relationship between trans-mitral thrust, anulus recoil, and ventricular suction/filling through the index of vortex formation. Artificial ventricles are used to simulate the viscoelastic properties of the ventricle and can be controlled to adjust the impedance of the flow path to better replicate the waveform from the heart [21].

The pump from ViVitro Systems can keep the working fluid isolated from the pump by using the elasic model of the heart as a separating membrane suspended inside a fluid filled acrylic case [44]. The piston pump from Vivitro systems is connected to the plexiglas case and by pumping fluid into and out of the case the ventricular sac is compressed and expanded to produce the desired cardiac actions to test the mitral valve. The mitral and aortic valves they used are Carpentier-Edwards' PERIMOUNT bioprosthetic heart valves. To get the waveform from a specific artery, a network of tubes that model the arterial tree can be created [45] and by controlling the impedance of the flow through the tubes the waveform can be controlled to match physiological measurements. The fluid used in the sac was purified water. They experimented with 3 types of waveforms. The 3 waveforms corresponded to 30 beats per minute (bpm), 60 bpm and 72 bpm. Each experiment was run for 10 seconds to ensure the consistency and reproducibility of the results.

The article from Sadasivan et al. investigated cerebral aneurysms and how stents can be used as a potential therapy to exclude the aneurysm from circulation [44]. Their In Vitro study involves using an elastomer model of a spherical aneurysm

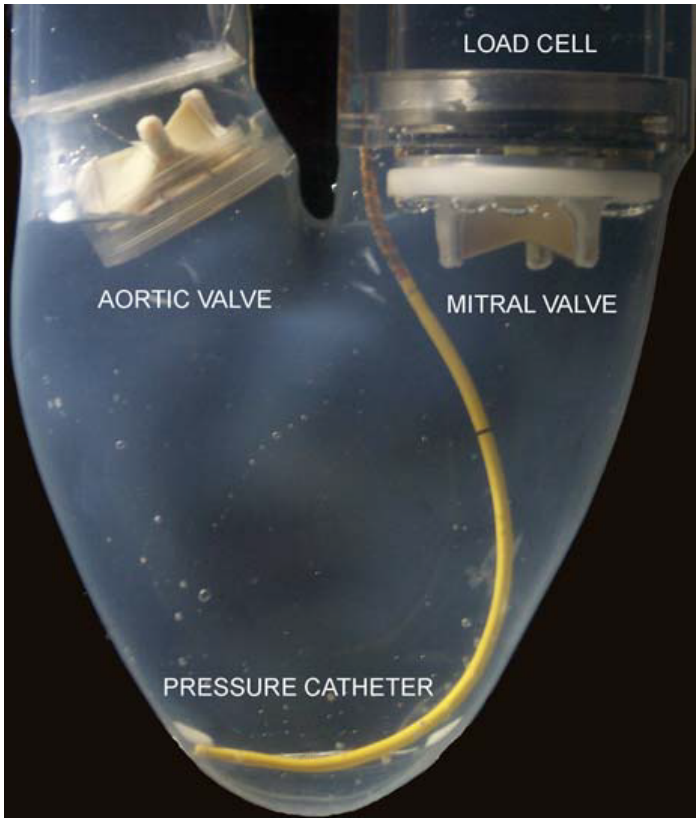

Figure 1.4: Elastic model of the heart [21]

and a physiological flow pump to evaluate the effectiveness of stents in reducing intraaneurysmal flow circulation. Similar to Kheradvar [21], their physiological flow pump is also from Vivitro systems. Figure 1.5 shows a diagram of their experimental setup.

Their system uses an elastic membrane to keep the working fluid separate from the pumps piston. The left ventricle is simulated by a thin walled sac like what is used by Kheradvar and Gharib. There are ventricle impedance adapters, also from Vivitro systems, that use resistive compliant elements to simulate viscoelsatic properties of the ventricle. The working fluid used in their tests is a mixture of 58% glycerin and 42% saline solution. This was chosen to match the index of refraction with the elastomer aneurysm model for optical measurements in another study. This study used four different waveforms to test the before and after effects of stent placement. The waveforms used were sinusoidal, with a constant ventricular output of 5 L/min at 60 bpm, 70 bpm, 80 bpm, and 100 bpm. Other parameters such as Reynolds

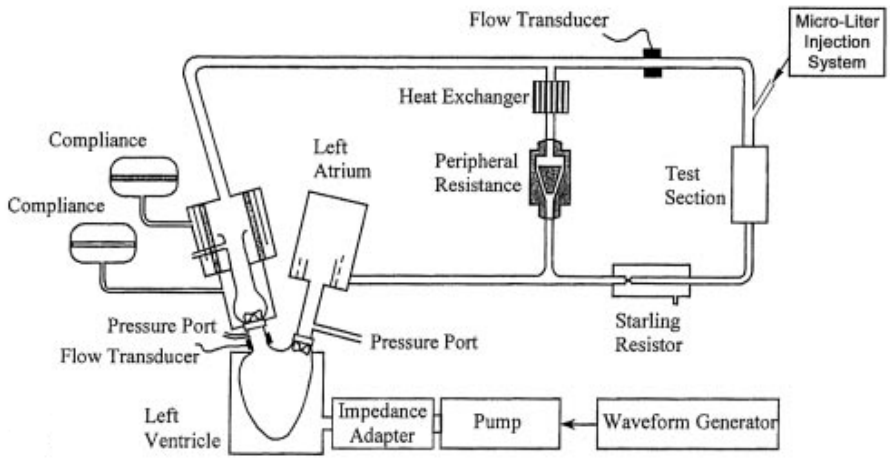

Figure 1.5: Schematic diagram of experimental setup [44]

number and Womersley number were varied for the four waveforms.

The waveform at a specific artery can also be created directly with the use of a piston pump. This is often done with two cylinders that are connected to one actuator. The cylinders are usually mechanically attached such that the linear actuator is in between them. A valve switches the fluid output between the two cylinders to select which one is producing the pulsatile waveform, while the unselected cylinder refills with fluid. One such pump uses a rack and pinion to drive the two cylinders [17]. The pinion is driven by a stepper motor where one step from the motor displaces 0.510 μL [17] of fluid.

The size of the pistons used in this pump limit the total volume that can be output in one waveform to $180mL$. To achieve negative flows the piston needs to be able to draw fluid back through the output line. This pump uses a four-way valve to switch the two pistons between the inlet and outlet lines. This pump is intended for peripheral vasculature where the peak flow rates are in the range of $30mL/s$ [17]. Testing and validating of this pump involved measuring the flow with a Doppler ultrasound machine. The fluid used was a mixture of glycerol and water to approximate the viscosity of blood [36].

Frayne et al., [12] discuss a similar pump to Holdswroth et al. [17] that uses a double piston design driven by a lead screw attached to a stepper motor. This design is more compact in that there is only one piston head, that divides the cylinder into

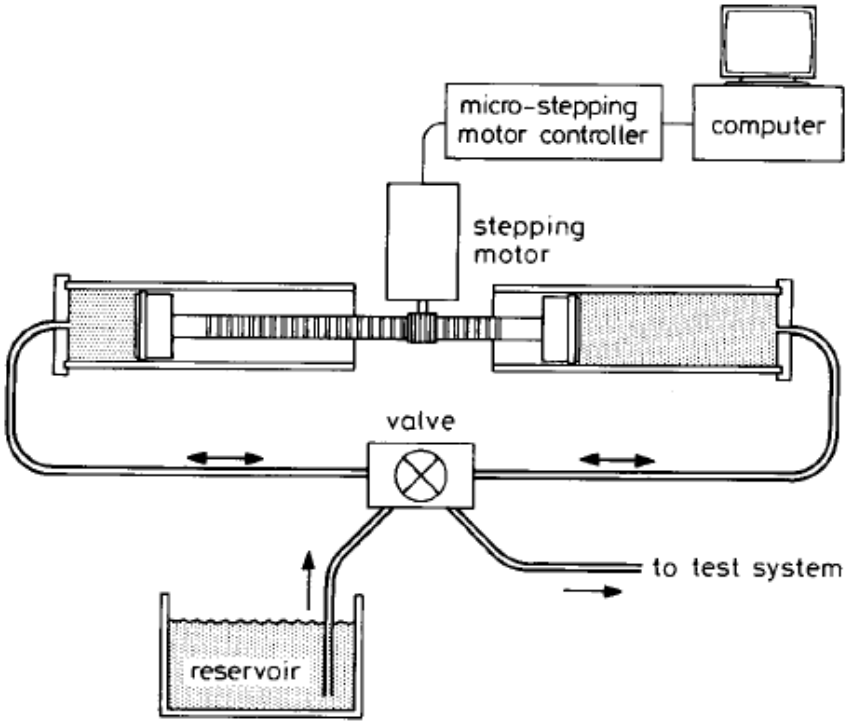

Figure 1.6: Schematic diagram of pulsatile flow simulator[17]

.

two separate chambers. Unfortunately, the lead screw used to drive the piston is in direct contact the working fluid. A 4 way valve switches between the two chambers of the pump, allowing the pump to output negative flows. The working fluid used was a mixture of machine cutting fluid and water with a viscosity of 4.0 cP [12].

Verdonck et al. studied mitral valves and how different characteristics effect the transmitral flow [52]. This study used elastic tubes to simulate the arterial network. They also use a synthetic heart chamber that is used to keep the working fluid separate from pumping fluid. The pulmonary veins, left atrium, left ventricle and aortic arch are all made of latex. They can then swap in different mitral and aortic valves for testing. They surround the synthetic heart in a box filled with water and use compressed air and a vacuum to contract and expand the heart model to produce the desired cardiac flow. Their working fluid is a mixture of water, glycerin and clay particle to simulate blood, and provide good reflective quality for Doppler measurement. This heart model will mostly be used for prosthetic valve testing.

Similar to Verdonck, Segers et al. [45] recreated the entire arterial network using

elastic tubing. This includes the aorta, the upper and lower limb arteries, the branches to abdominal organs, and 28 vascular beds to terminate the arteries with adjustable resistances and compliance. They used the same synthetic heart chamber as Verdonck [52] for their flow source. The goal of the work was to get their arterial network model to match well with In Vivo data. Their model could then be used to develop and calibrate new non-invasive diagnostic protocols surrounding the arterial network [45].

Hoskins et al. use a gear pump that is driven by a stepper motor. The pump outputs $0.316mL$ per revolution. This low volume of fluid was chosen because of the focus on umbilical and arcuate/uterine arteries [19]. Their goal was to reproduce a variety of physiological waveforms that could meet their custom needs. Instead of recreating the flow from the heart and simulating the arterial network all the way down to the arcuate/uterine arteries this gear pump would output the desired waveform directly. An important observation they make is that there are large changes in the waveform along the length of an elastic tube. Blood is a non-Newtonian fluid, however McDonald [34] says that the non-Newtonian behaviour at high shear rates are important only in small vessels of arteriolar dimension. To simulate blood a mixture of 42% glycerol to 58% water by mass is used to give a viscosity of 0.004 kg/ms [39].

Eriksson [11] uses a progressive cavity pump driven by a stepper motor to create their desired waveforms. Figure 1.7 shows the setup Eriksson used with their progressive cavity pump.

Their pump is intended to produce waveforms such as sine waves, square wave, and triangular wave. The physiological waveforms they want to reproduce are the carotid, femoral, and the aorta. The working fluid used is a glycerol and water mixture with a viscosity of 0.004 kg/ms [39]. If the waveform has very high peaks or very steep slopes exceeding 2210 mL/s^2 it may not be properly generated. Because this is a progressive cavity pump it is capable of bidirectional flow.

Plewes [40] discusses the use of a flow simulating pump for use in a magnetic resonance (MR) machine. A gear pump is used to generate the required waveform and is able to operate at an $8m$ distance from the MR machine, since no ferrous objects are allowed near the machine. An 8 m long section of 1.3 cm nylon reinforced tubing is used to connect the gear pump to the flow phantom in the MR machine. To tune the controller for the pump they preformed iterative tests that required 5-7

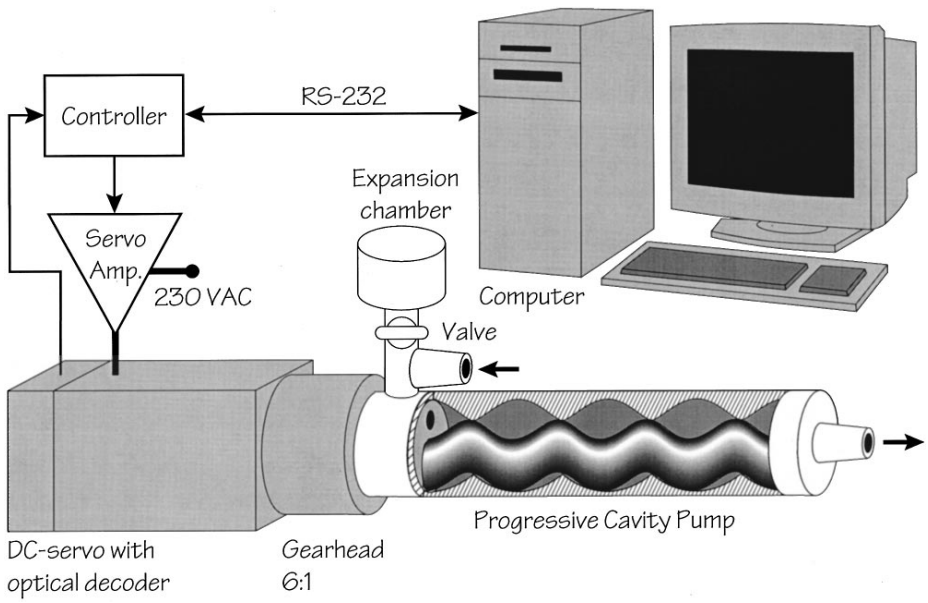

Figure 1.7: Progressive cavity pump with arbitrary flow generator setup[11]

.

minutes to arrive at the desired pressure waveform [40]. The peak flow rate for this pump is 125 mL/s. For most of their testing they use a sinusoidal pressure wave.

Law et al. [26] used a modified roller (peristaltic) pump to simulator carotid artery waveforms. This type of pump was chosen because they did not want to use a gear pump because the gears will damage sensitive particles that are intentionally in the fluid. As it is a positive displacement pump no check valves are required. Figure 1.8 shows a side view of the roller mechanism of the pump.

The modification Law et al. implemented was a back plate with screws that could be adjusted to change the degree of tube compression as a function of roller position. The rotation of the rollers was controlled by a stepper motor to generate the desired waveform. The waveform is imported to a computer from a digitizing pad and converted to 1000 equally spaced points using a cubic spline fitting algorithm.

A somewhat unique pump design by Hoppmann and Liu [18] consisted of two rubber hemispheres attached to the ends of a cylinder. The rubber hemispheres are compressed by a cam driven at constant speed by a motor. Check valves on the inlet and outlet to the cylinder control the direction of flow. As a result of using these check valves, this pump is not capable of negative flow. The shape of the cam is what controls the shape of the waveform being produced. The motor driving the cam

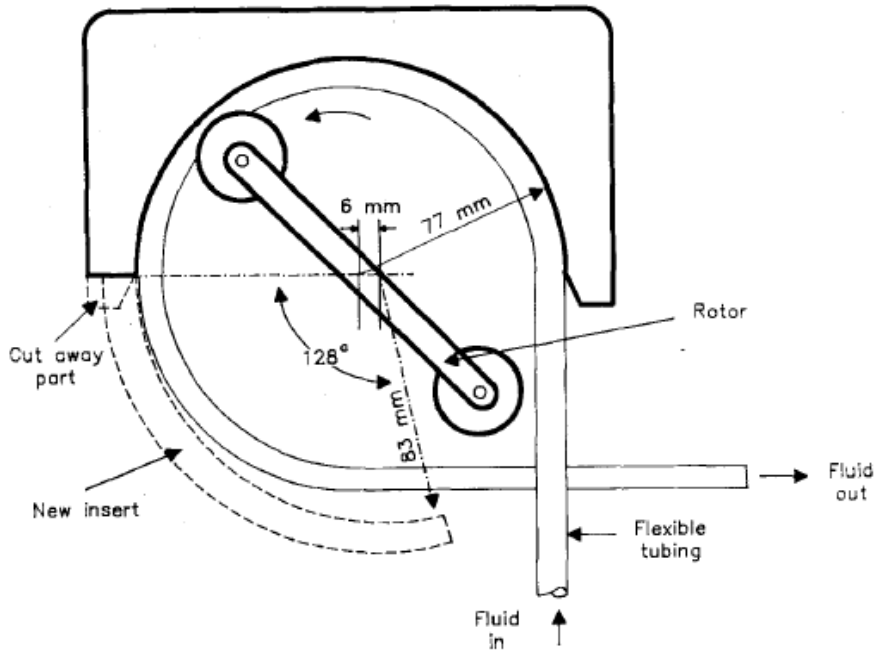

Figure 1.8: Modified roller pump side view[26]

rotates at approximately 70 revolutions per minute [18] that would correspond to about 70 beats per minute. The speed of the motor can be varied using a thyratron speed controller. The working fluid used was water. The specific waveform being used is not documented, and it would also be difficult to change to any arbitrary waveform since it would require that a new unique cam be made.

Ku and Giddens [23] needed physiological flow conditions to study the development of atherosclerosis in the carotid artery bifurcation. To create the flow required for their experiments they combined a steady state component with a pulsatile component. They used a servo controlled shaker valve connected to a constant pressure head to produce a half-sine wave with DC offset [23] which simulates the carotid pulsatile flow. They used a blown glass model of the carotid bifurcation with the average geometry taken from 22 adults. Their carotid bifurcation test section was placed downstream from the valve and they measured the flow with a electromagnetic flow meter. Additionally, they added hydrogen bubbles to the fluid to photograph and analyze bubble patterns to further study the flow phenomenon. The fluid used for their tests was a water and glycerin mixture, and the flow was pulsed such that it corresponded with a heart rate of 80 beats per minute.

Continuing with their previous work [23] in regards to the carotid bifurcation, along with work from Bharadvai et al. [3], Ku and Giddens further investigated separation, secondary flow, and flow disturbance near the model walls that might be caused by the pulsatile nature of the incoming flow [8]. In this study they used laser Doppler velocimitry for their measurements. The same carotid bifurcation model and flow system used by Bharadvai et al. [3] was used by Ku and Giddens in this study. Similar to they earlier study with a constant pressure head, this flow system uses two valves downstream of the branches of the bifurcation to control the individual flow rates in the branches. So these studies show an alternative to having a controllable flow source with constant resistance is to have a constant pressure source and controllable resistance.

Cassanova and Giddens [41] did work on measuring the velocity and energy spectra in a rigid tube downstream from a modeled stenoses with both steady and pulsatile flow. To achieve the pulsatile flow they superimposed a sunisoidal pulse from a piston pump on to a steady flow centrifugal pump. Figure 1.9 shows the schematic of their entire flow system. The working fluid used in this flow system is water. Not much detail is given to the pump setup in this article. For their tests with stenoses they vary the Reynolds number of the flow as well as how much the stenoses occluded the flow path. To measure the flow in the distal region of the stenoses they used a hot film anemometer. They also photographed the flow in acrylic sections with a fine stream of dye added for flow visualization

Similar to Cassanova and Giddens, Tsai and Ömer combined in series a piston pump for the pulsatile flow with a gear pump for the steady flow. Their system is capable of negative flows by having the piston draw in more fluid than the gear pump is outputting. Figure 1.10 shows a diagram of their flow system. The working fluid they used is distilled water. For their flow measurements they use a Transonic 4N ultrasonic flow probe along with a T206 flow meter. The flow profiles they produced in their tests were sinusoidal, carotid and coronary waveforms. An important observation they make is that their system is sensitive to the fluid impedance, and that the tuning of the system should be done when connected to the experimental flow loop. They also observed that the output flow had the least error at constant acceleration, and the largest error during diastole where there are small oscillations. The control system

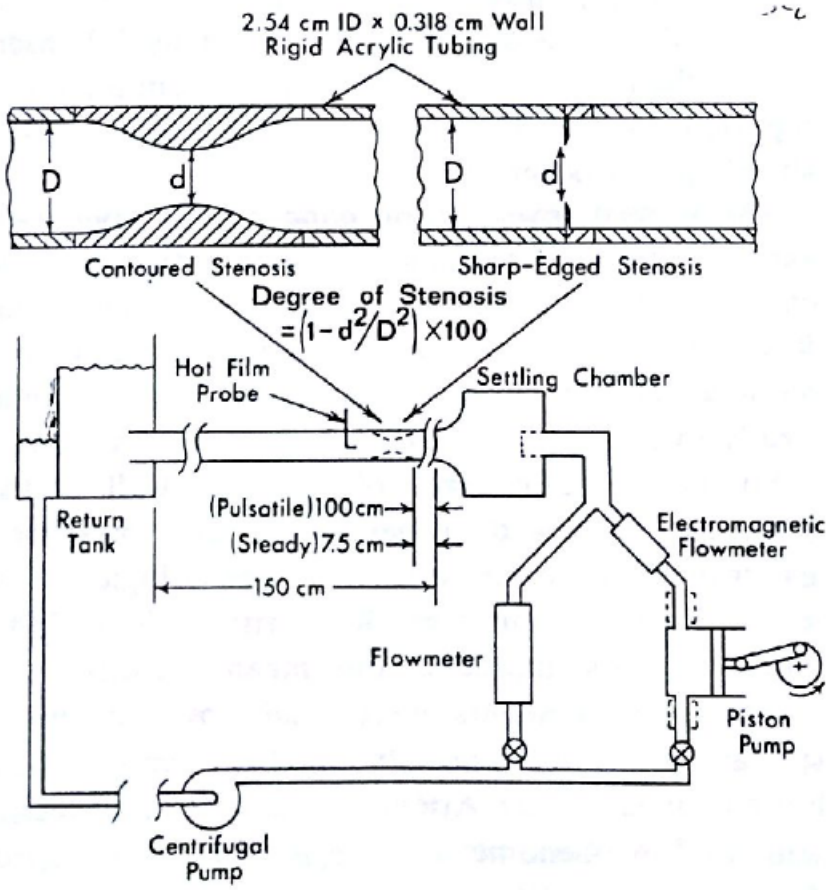

Figure 1.9: Schematic of the flow system with centrifugal and piston pump [41]

.

for this pump does not used any flow feedback.

What all these articles clearly show is that there are many different ways to make a physiological flow pump. These pump are also used in a wide range of research applications. Most pumps seem to be positive displacement type pumps so that they can produce negative flow. Few pumps were able to keep the working fluid sterile. Most pumps also use a stepper motor to drive the pump as it is relatively easy to control and generate arbitrary waveforms.

What was discovered early on is that the voice coil type actuator used to drive the piston needs to accurately estimate and compensate for friction to be able to track a reference profile. There are a few different methods of friction compensation in literature that were considered for use in this project. Because the pump operates close to zero velocity and frequently switches between positive and negative velocities,

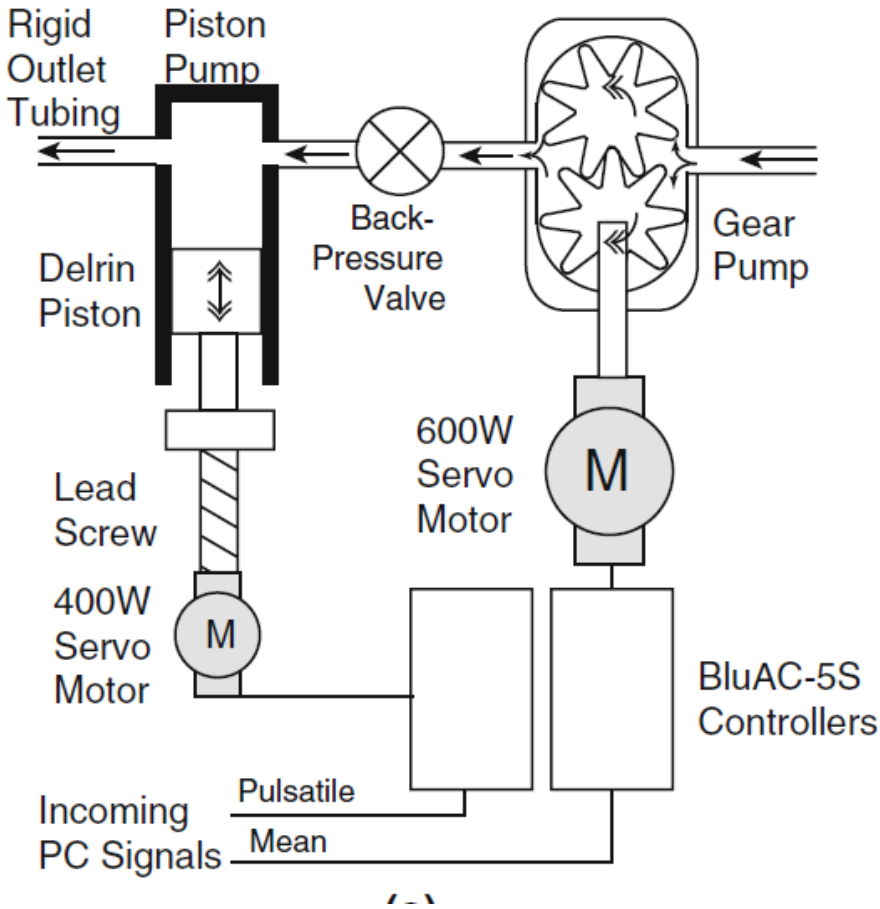

Figure 1.10: Diagram of flow system with gear pump and piston pump in series [51]

a robust method for friction compensation needs to be implemented.

The first method of friction compensation that was considered was a Maxwell slip model [2, 25, 50]. The Maxwell Slip model involves having several elasto-slide operators in parallel that share a common displacement excitation $x(t)$ [42]. Figure 1.11 from Rizos and Fassois illustrates the structure of the model.

In the Maxwell Slip model each operator has negligible inertia, stiffness k_i, and a maximum spring deflection Δ_i. For a spring deflection smaller than $\Delta_i[|\delta_i(t)| < \delta_i]$ the operator sticks, else it slips $[|\delta_i(t)| = \delta_i]$. The whole system sticks if and only if at least one operator sticks, and slides if and only if all operators slip[42]. The nonlinear state equation for each operator is:

$$\delta_i(t+1) = sgn[x(t+1) - x(t) + \delta_i(t)] \cdot min\{|x(t+1) - x(t) + \delta_i(t)|, \Delta_i\} \quad (1)$$

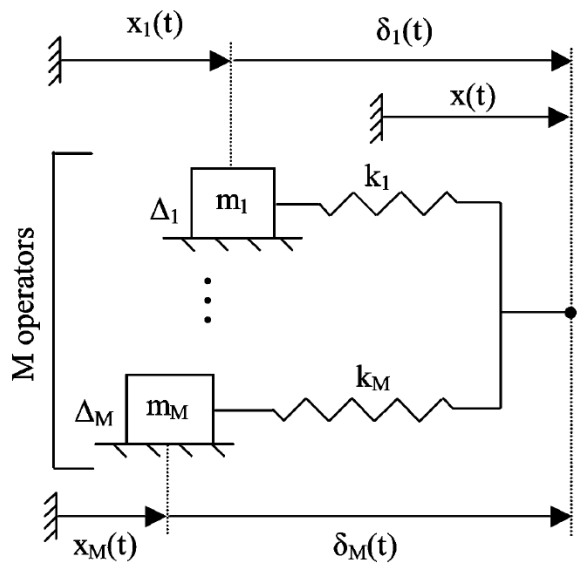

Figure 1.11: Basic Maxwell Slip model structure [42]

.

The force of friction from the model is the sum of the operator forces:

$$f_M(t) = \sum_{i=1}^{M} k_i \cdot \delta_i(t), \quad t = 1, 2, \ldots \tag{2}$$

An attempt was made to use this model for friction compensation, but the number of operators required, along with the identification of the operator parameters made it difficult to properly implement. As the number of operators increases the calculation time for each control cycle increases, so this was not a desirable trait. The literature from Rizos and Fassois [42] does describe how to identify parameters for the Maxwell Slip model, but at the time it was not possible to successfully implement the identification method.

The next method that was considered was the LuGre model [10, 9, 53, 15, 29, 35, 37, 43, 47, 54]. The LuGre model is used because it captures the features of dynamic friction such as breakaway forces, presliding displacement, viscous friction, and the Stribeck effect [53]. The article *LuGre-Model-Based Friction Compensation* by Freidovich and Robertsson discusses a tracking problem with a feedback controller with a dynamic LuGre friction model [13]. For a simple system with mass M, motor constant k_c, control signal u, and friction force F, the system can be expressed as:

$$M\ddot{x} = k_c u - F \tag{3}$$

The LuGre friciton model treats the interaction between surfaces as bristles brushing past each other. The model uses an internal state z as the average deflection of the bristles, and is used to calculate friction force as:

$$F = \sigma_0 z + \sigma_1 \dot{z} + \sigma_2 \dot{x} \tag{4}$$

$$\dot{z} = \dot{x} - \frac{|\dot{x}|}{g(\dot{x})} z \tag{5}$$

$$g(\dot{x}) = f_c + (f_s - f_c) e^{-(\dot{x}/v_s)^2} \tag{6}$$

Static and coulomb friction coefficients, as well as the stribeck velocity coefficient as seen in Equation (6) are used to model friction around the zero velocity region. The viscous friction term σ_2 dominates the other terms once away from the zero velocity region. Figure 1.12 from Wang and Wang [53] shows and example curve of the friction velocity relationship.

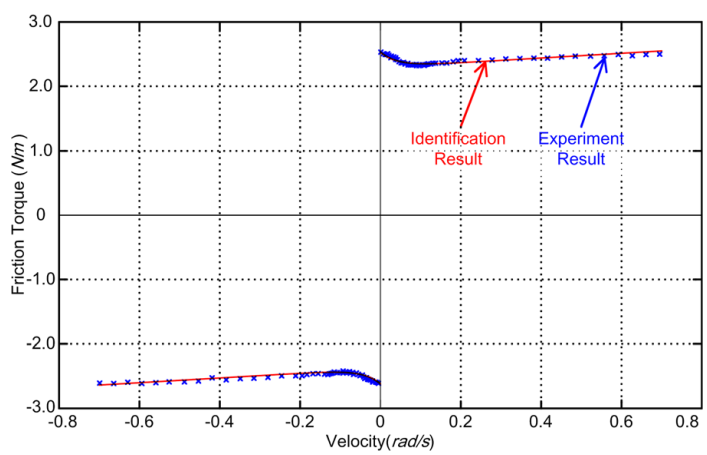

Figure 1.12: Stribeck curve example [53]

The LuGre model captures the dynamic characteristics of friction around the zero velocity point very well. The LuGre model is also relatively simple in terms of the math required to implement. The article by Freidovich and Robertsson [13] was a good introduction to the LuGre model and its basic structure. However, that article

did not discuss the identification process for the friction coefficients used in the LuGre model.

An article published by Wang and Wang [53] was informative as it covers the compensation and identification aspects of the LuGre model. The article involves tracking a motion trajectory with a hydraulic motor. An encoder provides feedback from the motor and the controller actuates a servo valve to drive the motor. To achieve accurate position tracking they use the LuGre model to capture the friction characteristics of the hydraulic motor. From a controls point of view, the mechanical setup in the article is similar to the one in this project. The control theory needs to be adjusted from rotational to linear motion.

The friction parameters are divided up into static and dynamic parameters. The static parameters are f_c, f_s, v_s, and σ_2. The dynamic parameters are σ_0, and σ_1. The static parameter identification involves constant velocity experiments to map the friction-velocity relation. When at constant velocity, the bristle deflection is also constant, so $\dot{z} = 0$. As a result of this, the steady state friction force is:

$$f_{ss} = \left[f_s + (f_s - f_c)e^{(\dot{x}/v_s)^2}\right] sgn(\dot{x}) + \sigma_0 \dot{x} \tag{7}$$

A novel evolutionary algorithm (NEA) is used to find optimal parameters by minimizing and objective function J_s [53]. The objective function used by Wang and Wang is:

$$J_s = \frac{1}{2} \sum \left[f(t_i) - f_{ss}(\Omega_s, \dot{x}_m, t_i)\right]^2 \tag{8}$$

where $f(t_i)$ is the measured friction force at time t_i and $f_{ss}(\Omega_s, \dot{x}_m, t_i)$ is the modeled friction force, $\dot{x}_m$ is the measured velocity, and Ω_s is a vector that contains the static friction parameters. The steps to implement the NEA [53] are discussed in detail by Wang and Wang. Basically, it is an iterative process that compares the modeled friction force to the measured friction force to find static friction parameters that best minimize the objective function J_s in Equation (8).

The dynamic friction parameters σ_0, and σ_1 are identified through open loop experiments, with a slow ramp input force. The previously obtained static friction parameters are also used to help identify the dynamic parameters. The cost function [53] shown in Equation (9) is used to evaluate the error between the model results

and the experimental measurements:

$$J_d = w_1 \sum_{i=1}^{N} {e_d}^2(x_d, t_i) + w_2 max\left\{|e_d(x_d, t_i)|\right\} \tag{9}$$

The error e_d is the difference between the measured results, and the system model results using the identified parameters from the NEA. The w_1 and w_2 terms are two weighting coefficients [53] to help optimize the objective function. Using the same NEA that was used to identify the static parameters, the optimal dynamic parameters can be found that best minimize the cost function J_d.

The next step Wang and Wang discuss is the observer design needed for the state z used in the LuGre model. A common problem pointed out by others [14] is that past a certain velocity point a typical observer becomes unstable. Part of the solution that Wang and Wang propose is a smooth transfer function based on the velocity of the system that will stop the observer from updating once z has reached a steady state at high velocities. The other part of solution Wang and Wang propose is that a modified dual observer is used to estimate the state z.

The final step is to combine everything into a robust controller. The system identification process gives initial values for the friction parameters for the controller to use. The modified dual observer should accurately estimate the internal state z to be used by the controller. The control expanded out with all the terms is:

$$u = -k_s(\dot{x} - \dot{x_r} + k_r(x - x_r)) + \hat{\sigma_0}\hat{z_0} + \hat{\sigma_1}\left[\dot{x} - \frac{|\dot{x}|}{g(\dot{x})}\hat{z_1}\right] + \hat{\sigma_2}\dot{x} + \hat{d} + \hat{m}\ddot{x_r} \tag{10}$$

The first few terms are a PD type controller. This controller also has a disturbance estimation term $\hat{d}$ as well as a feed forward component $\hat{m}\ddot{x_r}$. The identification process is not incredibly accurate and some of the parameters can vary over time and over the range of motion of the actuator. So, the parameters $\hat{\sigma_0}$, $\hat{\sigma_1}$, $\hat{\sigma_2}$, $\hat{d}$, and $\hat{m}$ are estimated values that start with the identified values, but are updated based on the filtered tracking error of the system.

The detailed description of the identification process, along with the controller design makes this article a invaluable resource in the development of this project. The information provided by this article is the reason that the LuGre friction model was selected for use in this project.

Chapter 2

Custom Voice Coil Based Pump System

2.1 Introduction

This project started with the desire to build a pump to mimic cardiovascular flow with the specific design challenge of using a voice coil type actuator to drive a piston. Early research into how voice coils operate lead to the idea to integrate the piston and actuator into one compact unit. This is accomplished by having the moving magnet of the voice coil actuator be the piston that is in contact with the working fluid. Figure 2.1 shows a labeled cross section of the pump to illustrate how the component of the voice coil and piston pump are configured.

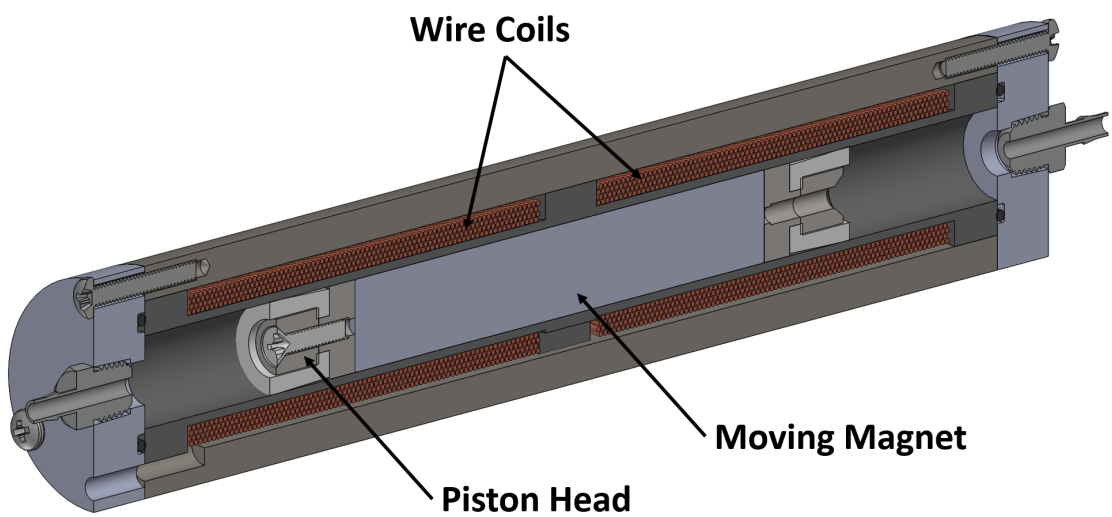

Figure 2.1: Labeled cross section of the prototype voice coil with integrated pistons

There are two ends to the actuator, so it behaves like a double acting piston. A directional control valve switches between each side of the pump to control which side of the piston is producing the desired waveform, while the other side refills on fluid

from the reservoir. By integrating the pistons and actuator into the same physical unit, this would help compact the pump into a smaller form factor.

This chapter will discuss the design process for the electrical and mechanical aspects to the pump. The electrical section will discuss the design process based on the electromagnetic principles that apply to voice coil type actuators. The mechanical design section will show how to fit a magnet in a sealed cylinder with a coil of wire wrapped around the cylinder and all the problems that creates. The seal design section details a finite element model that was used as a tool to try and adjust the seal geometry to keep friction forces to a minimum. The testing section will briefly discuss what was done to evaluate the custom voice coil and what was learned from it.

2.2 Electrical Design

This prototype was a proof of concept to investigate if it is possible to have the magnet of the voice coil function as a piston. The prototype could then be used to test the control system. Once the control system is implemented an functioning, it could be used on a larger pump to meet the large flow range requirement.

Designing a pump that can keep the working fluid sterile is a difficult requirement to meet. With this prototype, there is a rod that goes through a shaft seal to get position feedback from the piston. The actuation of the shaft through the seal exposes the shaft to the air, and by moving in and out of the shaft seal the working fluid will loose sterility. This means that the piston displacement needs to be measured while being completely enclosed. So there is a need for none invasive position feedback. A magnetic film potentiometer was found that could be used to measure the displacement of the piston without have to physically connect to it. The magnetic film potentiometer works by having a magnet near its surface to move the wiper along the length of the conductive tracks of the potentiometer. Figure 2.2 illustrates how this would work with the pump.

For this first prototype a regular potentiometer was used for feedback. The next iteration of the design will implement the magnetic film potentionmeter for feedback in an effort to maintain fluid sterility during operation of the pump. Engineering drawings for all the parts of this prototype pump can be found in appendix A starting

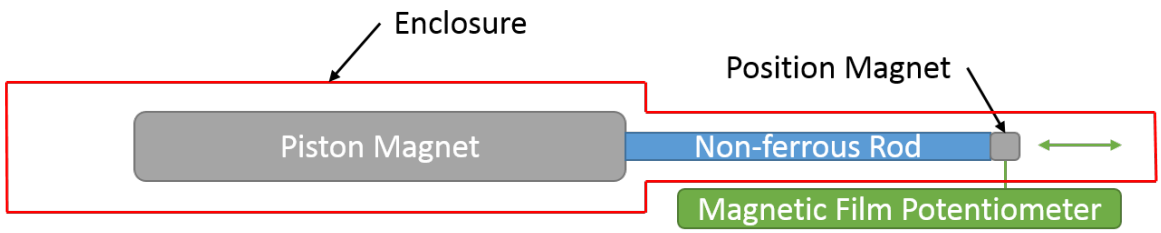

Figure 2.2: Sterile position feedback method

on Page 84.

The length and diameter of the moving magnet constrains most of the geometry of the design. The design started with selecting a 3 inch long, 0.5 inch diameter magnet. Two coils are wound around a spool and are located around the ends of the magnet [4, 6, 16, 20, 30, 48, 49]. The equation for the force of an N turn coil of average turn length L is [5]:

$$F = NBIL \tag{11}$$

B is the magnetic flux density perpendicular to the coil, and I is the current through the coil. Figure 2.3 shows the right hand rule for the Lorentz force to help illustrate the direction of the electric current I relative to the magnetic field B. The right hand rule is relevant because it shows what direction the wire needs to be wound around the magnet to produce a net force in one direction.

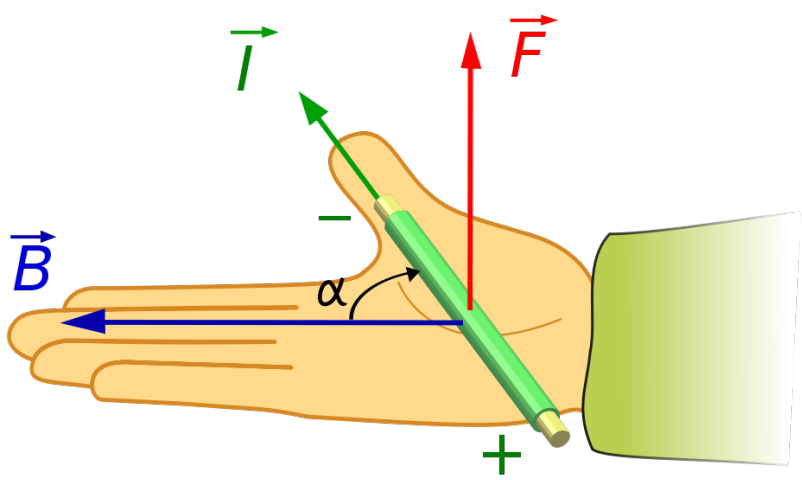

Figure 2.3: *Right hand rule for a current-carrying wire in a magnetic field B* by Quibik is licensed under CC BY-SA 3.0

The magnitude of the magnetic flux density B is determined by the grade of the magnet. For the actuator design it is crucially important how close the coil is positioned to the magnet. Since the flux density decays rapidly as you move away from the magnet, the coils should be as close as possible to the surface of the magnet to maximize the Lorentz force. With the moving magnet acting as the piston of the pump, the wall thickness of the cylinder determines how close the wire can be to the magnet. The minimum wall thickness depends on the chosen material and manufacturing process, to ensure the wall does not break or deform.

The magnet manufacturer does provide information for the flux density of the magnet, but only in the format of a color scaled image as seen in Figure 2.4. The image is too small to see a detailed view of the flux density near the ends of the magnet.

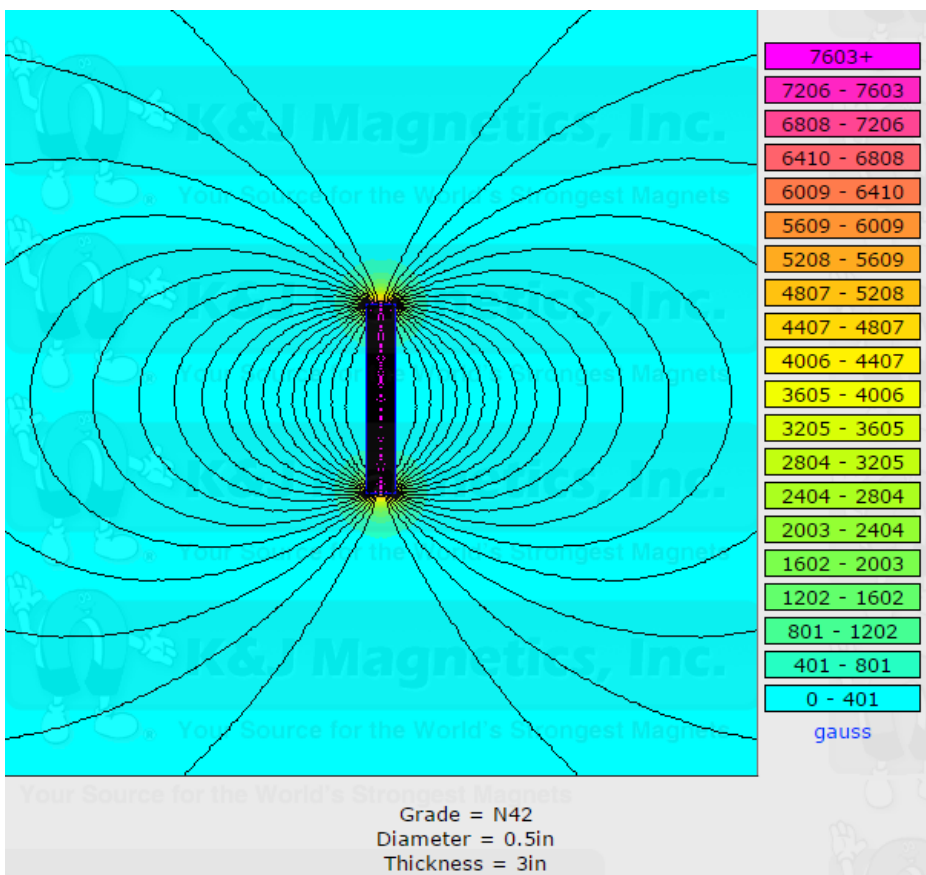

Figure 2.4: Magnetic field visualization for D8Z0 bar magnet from K & J Magnetics [31]

Figure 2.4 does give enough information to have a coarse estimate of what the order of magnitude of the flux density should be near the ends of the magnet. A 2D axisymmetric finite element model of the magnet was made to get a more detail into the flux density in the region around the ends of the bar magnet. The program used to create the mesh and run the analysis was QuickField Version 5.10. Figure 2.5 shows the model of the flux density at one of the magnet ends with a plot of the flux density in the middle of the air gap. This model was used get a value for the average flux density B that was within the range of flux density provided by the manufacturer for this specific magnet. From the plot of the flux density in Figure 2.5 the mean flux density in the air gap near the end of the magnet is 0.23 Tesla. This estimated value of the flux density is used in Equation (11) when calculating the force for the designed actuator.

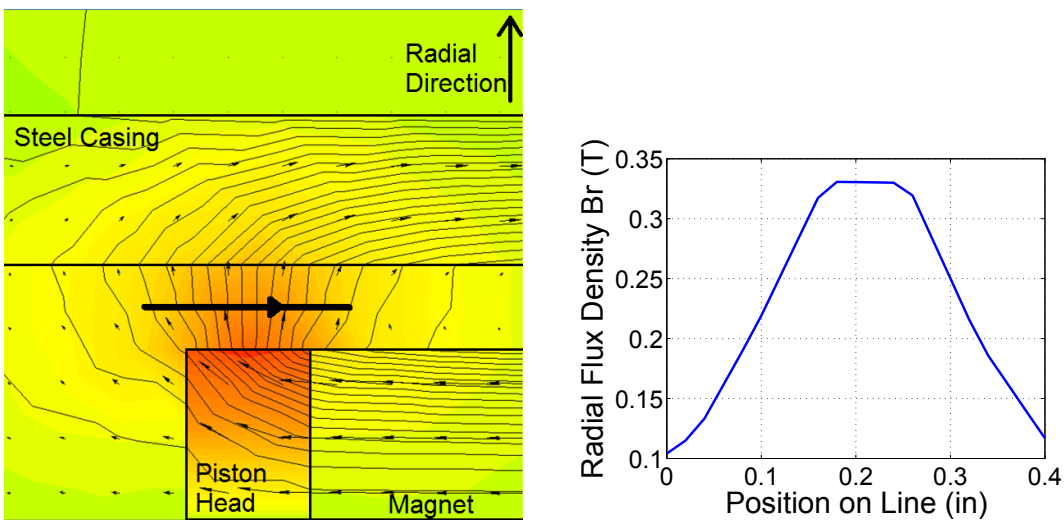

(a) Finite element model of flux density near the end of a bar magnet

(b) Flux density in air gap

Figure 2.5: Results of finite element model of the flux density for a 3 inch long 0.5 inch diameter N42 bar magnet

The terms I, N and L in Equation (11) are determined by the wire size and coil geometry. The wire size chosen was 22 AWG. The current I is determined using ohms law with the given voltage from the power supply. The resistance is estimated from the wire diameter and the total length of the wire in the coil. The resistance of the coil on half of the spool is calculated to be 1.1Ω. Measuring the resistance with a multimeter shows it to be 1.0Ω. For a nominal $5V$ power supply, the current should

be $I = 4.772A$. The number of turns N of average length L in the region of high flux density contributes the most to the total force output. N is assumed to be the number of wires that fit in the high flux density area shown in Figure 2.5. Based on the wire diameter and the number of layers in the coil, $N \approx 64$. L is the length of one turn around the coil and is calculated to be $L_{mean} = 0.0562m$. The estimated force produced from one end of the magnet is calculated in Equation (12).

$$F = (64)(0.227T)(4.772A)(0.0562m) = 3.9\ Newtons \tag{12}$$

This gives a force constant of:

$$k_{calculated} = \frac{3.9\ N}{4.772\ A} = 0.82N/A \tag{13}$$

Once the voice coil is constructed the maximum force can be measured to compare it with the calculated maximum force. This will be discussed further in the testing subsection.

Position feedback for the prototype was achieved using a simple linear slide potentiometer. An aluminum rod was threaded into the piston head on the end of the magnet and sticks out the end of the voice coil to be fixed to the potentiometer. The potentiometer is then wired so that the position is read as an analog signal from $0V$ to $5V$.

The initial control system for the prototype used Matlab to communicate with an Arduino Uno micro controller board to read in the potentiometer signal and to send a control signal to a motor controller board. The motor controller board powered the voice coil from a used computer power supply. A Matlab GUI was made to plot the position and velocity of the piston in real time, similar to how a heart rate monitor in a hospital displays heart beats.

2.3 Mechanical Design

The design started assuming a 3.000 ± 0.004 inch long, 0.500 ± 0.004 inch diameter magnet. The diameter of the magnet set the size for the bore of the cylinder. Figure 2.6 shows the magnet with the piston heads attached. An engineering drawing for the piston head and assembly are in appendix A pages 85 and 86. The rod sticking

out the end of the piston head is connect to the linear potentiometer for position feedback. A 33/64 inch reamer had to be used to machine the cylinder bore to accommodate the diameter and straightness tolerance of the magnet. The 33/64 inch bore diameter made commercial seals impossible to find. Custom piston cup seals had to be machined to fit the bore properly.

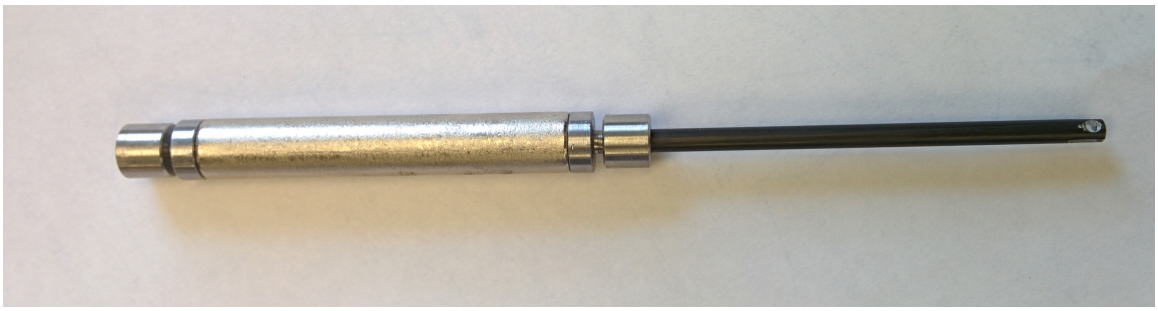

Figure 2.6: 3 inch magnet with piston heads (no seals)

Three cylinders were manufactured in total. See Appendix A Page 87 for the drawing of the spool assembly, and Page 89 for the spool part drawing. The first two cylinders were made of plastic to avoid shorting the coils to the spool. Using only a drill for the bore for the first acetal cylinder did not produce a good surface finish, so it was quickly scrapped. The second cylinder spool was made of acrylic, since it is a relatively hard plastic. The bore was drilled and reamed to produce a good surface finish to seal against. Figure 2.7 shows the second cylinder spool that was made. The friction between the PTFE piston seals and the acrylic cylinder was a problem for the second cylinder. The third cylinder was made of brass to try to reduce the seal friction. A tiny thermistor was placed on the brass spool and had the coil wound around it. This thermistor would have been used to monitor the temperature of the coil to make sure it doesn't exceed the maximum temperature of the coating on the wire. As feared, the wire shorted to the brass so this cylinder was not powered.

Figure 2.7: Second manufactured cylinder spool

There are 4 layers of coils on each side of the cylinder spool. The coiling starts in the center and is wound on one side clockwise with 4 layers. There is a little slot milled into the middle of the cylinder spool for the wire to cross over to start the second coil. The second coil is wound counter clockwise. The reason why the coils need to be wound in opposite directions is because the flux density is positive at one end of the magnet, and negative at the other. This is where the right hand rule is relevant in the coil design. Winding the coil in opposite directions means that the current through one coil will be negative when applying the right hand rule. By putting the negative flux density end of the magnet with the coil with negative current, the resulting force (following the right hand rule) will still be positive. This arrangement means that each end of the magnet contributes to the total force output of the actuator. Figure 2.8 shows an axisymmetric cross section of a cylinder magnet with steel caps on the ends placed inside a steel tube with a small air gap. The magnet in this model is the 3 inch long, 0.5 inch diameter grade N42 magnet from figure 2.6. The highest regions of flux density are located at the ends of the magnet with the steel end caps helping direct the flux out in the radial direction.

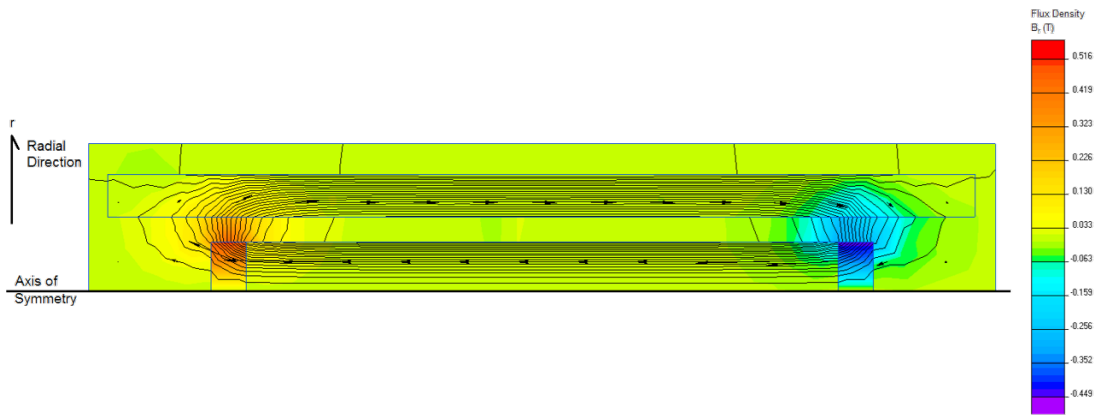

Figure 2.8: Axisymmetric model of bar magnet flux density in the radial direction

Figure 2.8 was used to estimate the flux density value when calculating the maximum force of the actuator. Testing will show that this relatively simple model was fairly accurate.

The cylinder is the critical part to the prototype pump, but there was also the surrounding hydraulic circuit around the piston actuator. To keep the fluid system simple the piston is connected so that it sucks water from a reservoir, and then expels it back out into the same reservoir. This was achieved with two low pressure check valves. Figure 2.9 illustrates the simple hydraulic circuit.

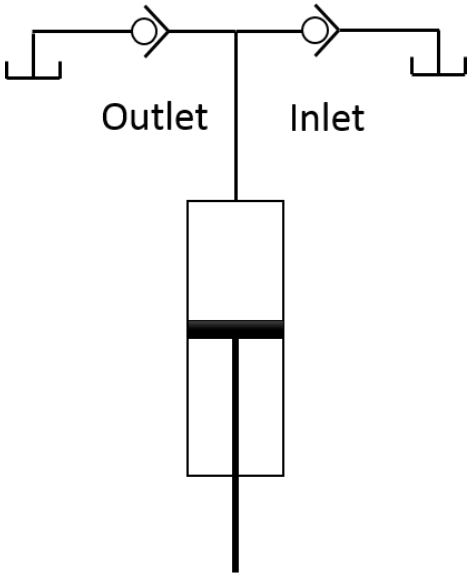

Figure 2.9: Simple hydraulic circuit diagram of prototype pump

This setup was used as a proof of concept to show that the pump could move water. While the setup did function as intended, the low pressure check valves still provided significant resistance that the piston had difficulty overcoming. The check valves require low pressure to activate, so this difficulty is caused by the actuator being under powered and is not really an issue with the check valves. However, replacing the check valves with a directional control valve would reduce the the pressure required and allow the pump to perform better.

2.4 Seal Design

Since the spool has a bore of 33/64 inch the piston cup seals were machined out of a solid piece of PTFE to fit the odd fractional size(Drawing on page 94). Testing the seals in the acrylic cylinder spool showed that the friction forces from the piston seal was much larger than expected. A simple spring scale test measured the breakaway friction force to be about 9 N. This is rather close the the maximum force the prototype was designed to produce. This test showed that dealing with friction will be critical to the design and control of the pump.

A finite element(FE) model of the piston cup seals was created as a tool for estimating the friction of different seal geometries. Figure 2.10 shows a cross section of the seal that was used in the FE model.

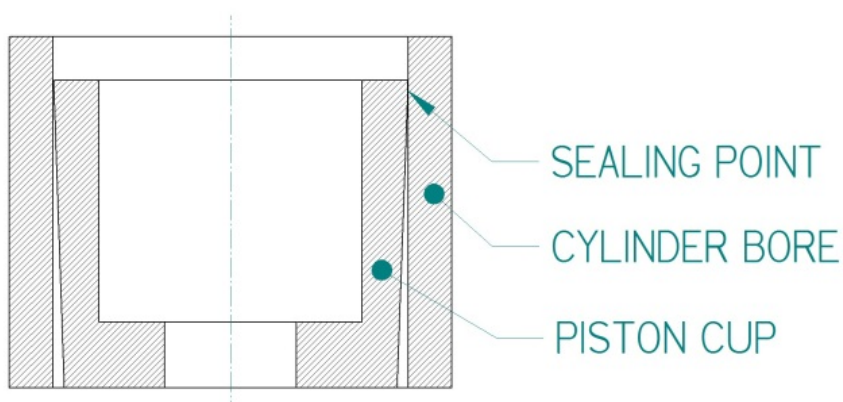

Figure 2.10: Axisymmetric model of piston cup seal

The piece of data from the model that will be useful is the contact force between the PC and the cylinder. Specifically, the contact force in the radial direction, as it is

directly related to the friction. Multiplying the radial contact force by the coefficient of friction should yield a friction force that the piston actuator needs to overcome. Since the seal and cylinder was already made, this model could be validated. The PC and cylinder parts are both axisymmetric.

The prescribed motion in the model is a constant velocity in the axial direction. This allows the use of a 2D axisymmetric model. The PC is made of PTFE. This material is used because it is well known for its low coefficient of friction, which is desirable for this application. Both the static and dynamic coefficients of friction are often listed as between 0.04 and 0.08 (MatWeb LLC). To be conservative, the model assumes that $\mu_s = 0.08$, and $\mu_d = 0.08$. A simplified Johnson Cook model is used for the PTFE material. The material model, as taken from the LS-DYNA manual (Livermore Software Technology Corporation), expresses the flow stress as:

$$\theta_y = (A + B\epsilon^p)(1 + c \log \dot{\epsilon}) \tag{14}$$

A, B, C and n are input constants and $\bar{\epsilon}^p$ is the effective plastic strain. The input constants used are: $A = 11\ MPa,\ B = 44\ MPa,\ n = 1,\ C = 0.12$ (Herbold).

Acrylic is used in the model because the existing prototype is made with acrylic. By keeping the model as similar to the prototype as possible, it will be possible to experimentally validate the results. The acrylic is modeled as a linear elastic material. The material properties for the cast acrylic were taken from MatWeb (MatWeb LLC) and can be seen in Table 2.1. MatWeb does not list a Youngs modulus for PTFE, so material properties are used from a PhD thesis (Herbold). This is the same source for the Johnson Cook model in an effort to keep the material properties consistent.

Table 2.1: Material properties used in LS-DYNA model

Material	**Density**	**Young's Modulus**	**Poisson's Ratio**
PTFE	2200 kg/m^3	1.46 GPa	0.46
Cast Acrylic	1190 kg/m^3	3.10 GPa	0.35

As mentioned previously, this model will be 2D and axisymmetric. This should allow the use of small sized elements without having relatively long solution times.

Figure 2.11 shows a mesh with 0.007 inch elements. There are approximately 1000 elements in the PC for this mesh. This is a moderately fine mesh, and has a relatively short solution time for this model

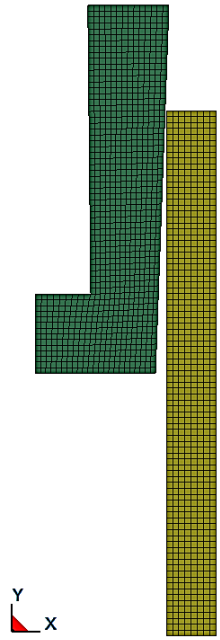

Figure 2.11: Model mesh with 0.007 inch element size

There are two important node sets within the mesh. There is the set for boundary conditions, and the set for the prescribed motion of the PC. Figure 2.12 shows where the two node sets are on the mesh. The node set 1 is used to prescribe the motion of the PC. For this model, the prescribed motion is a constant velocity of 12 in/s in the negative Y direction. Node set 2 is the rigid boundary condition with the nodes constrained in all degrees of freedom. The total simulated time is 0.090 seconds. This allows the PC to enter, traverse, and exit the cylinder.

A convergence study was performed to determine if the model converged on a value for the radial contact force as the element size decreased. Note that the X direction labeled in the figures is actually the radial direction, so the X force is the radial contact force that is the focus of the model. The element size of the piston cup seal mesh was varied from as large as 0.200 inch with 3 elements, down to 0.0015 inch with over 20000 elements. For the convergence studies the cylinder mesh was kept constant at 0.007 inch element size. The cylinder material itself was also made

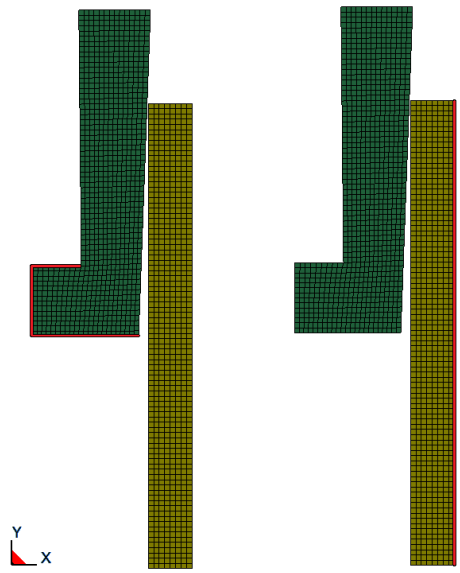

Figure 2.12: Node sets highlighted in red, 0.007 inch element size

completely rigid for the convergence study. The large element sizes in the first several studies means that the solution time is very fast. This allowed 10 studies to be done while gradually reducing the element size. The results of the 10 studies are listed in Table 2.2.

The contact force stays fairly constant as the PC travels through the cylinder. To keep the numbers consistent between the different studies, the contact force is averaged between 0.025 seconds and 0.060 seconds for each study. This should minimize any transient effects from entering and leaving the cylinder.

The results from the convergence study are plotted in Figure 2.13. It is clearly visible that decreasing the element size below 0.007 inches starts to increase the solution time dramatically with minor variation in the X force.

The results of the study show that the X force is converging to an X force in the range 14.5 lbf to 14.9 lbf. To maintain some level of accuracy without incurring longer solution time, an element size of 0.007 inch will be used for the validation and results discussion.

By using the existing prototype it should be possible to experimentally validate the model. Some preliminary experiments were performed to estimate the friction force of the PC. A spring gage was used to manually actuate the piston while monitoring

Table 2.2: Convergence study results

Study	**X-Force**	**Time**	**Element Size**
-	(lbf)	(s)	inch
1	0.633	117	0.200
2	13.3	14	0.050
3	13.9	32	0.030
4	14.5	41	0.025
5	14.6	56	0.020
6	14.4	61	0.015
7	14.5	213	0.007
8	14.8	2133	0.003
9	14.7	22397	0.002
10	14.9	20632	0.0015

the force required on the dial indicator. The force required to move the piston was in the range of 1 lbf to 2 lbf. Peak forces of close to 2 lbf were experienced, but under smooth running conditions the force was closer to 1 lbf. These measurements are not very accurate, but should provide enough information to validate the model with low to moderate accuracy. By taking our X force from study 7 of 14.5 lbf and multiplying by d = 0.08, the friction force is estimated to be 1.16 lbf. Given the accuracy of the experimental results, this should be considered a low to moderately accurate model. The key numerical result to take away from this model is the radial force of 14.5 lbf, and the resulting friction force of 1.2 lbf. Keep in mind that the accuracy of this model is low to moderate. This model can now be used to minimize the seal friction in future pump designs by adjusting the part geometry, as well as providing an estimate of the force required to actuate the piston. A friction coefficient of 0.08 is also assumed, which may or may not be accurate for PTFE on acrylic contact. This model is only trying to estimate the dry running friction force resulting from compression of the piston cup seal. One major improvement to the model that is recommended is to find, or measure, accurate coefficients of friction to input into the simulation. It may be possible to use the prototype to determine the coefficients of friction experimentally for this specific case. This would allow for a more detailed representation of the friction forces with static, dynamic, and viscous coefficients, as well as a decay parameter being included in the contact analysis. The model could

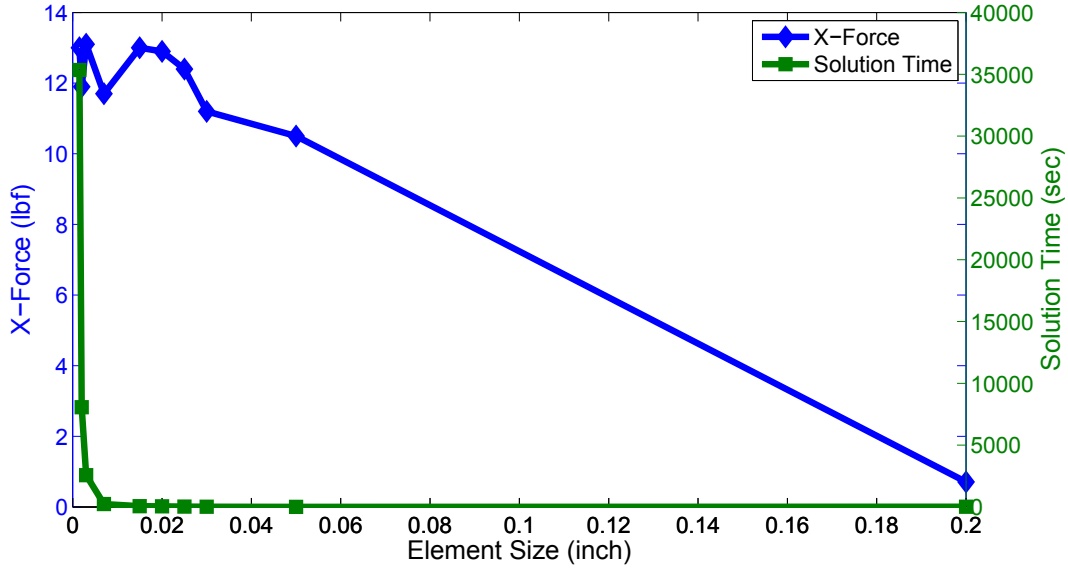

Figure 2.13: Convergence study results

then directly output the force required to move the piston as the contact force in the Y direction. This might also allow for more variable velocity curves to be simulated, which could help achieve better controllability of the pump.

2.5 Testing

The first attempt at controlling the voice coil used Matlab to communicate with an Arduino Uno microcontroller board. The Arduino read the position from the linear potentiometer, and communicated with the motor driver to power the voice coil. The downside to using this simple setup is that the control cycle only operated at 70 Hz. Desktop computers do not work well for real time deterministic control applications.

The first controller was a PID controller with the reference changing over time. The Arduino Uno microcontroller was too slow to save the the position data while controlling the pump, so no results could be recorded. This first controller was still useful as a proof of concept for the pump. The goal at this stage of the design was to observe it simply moving fluid while trying to track some reference waveform. It was during this testing that high friction forces from the piston seals where observed as a problem for the pump. The pump was operating near its maximum designed current just to overcome static friction. This indicated a problem with the voice coil

being under powered for this application. When testing the pump without the seals and fluid, friction from the slide potentiometer was still and issue. The pump didn't need to be near maximum current to overcome the potentiometer friction, but it was observed that the non-linear nature of friction[32, 33, 35, 46] is a problem when trying to control the pump.

The key test for the custom voice coil is to see if the measured force output matches the calculated force from the design stage. The coil on the brass cylinder had to be rewound for this test. To minimize the risk of shorting the coil again, lacquer was applied to the spool in an effort to insulate the brass from the coils. A multimeter was used to verify that the coil was not shorting to the cylinder. The prototype was connected to a $5V$ power supply and the force and current were measured. The measured force was $3.2N$ and the current draw was $3.72A$. The corresponding force constant is:

$$k_{measured} = \frac{3.2\ N}{3.72\ A} = 0.86\ N/A \tag{15}$$

The calculated force constant was $0.82\ N/A$. The error between the calculated force constant and the measured force constant is 5%. The calculated force constant underestimates the measured force constant which will be good when designing future voice coils. Although the calculated and measured force constants were close in value, the maximum force output was still small. For reference, the commercial voice coil has a force constant of $17.8\ N/A$. When first testing the pump with the PTFE seals, the voice coil had to be near maximum current just to overcome static friction. This under powered voice coil contributed to the list of reasons to switch over to the commercial voice coil for further development of the control system for the pump. In the future, the commercial voice coil should be disassembled to see how it is made with such a large force constant compared to the custom voice coil.

2.6 Summary

This chapter discussed the design process for the electrical and mechanical aspects of the custom voice coil type pump. It involved wrapping a coil of wire around a sealed cylinder for a magnet to sit inside. Current is applied to the coil to drive the magnet as a piston to produce flow. The main lessons learned from the design and testing of

this pump was:

- Non-linear friction forces make control difficult
- Custom voice coil is under powered
- Relatively low force constant

Chapter 3

Commercial Voice Coil Based Pump System

3.1 Introduction

As mentioned in the previous chapter, non-linear friction forces from the piston make control of the pump difficult. Additionally, having an under powered actuator makes the control even more difficult. Therefore, to better understand and implement a robust control system, a commercially available voice coil actuator was used to develop the control system for the pump.

This chapter will discuss all of the physical hardware used for developing this version of the pump. The hardware that will be discussed includes the voice coil actuator, the encoder, the custom switching valve, and the National Instrument devices. The pump setup described in this chapter is the setup used for validating the control system which will be discussed in the following chapters.

3.2 Hardware Setup

The commercial voice coil used is the NCM30-25-090-2LB from H2W Technologies. The important details of this actuator are the 3 inch stroke and 9 pounds of force (40 N) at 100% duty cycle. This pump set-up involves attaching a piston to each end of the actuator. A custom valve controls the flow direction to and from each piston. Figure 3.1 shows the labeled pump set-up.

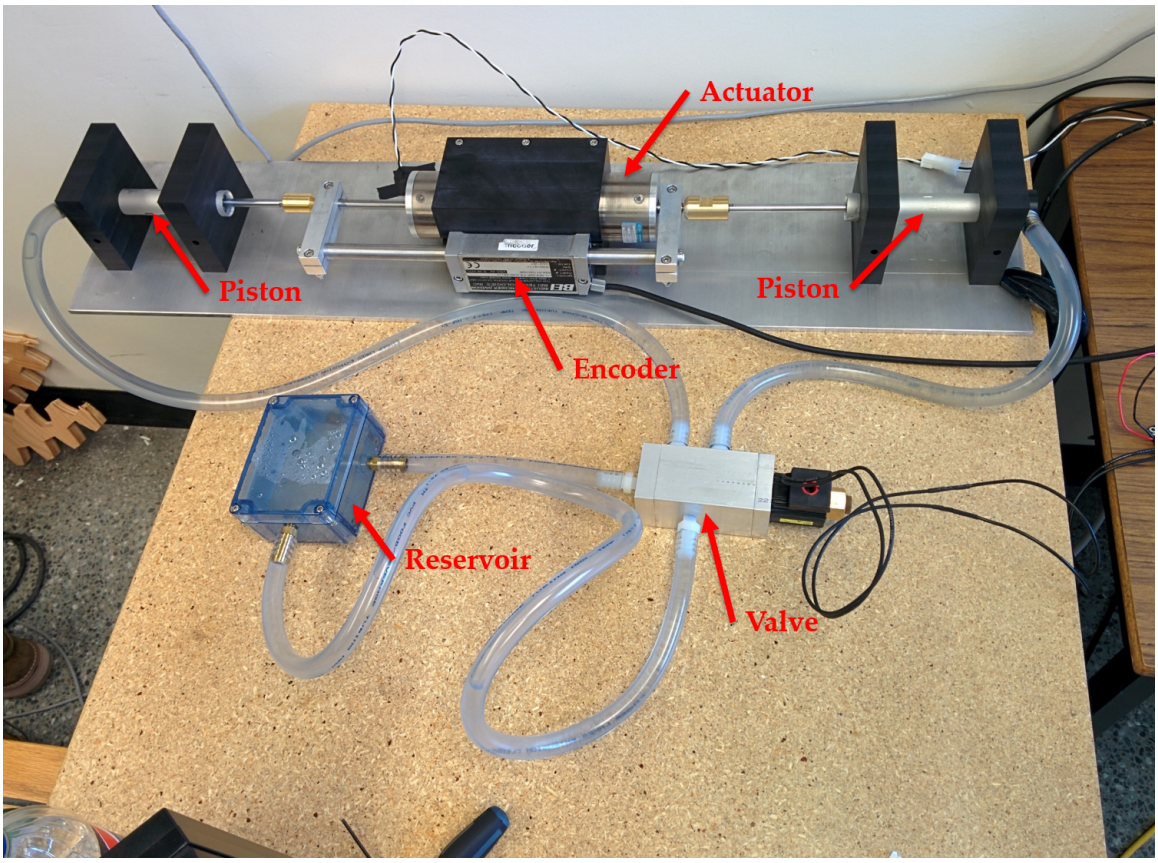

Figure 3.1: Pump setup with major parts labeled

This commercial actuator is much more powerful than the custom voice coil. For comparison, the commercial voice coil has a force constant of 17.8 N/Amp and the custom voice coil has a force constant of 0.87 N/Amp. This was the main reason for using it while implementing the control system. The actuator was purchased prior to the start of the work in this thesis, but was intended for use in the project so it was readily available to work with. The pistons are 20 millimeter diameter with 100 millimeter stroke length. The valve was custom made because the pump operates at a low pressure, and commercial hydraulic valves have such small orifices that it would restrict flow too much for the pump to overcome. The reservoir is a clear enclosure with a sealed lid with a two tapped holes for 3/8 NPT barbed tube fittings. The tubing used was 3/8 inch inner diameter, 5/8 outer diameter, flexible PVC tubing.

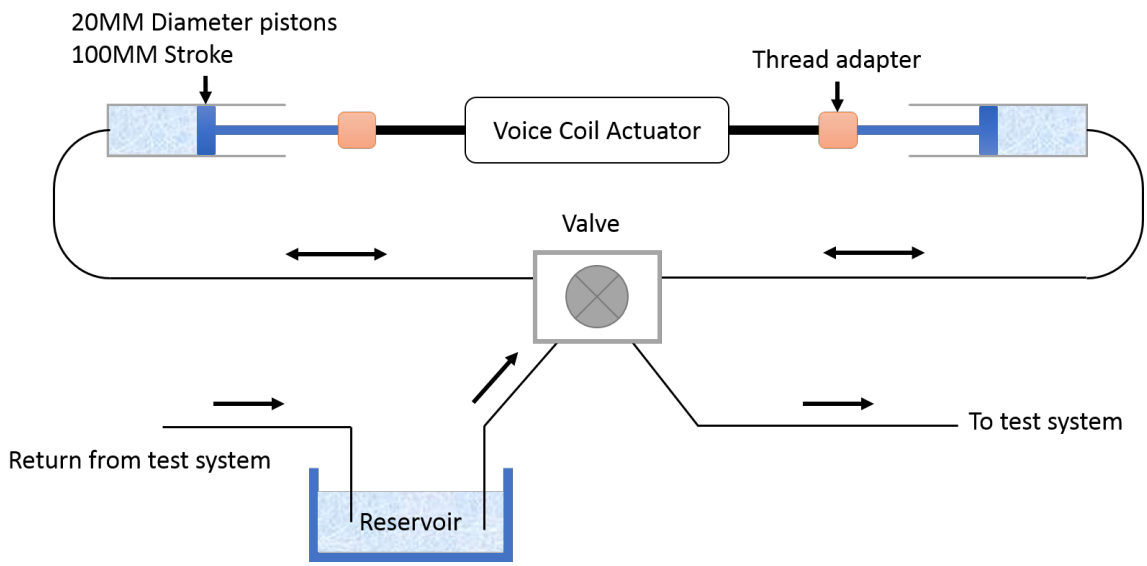

Figure 3.2: Block diagram of pump setup

Figure 3.2 illustrates a block diagram of the pump setup. In Figure 3.2 the line labeled as going to the test system is where the flow measurement will be taken. During the development and testing of the control system the line going to the test section just returns to the reservoir. The block diagram illustrates how the fluid in the lines connected to the pistons will flow back and forward. However, buy using the valve to toggle between the two pistons it is possible to have the test section experience net positive flow.

3.3 Simplified System Model

A simplified model of the system is illustrated in Figure 3.3. This is a linear time-invariant system. Although Figure 3.3 only shows one piston, there are two pistons in the physical system. To keep the system equations simple Figure 3.3 lumps all the parameters from the two pistons into this one piston model. This means the the mass M would be the mass of both pistons, in addition to the moving mass of the actuator itself. The term F is the force from the actuator. The resistance term R is used to represent all the fluid resistance in one term. Similarly, the viscous friction coefficient B lumps together all the sources of friction into this one term. Realistically the friction force is highly nonlinear, but this simplified model is a good starting point for the basic components of the controller. The piston area A is required for the state

equations, and is calculated from the 20 millimeter piston diameter.

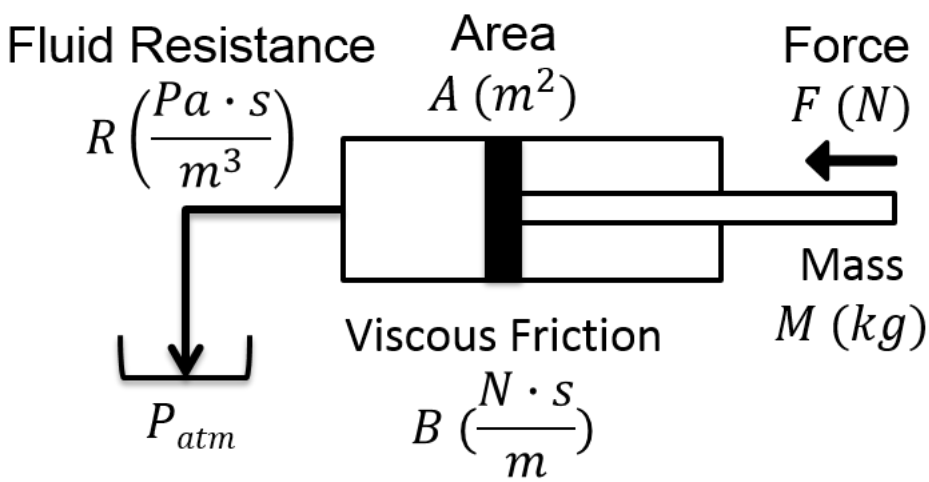

Figure 3.3: Pump system

The state equation for this simplified model is:

$$\frac{dV_m}{dt} = \frac{(RA^2 - B)}{M} V_m + \frac{1}{M} F(t) \tag{16}$$

The state space form of the system with the position added as a state is:

$$\begin{bmatrix} V_m \\ \frac{dV_m}{dt} \end{bmatrix} = \begin{bmatrix} 0 & 1 \\ 0 & \frac{(RA^2-B)}{M} \end{bmatrix} \begin{bmatrix} X_m \\ V_m \end{bmatrix} + \begin{bmatrix} 0 \\ \frac{1}{M} \end{bmatrix} F_s(t) \tag{17}$$

$$y = \begin{bmatrix} 1 & 0 \end{bmatrix} \begin{bmatrix} X_m \\ V_m \end{bmatrix} \tag{18}$$

The controllability matrix for this state space equation is:

$$W_c = \begin{bmatrix} 0 & \frac{1}{M} \\ \frac{1}{M} & \frac{(RA^2-B)}{M} \end{bmatrix} \tag{19}$$

Checking the rank of the controllability matrix yields:

$$rank(W_c) = 2 \tag{20}$$

The controllability matrix is full rank, which means this system is controllable. The observability matrix is:

$$W_o = \begin{bmatrix} 1 & 0 \\ 0 & 1 \end{bmatrix} \tag{21}$$

Checking the rank of the observability yeilds:

$$rank(W_o) = 2 \tag{22}$$

The observability matrix is full rank, which means this system is observable. A simulation of the system was create in Matlab and Simulink to test different controllers. On of the controllers used was a linear quadratic regulator (LQR) controller and Francis-Byrnes-Isidori (FBI) reference tracking. The values for the parameters used in the simulation were:

- $M = 0.6\ kg$
- $B = 100\ Ns/m$
- $R = 3.95 \cdot 10^6\ \frac{Pa \cdot s}{m^3}$
- $A = 1.2668 \cdot 10^{-4}\ m^2$

The general state space equation looks like:

$$\dot{x} = Ax + Bu, y = Cx \tag{23}$$

Looking at Equations (17) and (18) you can see that they follow the general form as seen in Equation (23). With the FBI reference tracking method along with the LQR controller gain, the controller u is:

$$u = F_1 x + F_2 y_d \tag{24}$$

In Equation (24) F_1 is the gain designed using the LQR method. The term x is the system states. The F_2 term is a feed forward gain that will be designed using the FBI method. The term y_d is the reference that the controller will try to track. The F_2 term can be expanded, and once expanded the controller looks like:

$$u = F_1(x - \Pi(y_d)) + \bar{F}_2(y_d) \tag{25}$$

The gains Π and $\bar{F}_2$ are calculated using the FBI method with the equation:

$$\begin{bmatrix} A & B \\ C & 0 \end{bmatrix} \begin{bmatrix} \Pi \\ \bar{F}_2 \end{bmatrix} = \begin{bmatrix} 0 \\ y_d \end{bmatrix} \tag{26}$$

Inputting the values for the mass M, the viscous friction coefficient B, the fluid resistance R, and the piston area A into equation (32) results in:

$$\begin{bmatrix} 0 & 1 & 0 \\ 0 & -166.7 & 1.67 \\ 1 & 0 & 0 \end{bmatrix} \begin{bmatrix} \Pi_1 \\ \Pi_2 \\ \bar{F}_2 \end{bmatrix} = \begin{bmatrix} 0 \\ 0 \\ y_d \end{bmatrix} \tag{27}$$

Solving Equation (27) system of equation shows that $\Pi_1 = y_d$, $\Pi_2 = 0$, and $\bar{F}_2 = 0$. Now the controller from Equation (24) becomes:

$$u = F_1(x - \begin{bmatrix} 1 \\ 0 \end{bmatrix} (y_d)) \tag{28}$$

The next step is to solve for F_1. To do this the performance criterion for the linear quadratic regulator must be considered [38]. The performance criterion is:

$$J = \int_0^\infty \left[x^T(t)Qx(t) + u^T(t)Ru(t)\right] dt \tag{29}$$

The matrix Q is non negative definite, and the matrix R is positive definite. The optimal control minimizing J is:

$$u(t) = -Kx(t) \ where \ K = R^{-1}B^TP \tag{30}$$

The symmetric matrix P is the unique positive definite solution to the matrix Algebraic Riccati Equation:

$$A^TP + PA - PBR^{-1}B^TP + Q = 0 \tag{31}$$

Using Matlab's LQR function, the gain K can be calculated given the input matrices, A, B, Q, and R. The matrices Q and R can be manually set to fine tune the controller. Looking at Equation (24) and comparing it to Equation (30) we see that for this case the optimal controller K is equal in magnitude to F_1.

3.4 Simulation Results of LQR Controller

Figure 3.4 shows the results of a Matlab simulation with the LQR controller and Francis-Byrnes-Isidori (FBI) reference tracking that was discussed in the previous section.

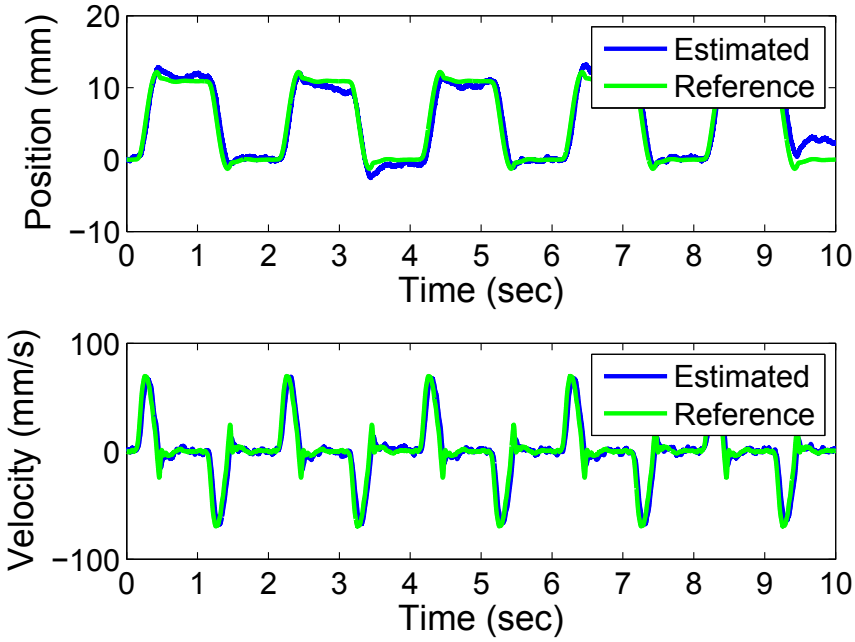

Figure 3.4: Matlab simulation results for LQR controller with FBI reference tracking

For the controller used to create Figure 3.4 the matrix R was [0.1]. The matrix Q was:

$$Q = \begin{bmatrix} 1500000 & 0 \\ 0 & 10 \end{bmatrix} \tag{32}$$

Other values for the matrices R and Q were tested to find a controller that tracked the reference with a small error. Decreasing the value of R induced high frequency oscillations is the estimated velocity. Decreasing the value of $Q_{1,1}$ made the controller more sluggish but also had the controller output a smaller control signal. Increasing $Q_{1,1}$ doesn't make the controller track any better, but does produce a larger control signal. Increasing $Q_{2,2}$ appears to filter out the high frequency components of the

control signal, so when high frequency movement of the system is required, the controller is sluggish to respond. In the end, the values for R and Q stated above were found to produced adequate tracking of the reference.

The Matlab simulation predicts that this controller tracks the reference closely. Unfortunately when this controller was applied to the real system, the controller did not work. The controller gains were insufficient in overcoming static friction. The gains were increased to the point of overcoming static friction, but it also made the controller unstable. The actuator to oscillate at high speed ramming into the ends of its stroke. The actuator would be quickly powered off to prevent it from damaging itself. This resulted in no useful measurements being collected with this controller on the real pump setup.

The non-linear friction dynamics is the source of the problem for this controller. Since the desired reference oscillates through zero velocity where friction forces are highly non-linear, this linear controller fails to track properly. This problem with non-linear friction will be addressed further in Chapter 4.

3.5 Control Hardware

The controller is implemented using a National Instruments cRIO-9074. It is a chassis with an embedded real-time processor and a reconfigurable field-programmable gate array (FPGA) along with 8 regular National Instrument module slots. This was used because it is meant for real-time deterministic applications and a chassis was available within the department. A digital signal processor was considered for the controller. The difficulty in learning how to program it combined with the high cost of the integrated development environment software is why it was not used. Programming the cRIO was challenging because it is significantly different than the more popular compact DAQ that the rest of the department uses. National instruments offers an online course in programming the cRIO that was useful for learning how to program and more importantly communicate and record data with the cRIO.

A NI 9505 full H-bridge brushed DC servo drive module is used to drive the linear actuator. This was the only brushed motor drive available from National Instruments and only functions with the cRIO chassis. The NI 9505 has an encoder connection for position and velocity feedback. The linear encoder used is from BEI Technologies

with $0.5\mu m$ resolution. This encoder was used because it was available. A NI 9402 LVTTL digital I/O module is used to control a MD10C motor driver that powers the directional control valve. The MD10C was used for its high current capacity, and because it was available. The maximum rate of the control loop is determined by its complexity because a more calculation intensive controller will require more time to execute. The FPGA is configured to read the encoder, generate a 20kHz pulse width modulated (PWM) signal for the actuator, and output two digital lines to the MD10C motor driver. Since the controller is running on the cRIO-9074 itself, a desktop computer is a requirement for it to run.

3.6 Voice Coil Linear Actuator

The commercial voice coil is the NCM30-25-090-2LB model from H2W Technologies that was purchased prior to the start of this work. Like most DC brushed motors, it is controlled with a PWM signal. Outputting a PWM signal with the NI 9505 module is a bit complicated. The PWM functionality is not built into the module, so the PWM signal needs to be created programmatically. The PWM signal needs to operate at 20kHz and the FPGA clock is 40MHz. So dividing the clock frequency by the PWM frequency tells how many clock ticks the period of the the PWM is (40MHz $\div$ 20kHz = 2000 ticks). The way the FPGA is programmed to interact with the NI 9505 H-bridge module means that if the PWM signal is high for 2000 duty cycle ticks that corresponds to the motor being fully powered (100% duty cycle). Figure 3.5 shows the block diagram used to program the FPGA to generate a PWM signal at the desired duty cycle at 20kHz. The top control structure in Figure 3.5 takes the specified duty cycle in ticks as an input and does some numerical manipulation before passing it on to the bottom control structure. The bottom control structure is a timed loop and uses the 40MHz FPGA clock for accurate time keeping. This is the loop that counts the number of ticks to keep the signal high and low to generate the specified duty cycle at 20kHz. The outputs to the NI 9505 are a simple direction and on/off signal. The on/off signal is where the PWM signal is being output.

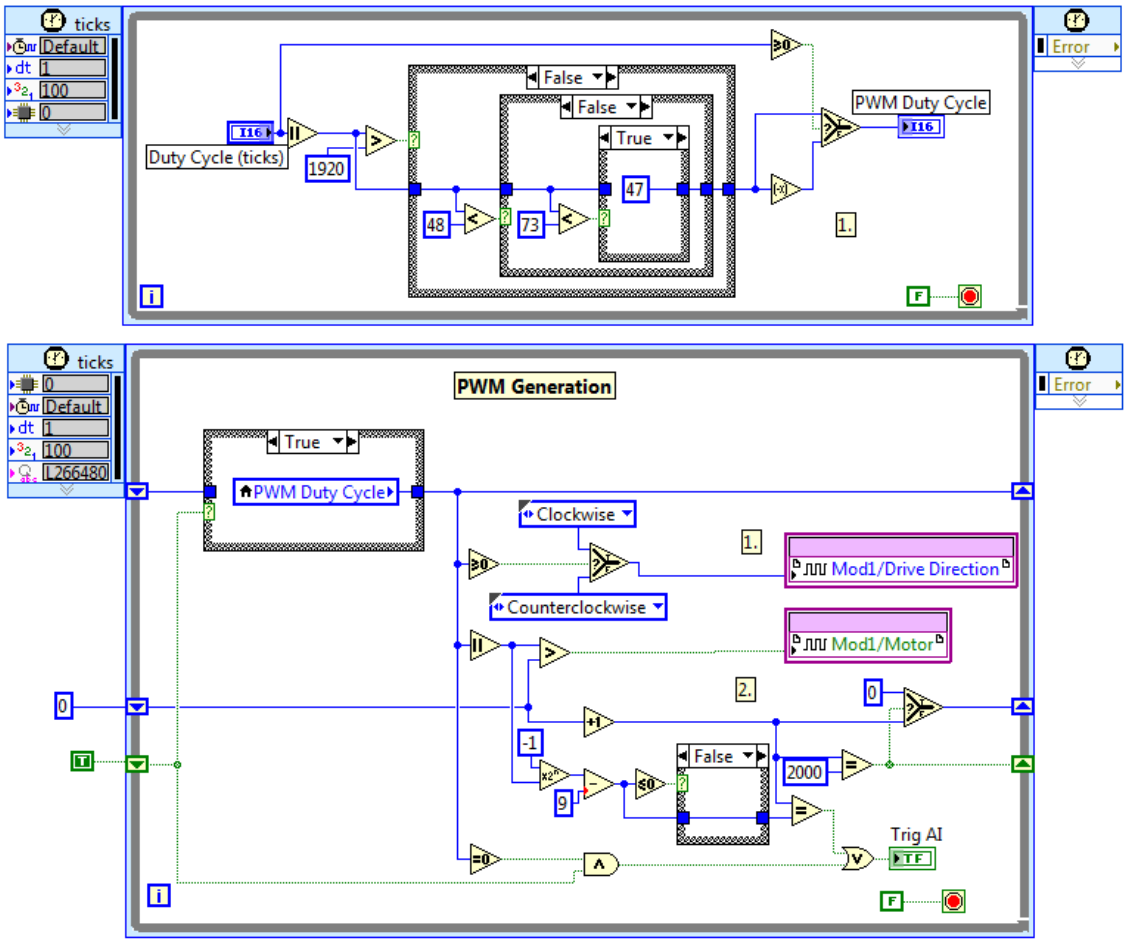

Figure 3.5: Control structure for PWM generation from the FPGA main virtual interface

This is actually a relatively simple block diagram. Figure 3.5 serves as an example of what the Labview code looks like, and why the more complicated algorithms will not be included in figures in this thesis.

When the control loop on the cRIO-9074 is executed it returns a force in Newtons that the actuator needs to output. In an effort to minimize any unit conversions or numerical manipulation, the force output of the actuator was directly measured using a spring scale over the full range of the motor controller. The range for the motor controller up to 300 ticks is measured using a 0 to 1 Lbf spring scale. Above 300 ticks is measured with a 0 to 10 Lbf spring scale. To maintain SI units for the controller, the force measurements are converted to Newtons. Figure 3.6 plots the measured force from the actuator over the duty cycle of the controller. The data starts at

200 ticks because below that value, the actuator can't overcome static friction so the spring scale reads zero.

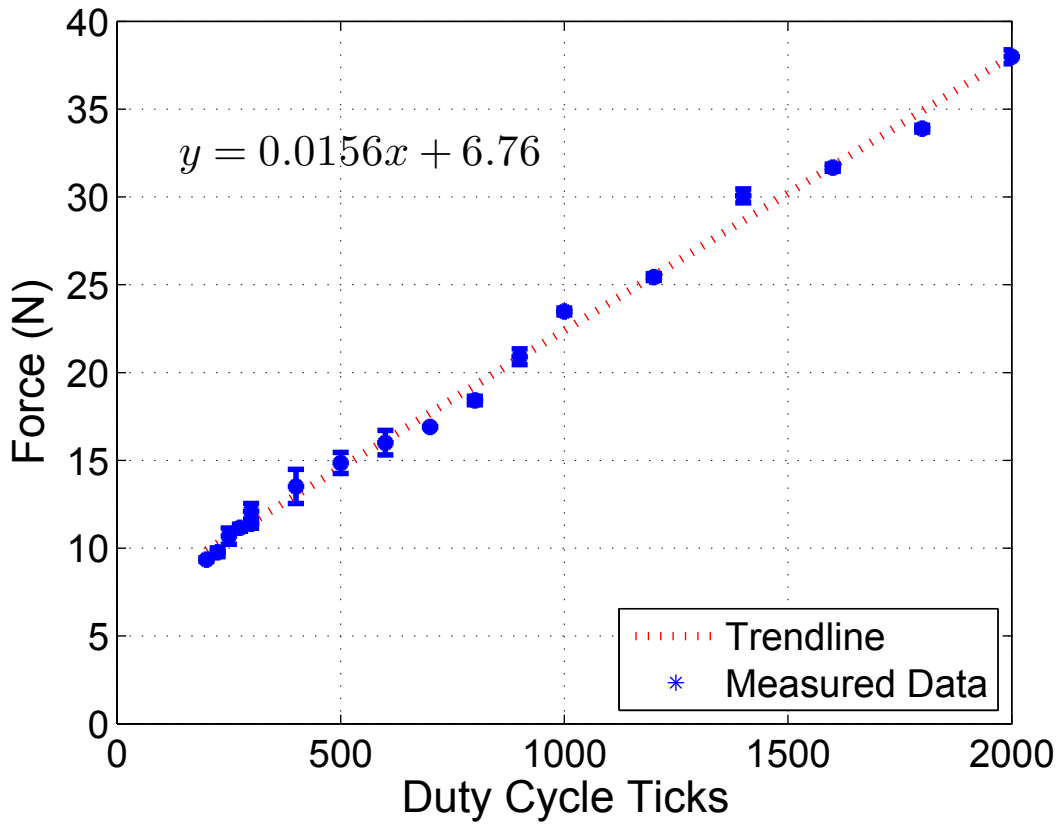

Figure 3.6: Actuator force

The trend line matches closely to the measured data ($R^2 = 0.995$). This is used to convert the force in Newtons required by the controller into ticks for the FPGA to output the correct PWM signal to the motor.

3.7 Valve

A commercial high pressure hydraulic valve had been considered, but the small orifice would likely restrict the flow too much for this low pressure application. Since the working fluid for this pump is water, corrosion of the hydraulic valve would also be of concern. The hydraulic valve was disassembled and its solenoid coil was reused in the custom valve. The reused solenoid coil can be seen on the right side of Figure 3.7.

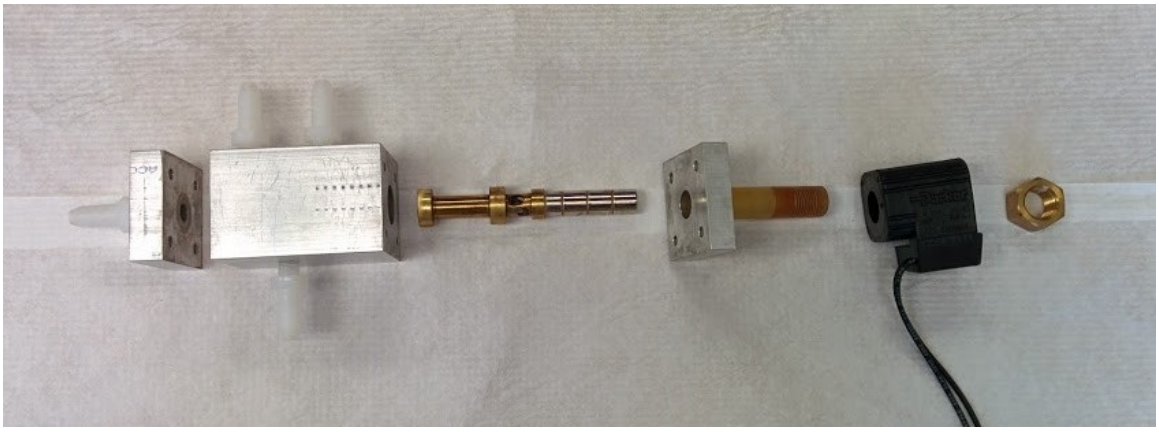

Figure 3.7: Exploded view of switching valve

A custom made two-position, four-way, directional control valve is used to switch between the two pistons on the pump. The valve serves to rectify the flow from the two pistons. Without the valve the fluid will oscillate back and forward with no net positive displacement. By having the valve switch between the two pistons after every pulse, flow is always going in the same direction in the test section. Figure 3.8 shows what two consecutive pulses in the test section look like with and without the use of the switching valve.

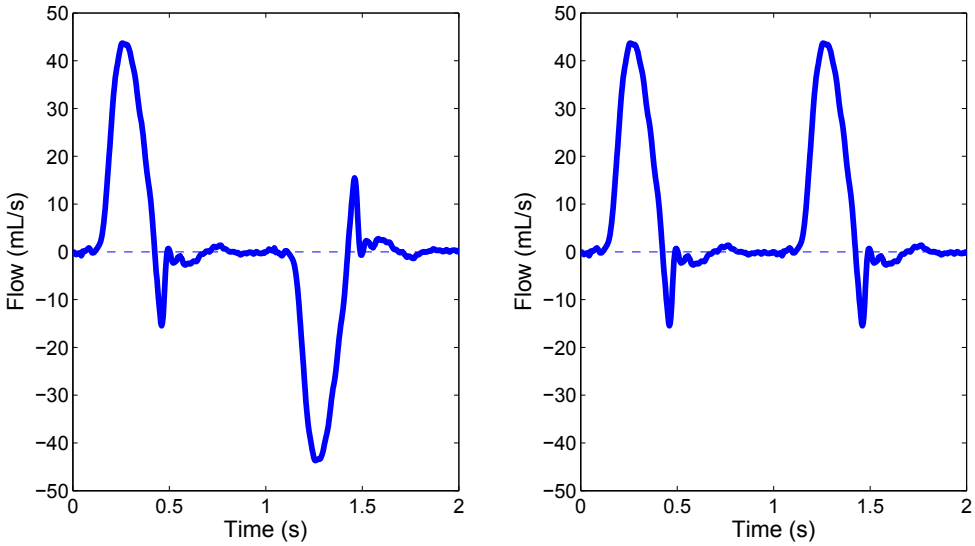

Figure 3.8: Example flow without switching valve is on left. Example flow with the switching valve on the right.

The valve was custom made to ensure the fluid is not restricted by any small

orifices. The valve spool has no seals and 0.002 inch clearance with the valve body. Fluid can move around the spool, but since the pump is operating at low pressure any leakage is neglected. The choice of aluminum for the valve body was not optimal as the bore corroded and sometimes made the spool stick in certain positions. Aluminum had been chosen because it is easy to machine. In the future the valve could be improved significantly by using brass for the body, and stainless steel for the spool.

3.8 Summary

This chapter discussed different components of the pump setup using a commercial voice coil actuator. The physical setup is similar to what is used by Holdsworth [17]. The pump setup described is used for testing and experimenting with the control system which will be discussed in the following chapter. The main components covered in this chapter were:

- Commercial actuator with attached pistons
- Custom made switching valve
- National Instruments hardware

Chapter 4

Control

4.1 Introduction

This chapter will discuss the control theory used to drive the pump. As mentioned in previous chapters, friction forces from the pistons make control difficult. To accurately track the desired reference waveform the controller needs to estimate the force of friction so it can compensate for it [1, 27, 28]. A lot of time was spent trying to implement different controllers with different friction compensation methods. The friction compensation model that worked the best was the LuGre friction model [10, 9, 53, 15, 29, 35, 37, 43, 47, 54].

It was not initially expected to be such a large part of the design of the pump, but ended up consuming the most amount time during the course of this project. Most other pumps use a stepper motor to drive pistons as stepper motors are relatively easy to control and have track a reference. Because a stepper motor moves in discrete steps, and as long as the motor is sized properly to the application, friction is not much of an issue for the control system. However, the voice coil type actuator used in this project does not operate in discrete steps. It operates with a force that is linearly proportional to the applied current. This fundamental aspect of its operation combined with the desired operating range that crosses through zero velocity makes controlling the pump difficult.

The LuGre model was thoroughly explained in an article from Wang and Wang [53] and the article was extensively used to help implement LuGre friction compensation with the pump. They explain how to implement an observer, as well as identify parameters for the LuGre friction model. This chapter will discuss the implementation of friction compensation with the LuGre model, adding an observer, and the identification of parameters.

4.2 Control with Friction Compensation

The LuGre model treats friction as the deflection of bristles between the surfaces. Think of is as though there are two brushes being rubbed against each other. An internal state z is used to capture the average behavior of these bristles [53]. With the LuGre model friction force is calculated as:

$$F = \sigma_0 z + \sigma_1 \dot{z} + \sigma_2 \dot{x} \tag{33}$$

$$\dot{z} = \dot{x} - \frac{|\dot{x}|}{g(\dot{x})} z \tag{34}$$

$$g(\dot{x}) = f_c + (f_s - f_c) e^{-(\dot{x}/v_s)^2} \tag{35}$$

In all the equations throughout this chapter, x is position, $\dot{x}$ is velocity, and $\ddot{x}$ is acceleration. The term z is the average deflection of the bristles from the model. Following from that, $\dot{z}$ is the rate of change of the deflection of the bristles.

Looking at Equation (33), the parameter σ_2 is the viscous friction coefficient. The other two terms in Equation (33), $\sigma_0 z$ and $\sigma_1 \dot{z}$, capture the frictional forces caused by these imaginary bristles. The coefficients σ_0 and σ_1 are dynamic friction parameters and represent viscous stiffness and damping respectively. Equation (34) defines the state z in relation to the velocity $\dot{x}$. Equation (35) contains the more common friction coefficients such as f_c for coulomb friction, f_s for stiction friction, and v_s for the Stribeck effect. There is a coupling effect between these parameters [53] which makes identification for some of them difficult. The internal state z will also need to be estimated as it does not exist physically and is a construct of the LuGre model.

Wang and Wang[53] have F estimated as:

$$\hat{F} = \sigma_0 \hat{z}_0 + \sigma_1 \left[\dot{x} - \frac{|\dot{x}|}{g(\dot{x})} \hat{z}_1 \right] + \sigma_2 \dot{x} \tag{36}$$

$$\dot{\hat{z}} = \dot{x} - \frac{|\dot{x}|}{g(\dot{x})} \hat{z} + \eta_z \tau_z \tag{37}$$

Initially the $\eta_z \tau_z$ term was left out of the controller because it was difficult to tune the parameters such that the system would not become unstable. The most common

problem was that the estimated friction force increased exponentially in one direction and drove the actuator to the end of its stroke and held it there with the motor 100% powered. A common problem with the LuGre model and the implementation of an observer for the state z, is that at high velocity above some critical value, the controller becomes unstable. Wang and Wang [53] proposed using discontinuous mapping and a smooth transfer function with a modified dual observer to estimate the state z. Their equations for estimating z are:

$$\dot{\hat{z}}_0 = \mathbf{Map}\left[\dot{x} - \frac{|\dot{x}|}{g(\dot{x})}\hat{z}_0 - \eta_{z_0} r\right] \tag{38}$$

$$\dot{\hat{z}}_1 = \mathbf{Map}\left[\dot{x} - \frac{|\dot{x}|}{g(\dot{x})}\hat{z}_1 + \eta_{z_1}\frac{|\dot{x}|}{g(\dot{x})} r\right] \tag{39}$$

$\dot{\hat{z}}_0$ and $\dot{\hat{z}}_1$ are the two estimates of z. The discontinuous mapping function from Wang and Wang [53] $\mathbf{Map}\langle\bullet\rangle$ is defined as:

$$\mathbf{Map}\langle\bullet\rangle = \begin{cases} 0 & if\ \hat{z}_0,\ \hat{z}_1 = z_{max}\ and\ \bullet\ > 0 \\ 0 & if\ \hat{z}_0,\ \hat{z}_1 = z_{min}\ and\ \bullet\ < 0 \\ s\left(\dot{x}\right)\bullet & otherwise \end{cases} \tag{40}$$

with $z_{max} = f_s/\sigma_0$ and $z_{min} = -f_s/\sigma_0$. The $s\left(\dot{x}\right)$ function is a smooth transfer function defined as [53]:

$$s\left(\dot{x}\right) = \begin{cases} 1 & |\dot{x}| < \nu_1 \\ \frac{1}{2}cos\left[\frac{\pi|\dot{x}|\nu_1}{\nu_2-\nu_1}\right] + \frac{1}{2} & \nu_1 \leq |\dot{x}| \leq \nu_2 \\ 0 & |\dot{x}| > \nu_2 \end{cases} \tag{41}$$

with $\nu_2 > \nu_1 > 0$ where ν_2 and ν_1 are transfer velocities arbitrarily selected based on characteristics of the system being controlled. What this observer does is to stop updating its estimation of the internal state z when the velocity is high. This is supposed to stop the system from becoming unstable when above the high velocity threshold.

The control law proposed by Wang and Wang [53] is:

$$u = -k_s(\dot{x} - \dot{x_r} + k_r(x - x_r)) + \hat{\sigma_0}\hat{z}_0 + \hat{\sigma_1}\left[\dot{x} - \frac{|\dot{x}|}{g(\dot{x})}\hat{z}_1\right] + \hat{\sigma_2}\dot{x} + \hat{d} + \hat{m}\ddot{x_r} \tag{42}$$

The parameters $x_r,\ \dot{x_r},\ \ddot{x_r}$ are the known continuous position, velocity and acceleration references to be tracked. Initial values for the friction parameters $\sigma_0,\ \sigma_1,\ \sigma_2$ can be identified through experiment. However, these parameters will vary when the system is being controlled. To make the controller more robust, the friction parameters $\sigma_0,\ \sigma_1,\ \sigma_2$, along with the mass m, and disturbance d will start at their identified values and then be continuously updated. Each parameter will be update by the following equations [53]:

$$\dot{\hat{\sigma}}_0 = -\eta_0 \hat{z}_0 r \tag{43}$$

$$\dot{\hat{\sigma}}_1 = -\eta_1 \left[\dot{x} - \frac{|\dot{x}|}{g(\dot{x})} \hat{z}_1 \right] r \tag{44}$$

$$\dot{\hat{\sigma}}_2 = -\eta_2 \dot{x} r \tag{45}$$

$$\dot{\hat{m}} = -\eta_m \ddot{x_r} r \tag{46}$$

$$\dot{\hat{d}} = -\eta_d r \tag{47}$$

Common between all of these equations is the filtered tracking error r. The term r is given by:

$$r = \dot{x} - \dot{x_r} + k_r \left(x - x_r \right) \tag{48}$$

Within r is the error between the reference profile and the measured profile. If r is small and close to zero, than that means the pump is tracking the reference profile very well. This should keep the parameters stable once they reach values that accurately track the reference.

To keep the first attempt at designing a controller as basic as possible, the parameters $\dot{\hat{\sigma}}_0$, $\dot{\hat{\sigma}}_1$, $\dot{\hat{\sigma}}_2$, $\dot{\hat{m}}$, and $\dot{\hat{d}}$ were not continuously updated. This actually means that the disturbance estimation term $\hat{d}$ was not include in the controller at all. For the first controller that was implemented the modified dual observer from Equations (38) and (39) was excluded to try to limit the number of different coefficients and parameters that would need to be tuned. To estimate z Equation (49) was used. This is different

that what was shown in Equation (37) because the $\eta_z \tau_z$ term is removed. As mentioned earlier when trying to implement the controller with an observer, the observer would often become unstable and exponentially increase the estimated friction force. Removing the $\eta_z \tau_z$ term stopped the observer from becoming unstable.

$$\dot{\hat{z}} = \dot{x} - \frac{|\dot{x}|}{g(\dot{x})}\hat{z} \tag{49}$$

As a result of all the changes to simplify the controller for the first attempt at controlling the pump with friction compensation, the controller [13] that was actually used for testing is:

$$u = -m(k_d(\dot{x} - \dot{x_r}) + k_p(x - x_r)) + \sigma_0 \hat{z} + \sigma_1 \left[\dot{x} - \frac{|\dot{x}|}{g(\dot{x})}\hat{z}\right] + \sigma_2 \dot{x} + m\ddot{x}_r \tag{50}$$

The parameter m is the total mass of all the moving parts to the pump combined into one term. The controller is actually very similar to the controller in Equation (42). The coefficients k_d and k_p are controller gains that tuned with iterative testing. The estimation of $\hat{z}$ was done differently than what was proposed in the paper by Wang and Wang in that there was no discontinuous mapping, no observer gain η_z used, and no continuous updating of $\dot{\hat{\sigma}}_0$, $\dot{\hat{\sigma}}_1$, $\dot{\hat{\sigma}}_2$, $\dot{\hat{m}}$, and $\dot{\hat{d}}$.

4.3 Identification of Parameters

To accurately control the system, the parameters of the model must be properly identified [22]. The methods for identifying the static and dynamic friction parameters are thoroughly explained by Wang and Wang [53]. The static parameters f_c, f_s, σ_2, and v_s are the first to identify. The simple system is defined by the equation:

$$m\ddot{x} + F = u \tag{51}$$

Where m is the moving mass of the system, F is the nonlinear friction of the system, and u is the input from the controller. A simple PI controller is used to run constant velocity experiments to map the friction-velocity relation. When moving at a constant velocity $\ddot{x} = 0$ and friction is at a steady state value. With $\ddot{x} = 0$ Equation (51) simplifies to $F = u$ and the steady state friction force is balanced with the input

force. Expanding F out into all of its components yields the equation for steady state friction as:

$$f_{ss} = [f_c + (f_s - f_c)e^{-(\dot{x}/v_s)^2}]sgn(\dot{x}) + \sigma_2\dot{x} \tag{52}$$

The controller input u is being recorded, so f_{ss} is known. By using the PI controller over a range of constant velocities, the friction curve can be identified. Figure 4.1 shows the friction curve over the operating range of the pump. Each point on Figure 4.1 is a separate constant velocity experiment.

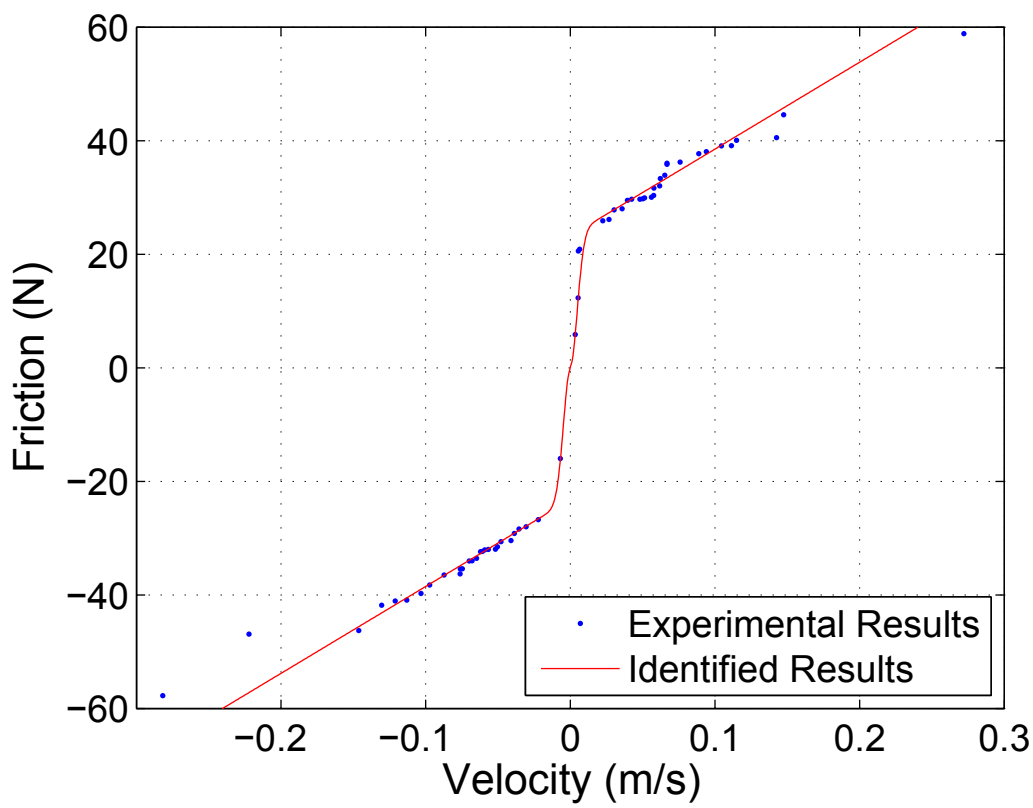

Figure 4.1: Identification results for friction curve

To find the best solution, a novel evolutionary algorithm (NEA) [53] was used to try finding that values for parameters f_c, f_s, σ_2, and v_s that best fit the experimental results. Keeping all initial conditions for the evolutionary algorithm the same, the values that the algorithm found varied greatly for the parameters f_c and v_s. Parameters f_s and σ_2 varied a little, but maintained a consistent order of magnitude.

Table 4.1 shows the parameters that were identified in 3 different iterations of the NEA algorithm. The Matlab curve fitting toolbox was also used to identify the 4 parameters based on Equation (52).

Table 4.1: NEA Parameter identification results

Identification Run	**Friction Parameter**			
	f_c (N)	f_s (N)	σ_2 $\left(\frac{\text{Ns}}{\text{m}}\right)$	v_s $\left(\frac{\text{m}}{\text{s}}\right)$
NEA 1	130450	21.6	160.6	-935
NEA 2	6342	22.1	152.2	-455
NEA 3	30941	21.2	162.9	-1669
MATLAB Toolbox	23.2	0.26	153.0	-0.0067

The σ_2 parameter had little variation over the different identification runs, so the confidence in that consistency of that value is high. The f_s parameter was consistent between the NEA runs. It is intriguing that the f_c term identified by Matlab is close to the f_s value from the NEA runs. This is likely related to the value of v_s and how each method tried to best fit the curve.

The NEA method produces values for v_s that seem unrealistic. Applying the v_s values only to the exponential term of Equation (52) over the full range of velocities show that it is effectively converged to 1 for all values of $\dot{x}$. With the exponential component of Equation (52) converged to 1 over the full range of the pump Equation (52) looks like:

$$f_{ss} = [f_c + (f_s - f_c)[1]]sgn(\dot{x}) + \sigma_2\dot{x} \tag{53}$$

Looking at the f_c and f_s terms in Equation (53) shows that the f_c terms will now cancel out. This basically means that the f_c terms does not matter when the v_s value is large. Since the NEA method always identified large v_s values, it never converged on values for f_c as they always canceled out when trying to fit the equation. So the v_s values from the NEA method is not accurate. The value for v_s that Matlab identified is actually a reasonable solution. The exponential term decays from 1 to 0 within about $0.03m/s$.

Since the Matlab toolbox seems to have identified more accurate parameters, these

were the ones that were used with the controller. Figure 4.1 was plotted with the Matlab parameters used to create the identified curve.

The remaining two parameter σ_0 and σ_1 are identified with open loop experiments with slow ramp input torque. The detailed procedure for this experiment is outlined by Wang and Wang [53]. The experiment involves slowly ramping up the input force and recording position, velocity and input force. The the data is then used with the NEA method to identify optimal parameters. Table 4.2 contains the values for the identified parameters for several runs with the NEA method.

Table 4.2: Ramp Input NEA Results

Identification Run	**Friction Parameter**	
	σ_0 $\left(\frac{\mathrm{N}}{\mathrm{m}}\right)$	σ_1 $\left(\frac{\mathrm{Ns}}{\mathrm{m}}\right)$
Ramp NEA 1	1 887 700	4096
Ramp NEA 2	1 397 900	2048
Ramp NEA 3	1 383 800	2496
Ramp NEA 4	1 577 600	2520

The parameters identified are fairly consistent, at least in terms of magnitude. Looking at the units shows that σ_0 has units of stiffness, and σ_1 has units similar to a coefficient of viscous friction. Remembering that the LuGre model treats friction as the average deflection of bristles, it makes sense that the parameter σ_0 would have units the same as a coefficient of stiffness. In equation 33 σ_0 is multiplied by the deflection z which equals a force. Similarly σ_1 is multiplied by a rate of deflection, which also equals a force. These parameters are trying to model a behavior that isn't actually physical, so it's hard to be certain if the values of the parameters are realistic. The best way to find out is by testing them with the controller on the physical setup.

4.4 Parameter Tuning

Now that initial values for the parameters have been identified, they can be used with the controller from Equation (50). Table 4.3 shows some sample values for the parameters that were used during the tuning of the pump.

Table 4.3: Friction and control parameters used for iterative testing

Set	σ_0 $\left(\frac{\mathrm{N}}{\mathrm{m}}\right)$	σ_1 $\left(\frac{\mathrm{Ns}}{\mathrm{m}}\right)$	σ_2 $\left(\frac{\mathrm{Ns}}{\mathrm{m}}\right)$	f_c (N)	f_s (N)	v_s $\left(\frac{\mathrm{m}}{\mathrm{s}}\right)$	m (kg)	k_d $(-)$	k_p $(-)$	**Comments**
1	$1.9{\cdot}10^6$	4096	153	23.2	0.26	-0.0067	5	1	1	Unstable
2	30	200	152	22.5	21.2	0.015	5	75	750	Undershoot
3	30	100	152	21	23	0.1	5	75	750	Undershoot
4	30	100	152	21	23	0.1	12	75	750	Good
5	80	200	152	21	23	0.1	12	25	750	Validation

To make tuning easier, Equation (50) was broken down into 6 terms and their values are monitored while the pump is in operation. The 6 terms were:

- $-m(k_d(\dot{x} - \dot{x_r}))$
- $-m(k_p(x - x_r))$
- $\sigma_0 \hat{z}$
- $\sigma_1 \left[\dot{x} - \frac{|\dot{x}|}{g(\dot{x})}\hat{z}\right]$
- $\sigma_2 \dot{x}$
- $m\ddot{x_r}$

Observing each of the terms made possible to see which specific terms were causing the controller to become unstable. When one term was observed to be unstable, the parameter associated with it could be increased or decreased to improve performance of the controller. The first set of parameters in Table 4.3 used the identified values to control the pump. That set of parameters made the controller unstable in that that estimated force of friction increased exponentially. By monitoring the individual terms of the controller it was observed that the instability mostly caused by the large value of σ_0. After a many iterations of reducing the value of σ_0 and changing a few of the other parameters, a stable set of values was found. Those values are shown as set 2. Set 2 undershoots the reference quite a bit, but was otherwise stable. The pump was allowed to run for at least 1 minute to make sure it would stay stable and that no terms would slowly grow and eventually become unstable.

The parameters continued to be changed to try to get better tracking of the reference waveform. The term that played a big role in the matching of the reference was actually the inertial mass of the system m. The parameter m change from set 3 to set 4 by 240%. However, there were many incremental steps to get from set 3 to 4. Figure 4.2 shows the average of 10 pulses produced using the parameter values from set 4.

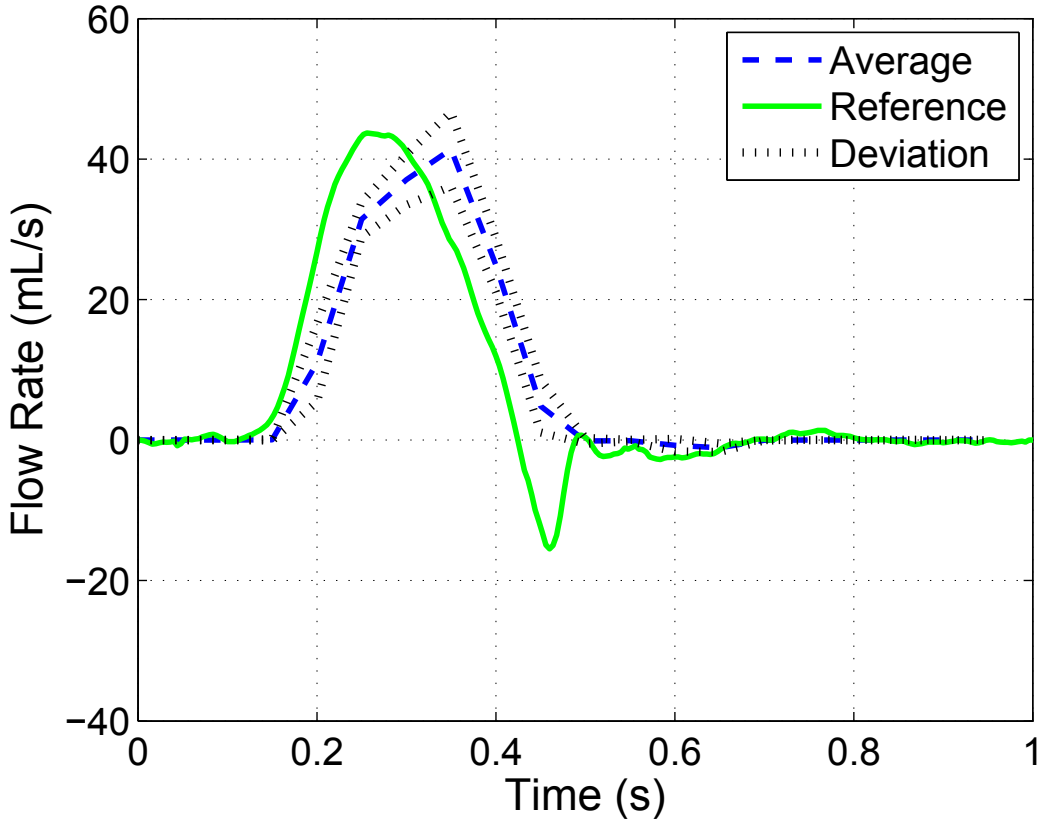

Figure 4.2: Average of 10 pulses produced using the parameter values from set 4 in Table 4.3

Figure 4.2 was a good result in that the peak flow measured was within about 10% of the reference waveform peak. Unfortunately it did not track the negative flow peak closely. More iterative tuning was done to get to parameter set 5 from Table 4.3. Parameter set 5 tracked the reference well enough that those parameters were used to control the pump when taking particle image velocimetry (PIV) measurements of the fluid. Chapter 5 will discuss the results from the PIV measurements.

4.5 Summary

This chapter discussed the implementation of friction compensation with the LuGre friction model, the use of a modified dual observer for state estimation, as well as the identification process for the friction parameters. The control system for this project was challenging and time consuming to figure out and try to implement properly. That having been said, it was still functional enough to test the pumps capabilities. The testing and validation of the pump will be discussed in the next chapter. The main point to remember from this chapter were:

- LuGre friction model for compensation
- Modified dual observer for state estimation
- Novel evolutionary algorithm for parameter identification
- Identified friction parameters through experiment
- Still requires trial and error for fine tuning parameters

Chapter 5

Validation

5.1 Introduction

To validate the control, parameter identification, and design of the pump, the measured flow should closely match the desired profile. The identified parameters were used as a starting point for the controller, and manually varied over many iterations in an effort to better track the desired waveform. An aorta waveform and femoral waveform were tested using particle image velocimetry (PIV) to measure the flow rate. This chapter will briefly explain the PIV measurement process, and then discuss the results.

5.2 Particle Image Velocimetry Results

A turbine flow meter was tried initially, but does not respond fast enough to measure the pulsatile flow. Additionally, the turbine type flow meter only measures flow in one direction. For theses reasons, particle image velocimetry (PIV) was used to measure the complex waveform created by the pump. The particle image velocimetry (PIV) measurement involves taking pairs of pictures with a high speed camera over time. Figure 5.1 shows a pair of images taken with the high speed camera at a rate of 4000 frames per second. The fluid, in this case water, is seeded with small glass spheres. A high powered laser is used to create a plane that is perpendicular to the camera and the middle of the clear rigid acrylic tube. The inside diameter of the tube is $10mm$ and is used as the reference scale when processing the images.

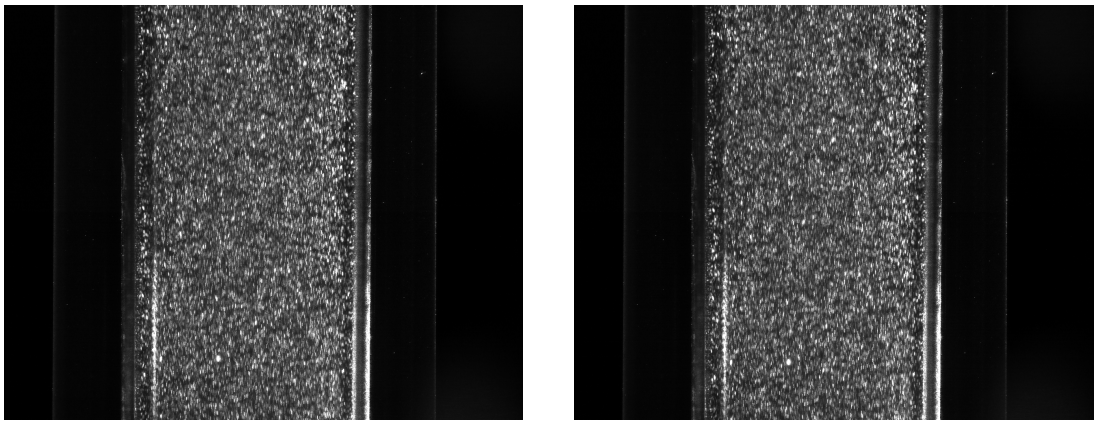

(a) PIV Frame 1 (b) PIV Frame 2

Figure 5.1: Pair of images taken at 4000fps

The open source Matlab program PIVLab is used to process the pairs of images. The programs measures the movement of the particles from one frame to the next at the known rate of 4000 frames per second to calculate the velocity of the fluid. Figure 5.2 shows the movement of the particles in the images from Figure 5.1 that is output by PIVLab.

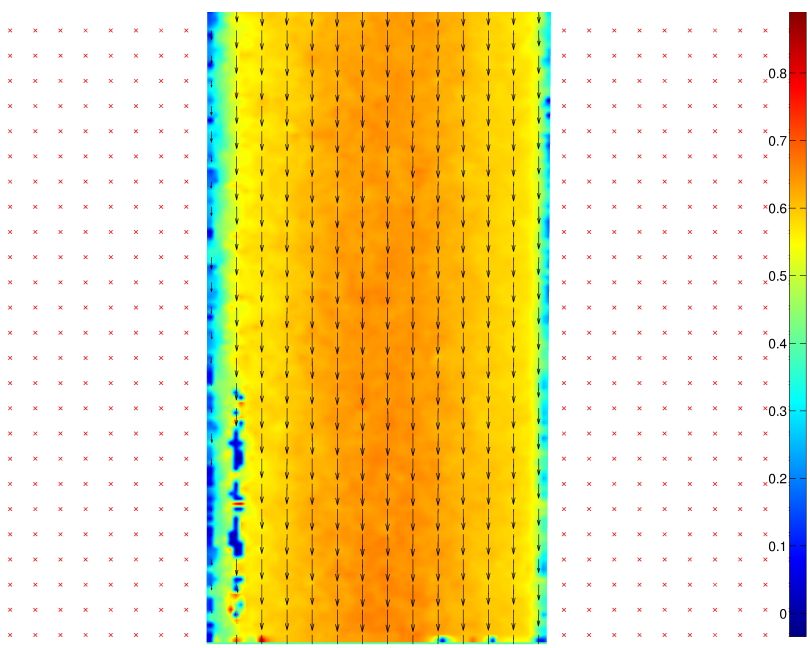

Figure 5.2: PIV Flow measurement results of water flowing in a 10mm tube. Color scale is m/s, with directional arrows scaled by magnitude of velocity

A cross section of the tube from Figure 5.2 is take to get the velocity across the

diameter as seen in figure 5.4. A revolution integral is applied to the cross section fluid velocity to calculate the average instantaneous volumetric flow rate. By capturing many pairs of images over time and processing as just described, the waveform being output by the pump is measured. This entire process is how the PIV measurements seen in Figure 5.5 and 5.7 were taken.

Figure 5.3 has 8 labeled points that correspond to the plots in Figure 5.4.

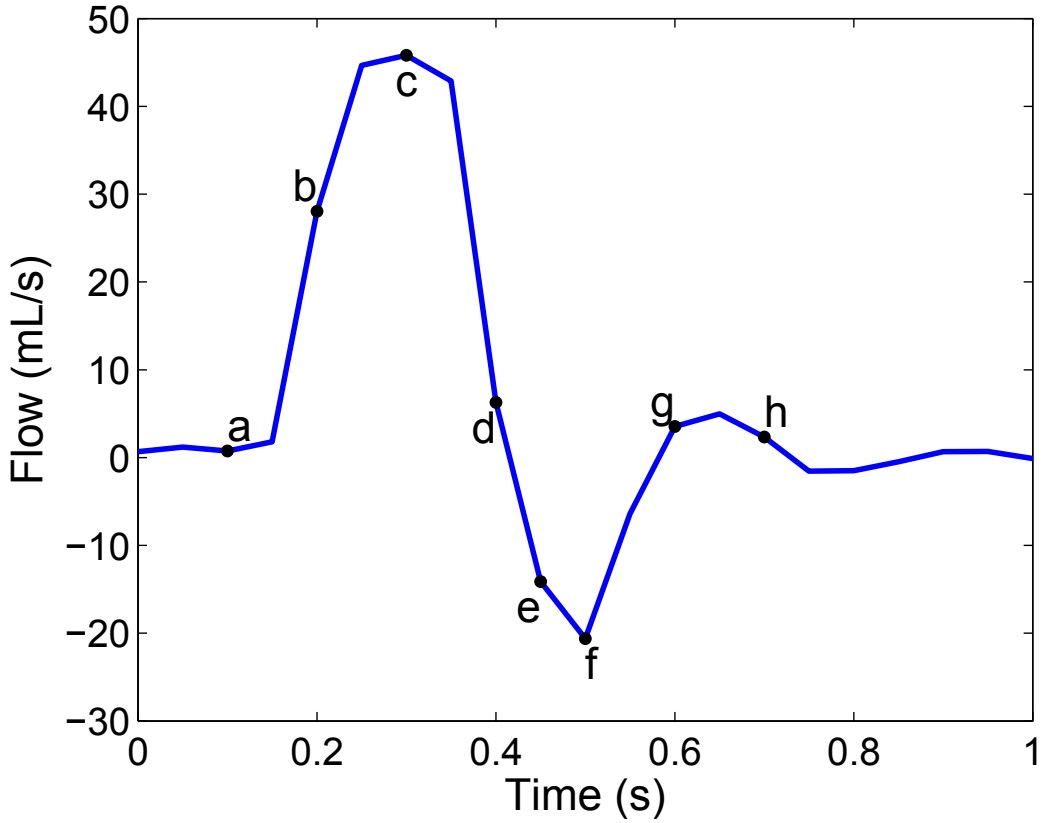

Figure 5.3: Single waveform with labeled points for cross section fluid velocity seen in Figure 5.4

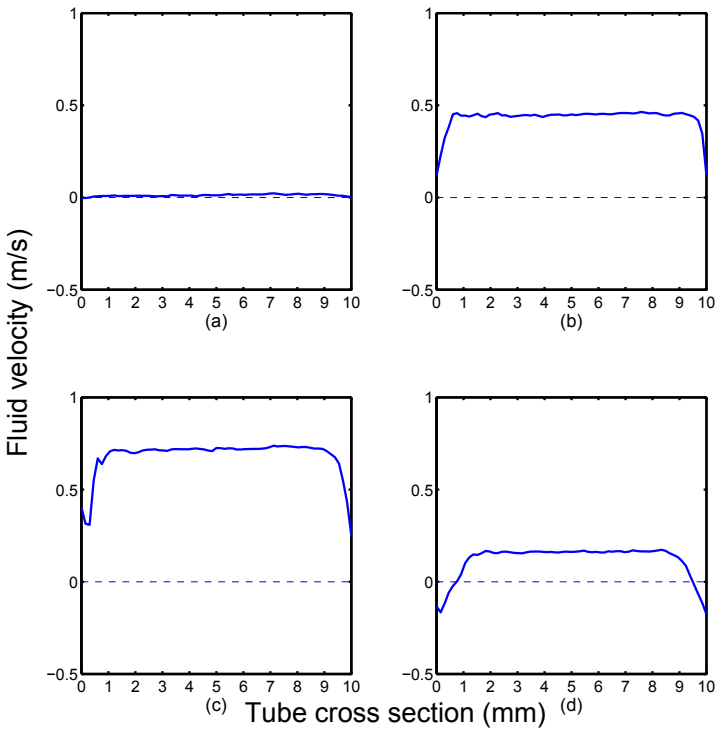

(a) points a, b, c, d from Figure 5.3

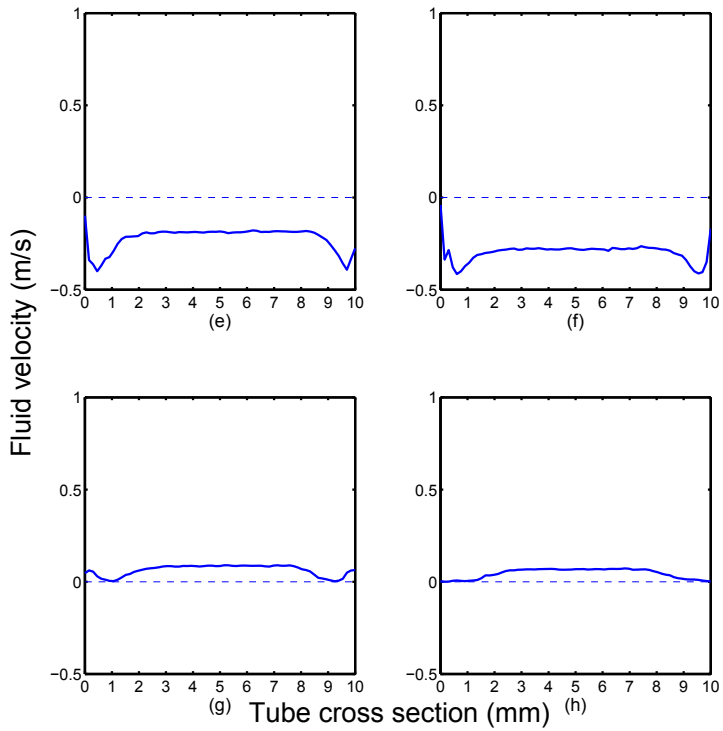

(b) Points e, f, g, h from Figure 5.3

Figure 5.4: Fluid velocity across tube diameter

Figure 5.5 shows the measured flow from the pump overlapped with the desired aorta waveform. PIV measurements were collected at 20 samples per second to measure the waveform being produced. For a 10 second test 400 images are captured and need to be processed.

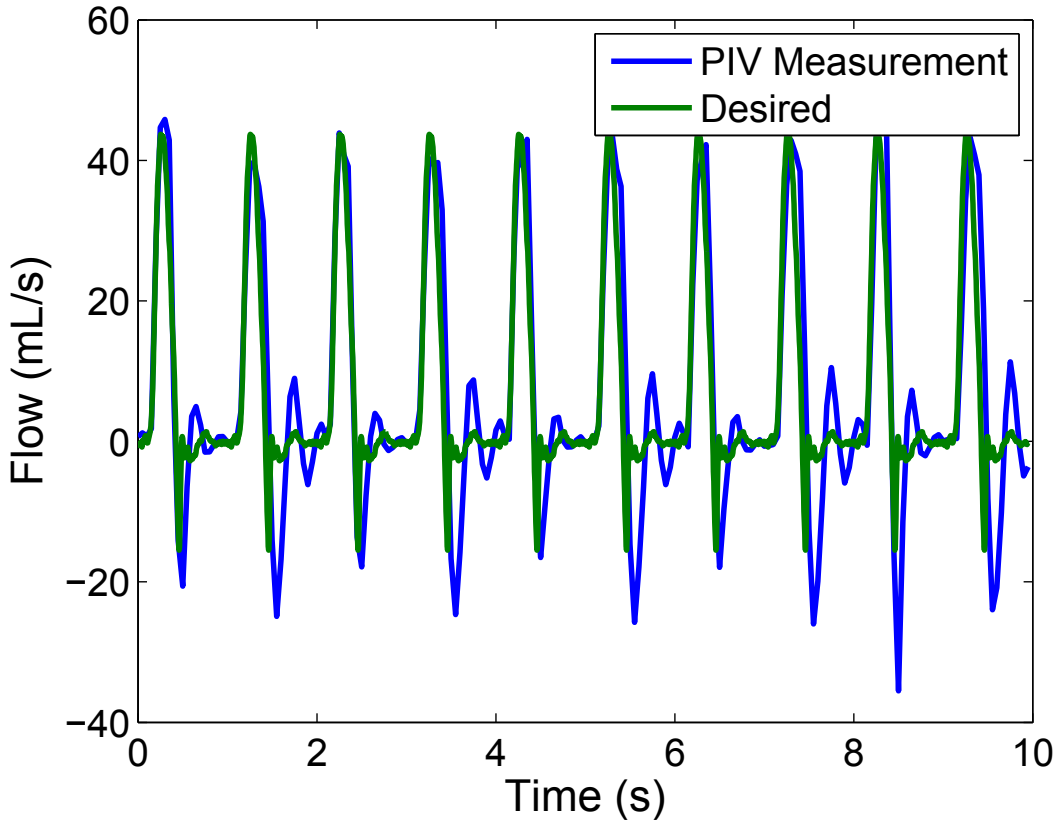

Figure 5.5: Flow measurement # 1

It is seen in Figure 5.5 that the measured flow overshoots the desired peak flow, and has oscillations in the flow near the zero flow regions. The measured oscillations can't really be damped out by the controller because it isn't directly receiving flow feedback. Figure 5.6 shows the 10 cycle average for the PIV flow measurement. The dashed lines in Figure 5.6 show the bounds of the standard deviation. While the rising edge of the pulse matches quite well, after the peak and during the change in flow direction pump lags behind the reference waveform. Tsai [51] also had results where their pump tracked the reference well during constant acceleration. While the general shape of the produced waveform is pulsatile, and could be used to approximate some

cardiovascular flow, its ability to accurately match the reference waveform is poor.

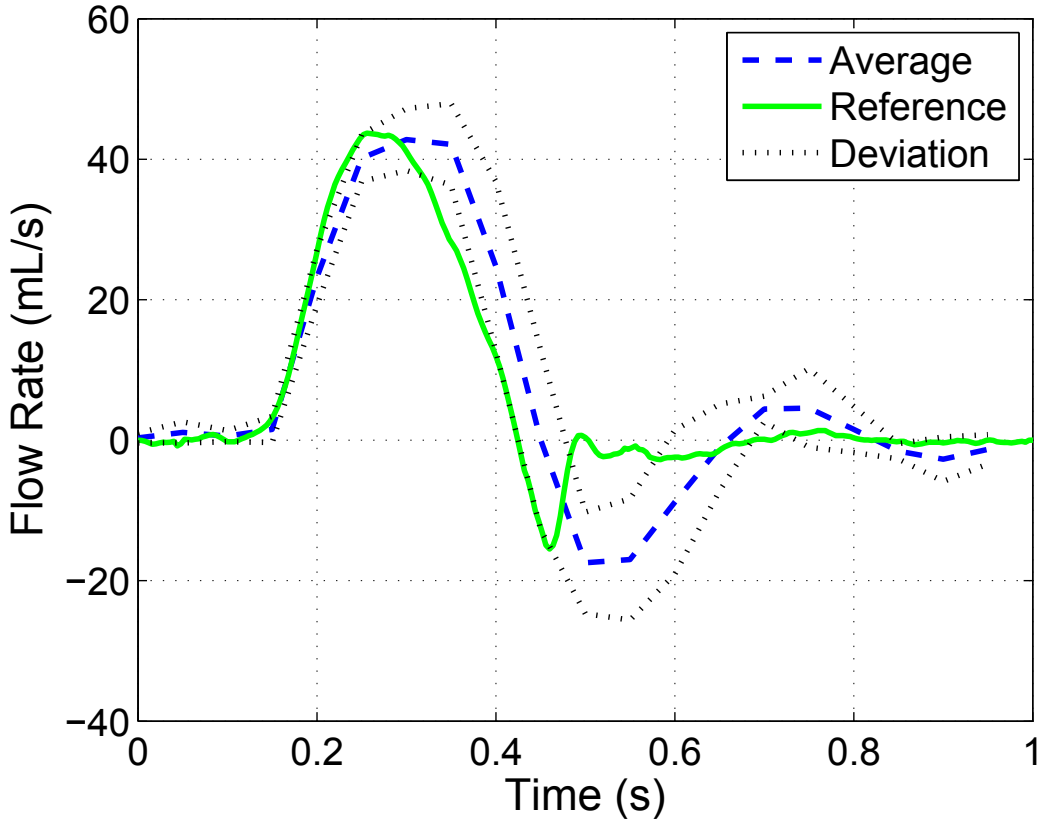

Figure 5.6: PIV measurement 10 cycle average

The other feedback worth analysing is the flow based on encoder measurements from the pump. The flow calculated based on the encoder measurements is shown in Figure 5.7 alongside the PIV measurements. When the encoder is near zero flow, the PIV measurement still records some small flow oscillations. These oscillations are likely caused by the compliance of the tubing that was used. Additionally, the inertia of the moving fluid also contributes to the oscillations when the pump should be at zero flow. It is not really possible for the controller to eliminate the oscillations since that would require in the loop flow feedback. This might be possible with ultrasonic flow measuring devices, but one was not available for use in this project.

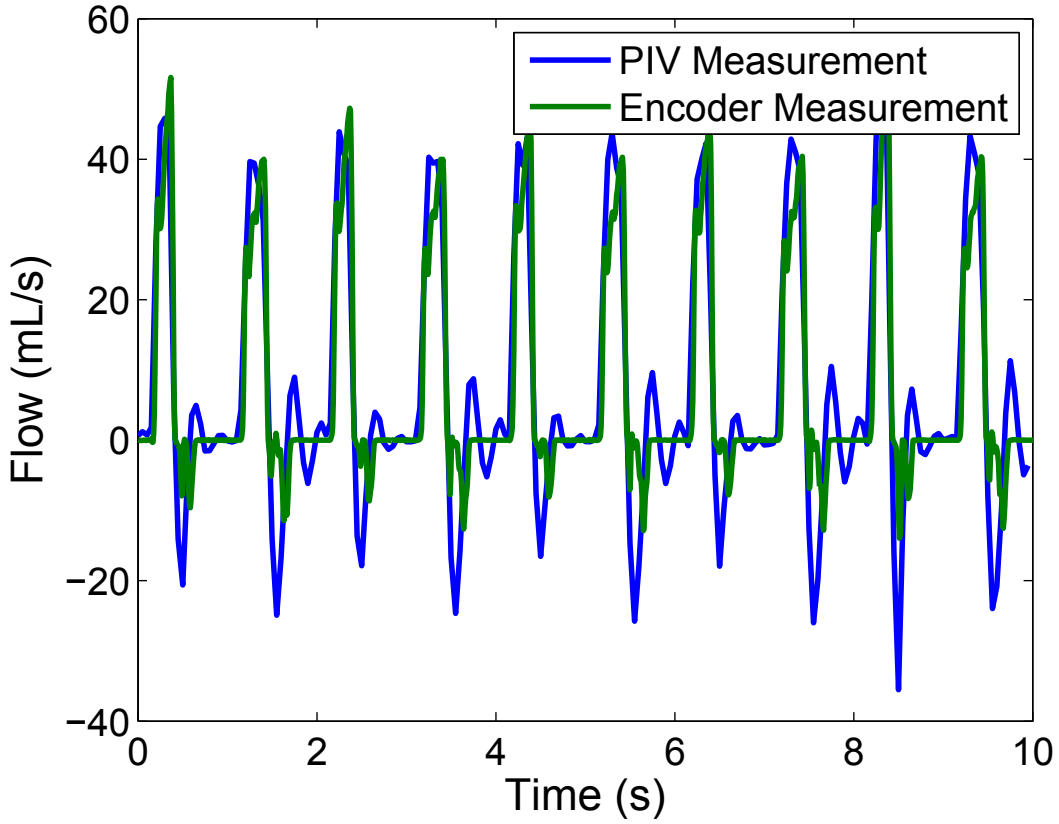

Figure 5.7: Flow measurement compared with encoder data

Figure 5.8 shows the average flow based on encoder feedback from the 10 cycles in Figure 5.7. Similar to what is seen in Figure 5.6, the encoder calculated flow lags behind the desired waveform. This seems to indicate that the pump is not outputting a strong enough signal during the flow reversal to dampen out both the flow and inertia of the pistons and actuator. Interestingly the encoder does not show a much negative flow like what is seen in Figure 5.6. This seems to mean that the negative flow in the PIV measurement is from the fluid oscillating due to the fluids inertia combined with the elastic nature of the tubing [19] and is not a result of the piston oscillating. More rigid tubing should probably be used in the future to try to reduce this source of error.

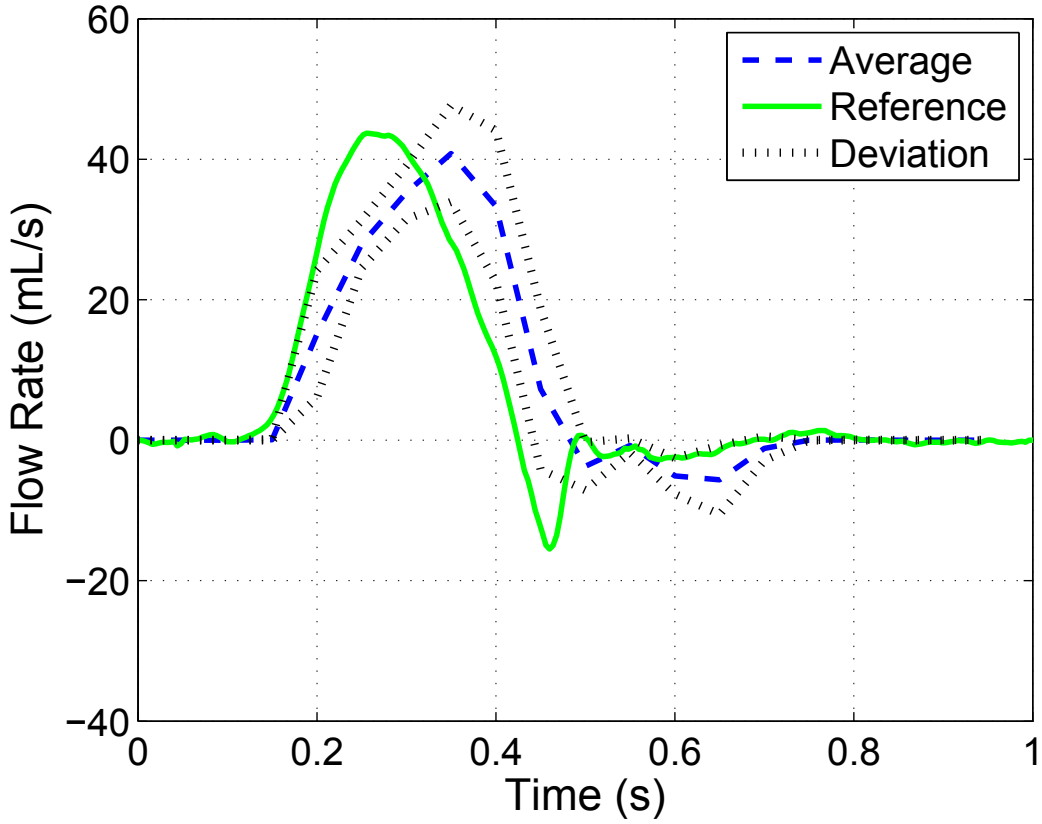

Figure 5.8: Encoder measurement 10 cycle average

Comparing the different measurements to the reference is useful, but so is comparing the two measurements to each other. Figure 5.9 shows the two flow measurements averaged over 10 cycles along with the standard deviation for each measurement method. Looking at the encoder measurement it can be seen that the PIV measurement is slow to respond to the pistons displacement. This is slow response can be attributed to fluid inertia.

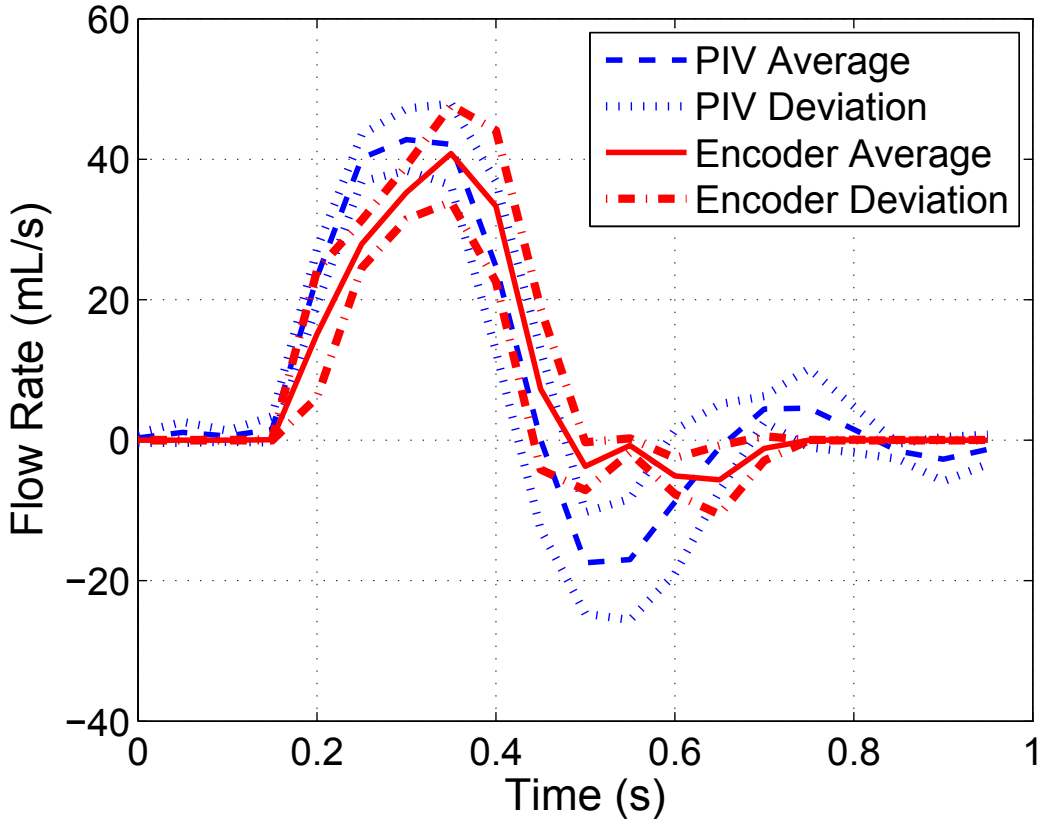

Figure 5.9: PIV and encoder measurement comparison

So the two measurements clearly do not agree well. This is not a good result as it means that the encoder cannot be relied on to accurately calculate the flow. This also means that using the encoder for feedback wont be accurate when trying to reproduce these kinds of pulsatile waveforms. This also means that using the encoder feedback to try and tune the pump to accurately match the reference probably wont produce a good match when measured with the PIV system.

A femoral waveform was also produced and measured to test the capabilities of the pump. The data for this waveform was collected by another member of the research group for their experiments [7]. Smaller pistons were used to produce this waveform. The pistons used were 0.438 inch in diameter. Additionally, the PIV measurement was taken differently for this waveform by having the pump run for 20 seconds instead of 10 seconds. To calculate the average waveform, every second pulse was counted towards the average. This still results in 10 pulses being included in the average, but its only 10 pulses produced from one piston of the pump, not both. In Figure 5.5 the

negative flow peaks measured are not the same from one pulse to the next. There is an alternating pattern of low and high in the negative peaks that increases the deviation when all the pulses are average together. By averaging every other pulse the deviation caused by the high and low peaks in the negative flow is reduced. What this also shows is that the flow produced by one single piston is consistent when only compared to itself. The likely cause of the low and high peaks in the negative flow region of the waveform is that the pistons have different flow paths through the valve. The slightly different flow paths through the valve causes more fluid resistance for one piston compared to the other, and this results in the low and high peaks observed in Figure 5.5.

Figure 5.10 show the PIV measurement compared to the reference waveform. The peak flow produced matches the peak of the reference waveforms. The general shape of the measured waveform is similar to the reference. It looks as if the 1 second reference waveform was squeezed into 0.7 seconds for the measured waveform.

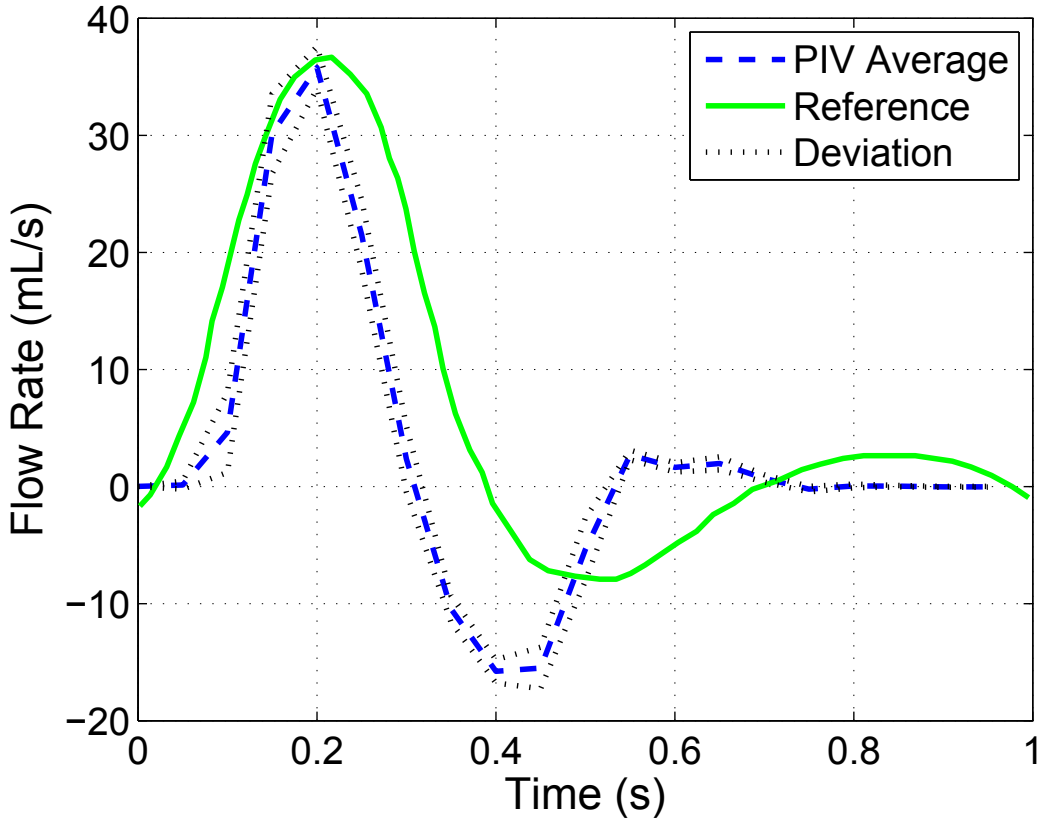

Figure 5.10: PIV measurement of femoral waveform [7]

Figure 5.11 shows the encoder data for the femoral waveform seen in Figure **??**. The encoder for this waveform significantly undershoots the peak flow of the reference. The general shape of the encoder measurement looks similar to the reference, but the scale is off significantly.

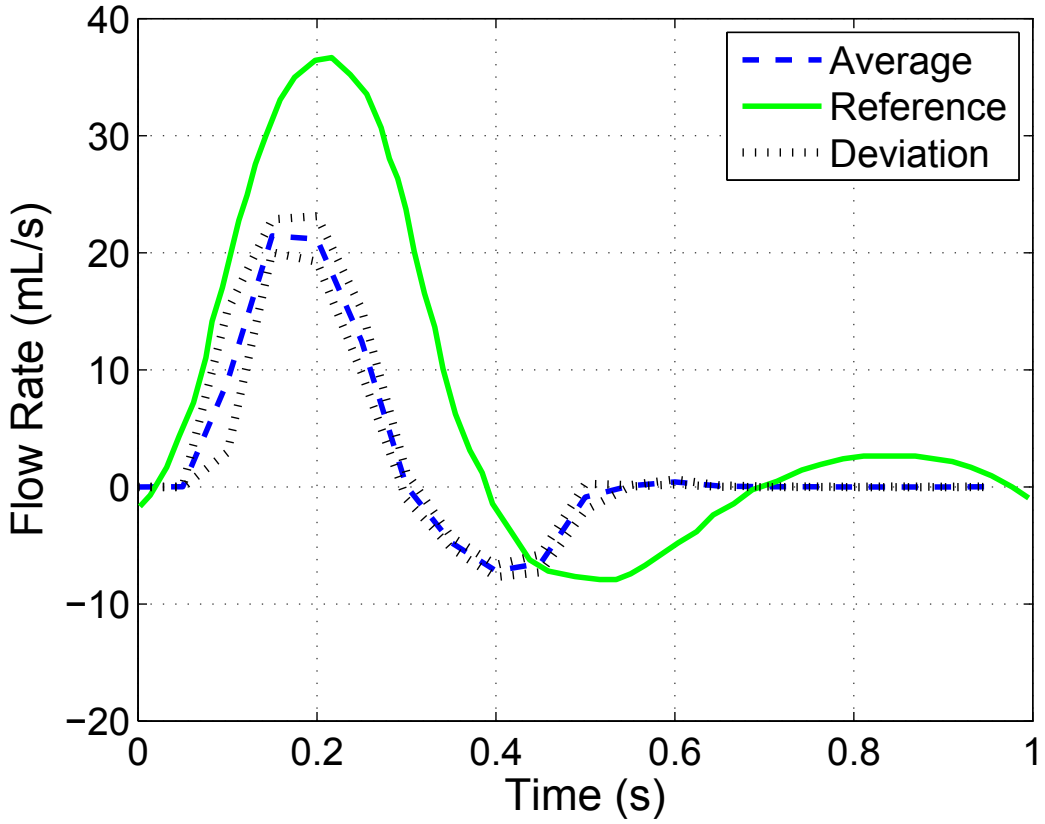

Figure 5.11: Encoder measurement of femoral waveform [7]

Again, comparing the two measurements to each other is useful. Figure 5.12 shows the two flow measurements averaged over 10 cycles along with the standard deviation for each measurement method. For this waveform the PIV flow greatly overshoots the encoder flow. Unfortunately there is not enough information to form a hypothesis for why this waveform overshoots the encoder measurement so much.

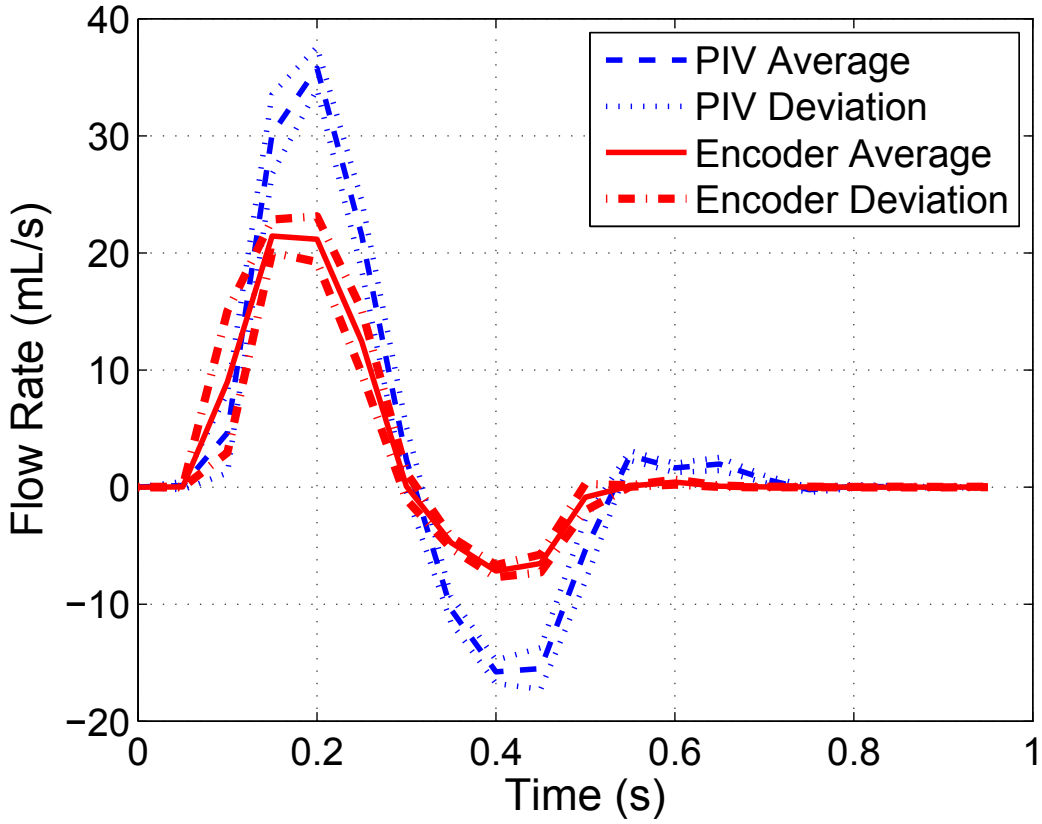

Figure 5.12: PIV and encoder measurement comparison for femoral waveform [7]

Even though the identification of the friction parameters can be done to help tune the system, time consuming trial and error is still required to get the system to perform well and not become unstable. Once good parameters are found though, the pump can be very consistent in the flow it produces. Figure 5.10 shows the standard deviation around the measured waveform and it is relatively small for the entire waveform. Although not ideal, it might be possible to compensate for the tracking error by changing the input waveform to the controller so that even though the pump doesn't accurately track the input waveform, what is produced would actually be the desired waveform. Comparing Figure 5.6 to Figure 5.10 again, it looks like the femoral flow measured is closer to the reference waveform from the aorta than the femoral. This is something that can be explored in future work on this project, but it is not a good solution to the tracking error. The better solution would be to fix the tracking error by changing the control system so that it accurately tracks the reference instead of just accepting the error and manipulating the input until the produced waveform

matches the desired waveform.

5.3 Summary

Particle image velocimetry was used to see if the measured flow would match the desired waveform. Two waveforms were produced by the pump and measured using PIV. One waveform was from the aortic artery, the second waveforms was from the femoral artery. The results were promising for a first attempt, but the pump did not quite manage to track the references accurately. Although the pump was fairly consistent from one pulse to the next. Unfortunately time consuming trial and error is still required to get the system to perform well when tracking the reference waveform.

For both waveforms the PIV and encoder measurements do not agree well. This means that the encoder cannot be relied on to accurately calculate the flow. This also means that using the encoder feedback to try and tune the pump to accurately match the reference probably wont produce a good match when measured with particle image velocimetry.

Chapter 6

Conclusions & Recommendations

6.1 Conclusions

This project started with a need for a pump that could produce waveforms like those found in the human cardiovascular system. The project began with an idea to use a voice coil actuator to make a positive displacement pump. The voice coil is used to actuate the pistons that could be interchanged with different diameter pistons and cylinders. This would give the pump a wide range of flow it could output with one actuator. This initial project plan used a commercial voice coil actuator with two piston cylinder assemblies attached to the ends of the actuator. Preliminary research into the operation of voice coil actuators lead to the idea to integrate the pistons into the actuator itself.

The development of the electrical and mechanical design of this pump is what was discussed in chapter 2. Developing this initial idea lead to figuring out that friction was a large obstacle for this project. Chapters 3 and 4 discuss the work that was done to try to resolve the friction problems that were discovered early in the project. Much time was spent trying to Figure out how to adequately compensate for non-linear friction dynamics in the operating conditions of the pump. A few methods of friction compensation were attempted, but the first method that produced positive results was the LuGre friction model. The friction compensation method was tested experimentally and discussed in chapter 5. For a first attempt the results were encouraging, but the control system needs improvement to better track reference waveforms. Future work with this pump should involve implementing a better controller.

The pump has been used to output two waveforms. Figure 6.1 summarizes the results from testing with aorta and femoral waveforms. It should be capable of a wide variety of profiles, but needs to be set up and tuned for each unique profile. This is time consuming and requires significant trial and error when fine tuning the controller. This is one reason what it was recommended to develop a better controller

in any future work with this project. A better controller would go a long way towards making the pump capable of a producing wider variety of waveforms.

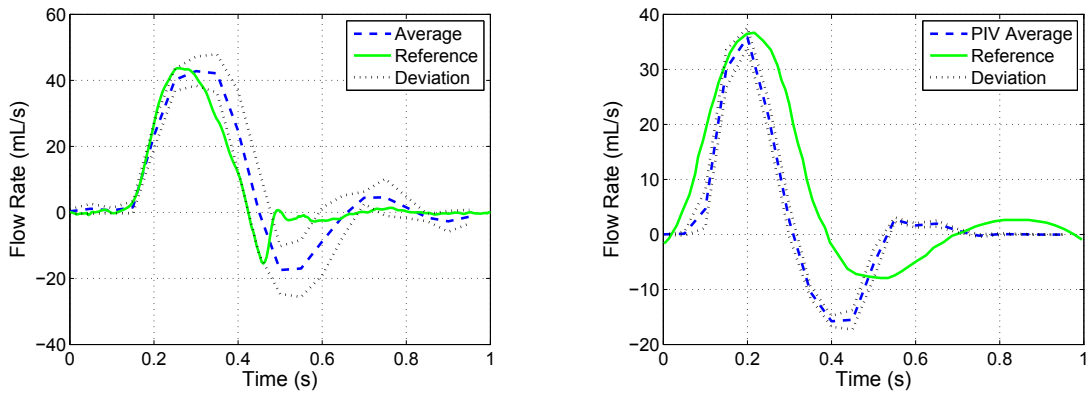

(a) Aorta 10 cycle average

(b) Femoral 10 cycle average

Figure 6.1: Waveforms produced by the pump for testing

6.2 Recommendations

The first recommendation for future work on this project is to address the sterility requirement of the pump. To make the pump sterile there needs to be a position feedback device that doesn't require a mechanical seal between the working fluid and the open air. There are commercially available sensors, such as a magnetic film potentiometer, that might have this capability and should be tested on the next iteration of the pump design.

More work should be done on on the control system for the pump. The results obtained so far are good for a first design, but the control should be improved in the future. Better parameter identification, better tuning methodology, and a more robust friction compensation method will greatly improve the ability of the pump to track a reference profile.

The commercial voice coil that was used in this project should be disassembled to see how the coil and magnet are configured inside the actuator. This information should help design a second prototype of the custom voice coil that has a much higher force constant than 0.87 N/Amp. Once that information has been incorporated into the design, another custom voice coil should be made and tested. So, next version

of the custom voice coil should have a higher force output, and include the magnetic film potentiometer in its design. This next version should than be used for implement the recommended improvements to the control system of the pump.

Pursuing commercialization of this pump is also a possibility in the future, provided that its development will continue. Specifically, if the control system can be significantly improved, and a sterile fluid maintained, it may be competitive with other pumps currently available commercially.

References

[1] Sören Andersson, Anders Söderberg, and Stefan Björklund. "Friction models for sliding dry, boundary and mixed lubricated contacts". In: *Tribology International* 40.4 (Apr. 2007), pp. 580–587. ISSN: 0301679X. DOI: 10.1016/j.triboint.2005.11.014. URL: http://linkinghub.elsevier.com/retrieve/pii/S0301679X05003154.

[2] Farid Al-bender, Vincent Lampaert, and Jan Swevers. "The Generalized Maxwell-Slip Model : A Novel Model for Friction Simulation and Compensation". In: *IEEE Transactions on Automatic Control* 50.11 (Nov. 2005), pp. 1883–1887.

[3] B. K. Bharadvai, R. F. Mabon, and D. P. Giddens. "Steady flow in a model of the human carotid bifurcation. Part I - flow visualization". In: *Journal of Biomechanics* 15.5 (1982), pp. 363–378.

[4] Bill Black, Mike Lopez, and Anthony Morcos. "Basics of Voice Coil Actuators". In: *PCIM* (July 1993), pp. 44–46.

[5] John Brauer. *Magnetic Actuators and Sensors*. Wiley, 2006.

[6] Yi Chen. "Lorentz force actuator and carbon fiber co-winding design, construction and characterization". Bachelors. Massachusetts Institute of Technology, May 2008. URL: http://18.7.29.232/handle/1721.1/45772.

[7] Amanda Colella-Centazzo and Clifton R Johnston. "The Quantification of Blood Flow Patterns Induced by Endovascular Stent Grafts Using a Non-Newtonian Blood Analog". In: *Summer Biomechanics, Bioengineering and Biotransport Conference*. 2015.

[8] Don P. Giddens David N. Ku. "Laser doppler anemometer measurements of pulsatile flow in a model carotid bifurcation". In: *Journal of Biomechanics* 20.4 (1987), pp. 407–421.

[9] C.C. De Wit et al. "A new model for control of systems with friction". In: *Automatic Control, IEEE Transactions on* 40.3 (Mar. 1995), pp. 419–425. ISSN: 0018-9286. DOI: 10.1109/9.376053.

[10] Nguyen B. Do, Aldo a. Ferri, and Olivier a. Bauchau. "Efficient Simulation of a Dynamic System with LuGre Friction". In: *Journal of Computational and Nonlinear Dynamics* 2.4 (Oct. 2007), pp. 281–289. ISSN: 15551423. DOI: 10.1115/1.2754304. URL: http://computationalnonlinear.asmedigitalcollection.asme.org/article.aspx?articleid=1394642.

[11] Anders Eriksson, Hans W. Persson, and Kjell Lindstrom. "A computer-controlled arbitrary flow wave form generator for physiological studies". In: *Review of Scientific Instruments* 71.1 (2000), pp. 235–242. ISSN: 00346748. DOI: 10.1063/1.1150189. URL: http://link.aip.org/link/RSINAK/v71/i1/p235/s1%5C&Agg=doi.

[12] R Frayne et al. "Computer-controlled flow simulator for MR flow studies." In: *Journal of magnetic resonance imaging : JMRI* 2.5 (1992), pp. 605–612. ISSN: 1053-1807.

[13] Leonid Freidovich and Anders Robertsson. "LuGre-model-based friction compensation". In: *Control Systems Technology, IEEE Transactions on* 18.1 (2010), pp. 194–200. URL: http://ieeexplore.ieee.org/xpls/abs%5C_all.jsp?arnumber=5291704.

[14] Leonid Freidovich et al. "Friction compensation based on LuGre model". In: *Decision and Control, 2006 45th IEEE Conference on*. Dec. 2006, pp. 3837–3842. ISBN: 1424401712.

[15] SS Ge, TH Lee, and SX Ren. "Adaptive friction compensation of servo mechanisms". In: *International Journal of Systems Science* 32.4 (2001), pp. 211–248. URL: http://www.tandfonline.com/doi/abs/10.1080/00207720119378.

[16] B.D. Hemond et al. "A Lorentz-Force Actuated Autoloading Needle-free Injector". In: *Engineering in Medicine and Biology Society, 2006. EMBS '06. 28th Annual International Conference of the IEEE*. Aug. 2006, pp. 679–682. DOI: 10.1109/IEMBS.2006.259918.

[17] D W Holdsworth et al. "Computer-controlled positive displacement pump for physiological flow simulation." In: *Medical & biological engineering & computing* 29.6 (1991), pp. 565–570. ISSN: 0140-0118. DOI: 10.1007/BF02446086.

[18] W.H. Hoppmann and J.C.C. Liu. "The mechanics of a certain class of pumps". In: *Journal of Biomechanics* 5.2 (Mar. 1972), pp. 153–158. ISSN: 00219290. DOI: 10.1016/0021-9290(72)90050-4. URL: http://www.sciencedirect.com/science/article/pii/0021929072900504.

[19] P R Hoskins, T Anderson, and W N McDicken. "A computer controlled flow phantom for generation of physiological Doppler waveforms." In: *Physics in medicine and biology* 34.11 (1989), pp. 1709–1717. ISSN: 0031-9155. DOI: 10.1088/0031-9155/34/11/018.

[20] Ian W Hunter and Nathan B Ball. "An Optimized Linear Lorentz-Force Actuator for Biorobotics and Needle-Free Injection by An Optimized Linear Lorentz-Force Actuator for Biorobotics and Needle-Free Injection by". MA thesis. Massachusetts Institute of Technology, 2007.

[21] Arash Kheradvar and Morteza Gharib. "On mitral valve dynamics and its connection to early diastolic flow". In: *Annals of Biomedical Engineering* 37.1 (2009), pp. 1–13. ISSN: 00906964. DOI: 10.1007/s10439-008-9588-7.

[22] Il-Hwan Kim et al. "Neural network-based system identification and controller synthesis for an industrial sewing machine". In: *International Journal of Control, Automation, and Systems* 2.1 (Mar. 2004), pp. 83–91. URL: http://ijcas.org/admin/paper/files/IJCAS%5C_v2%5C_n1%5C_p83-91.pdf.

[23] David N Ku and Don P Giddens. "Pulsatile Flow in a Model Carotid Bifurcation". In: *Arteriosclerosis* 3.1 (1983), pp. 31–39.

[24] DN Ku. "Blood flow in arteries". In: *Annual Review of Fluid Mechanics* 29 (1 1997), pp. 399–434. DOI: 10.1146/annurev.fluid.29.1.399. URL: http://www.annualreviews.org/doi/abs/10.1146/annurev.fluid.29.1.399.

[25] V. Lampaert, F. Al-Bender, and J. Swevers. "A generalized Maxwell-slip friction model appropriate for control purposes". In: *Physics and Control, 2003. Proceedings. 2003 International Conference*. Vol. 4. Aug. 2003, 1170–1177 vol.4. DOI: 10.1109/PHYCON.2003.1237071.

[26] Y. F. Law et al. "Computer-controlled pulsatile pump system for physiological flow simulation". In: *Medical & Biological Engineering & Computing* 25.5 (1987), pp. 590–595. ISSN: 01400118. DOI: 10.1007/BF02441756.

[27] Eduardo Licéaga-Castro et al. "Slow-motion control of an unloaded hydraulic robot arm". In: *Precision Engineering* 36.3 (July 2012), pp. 388–398. ISSN: 01416359. DOI: 10.1016/j.precisioneng.2012.01.001. URL: http://linkinghub.elsevier.com/retrieve/pii/S0141635912000049.

[28] Chih-Jer Lin, Her-Terng Yau, and Yun-Cheng Tian. "Identification and Compensation of Nonlinear Friction Characteristics and Precision Control for a Linear Motor Stage". In: *Mechatronics, IEEE/ASME Transactions on* 18.4 (Aug. 2013), pp. 1385–1396. ISSN: 1083-4435. DOI: 10.1109/TMECH.2012.2202679.

[29] Lu Lu et al. "Adaptive robust control of linear motors with dynamic friction compensation using modified LuGre model". In: *Automatica* 45.12 (Dec. 2009), pp. 2890–2896. ISSN: 00051098. DOI: 10.1016/j.automatica.2009.09.007. URL: http://linkinghub.elsevier.com/retrieve/pii/S0005109809004178.

[30] Diana Lui. "Design and Characterization of a Compact Voice Coil for a Needle-Free Injection Device". Bachelors. Massachusetts Institute of Technology, 2006.

[31] K & J Magnetics. *K & J Magnetics Magnetic Field Visualization Single Magnet in Free Space*. 2015. URL: https://www.kjmagnetics.com/magfield.asp?pName=D8Z0.

[32] N. Mallon et al. "Friction compensation in a controlled one-link robot using a reduced-order observer". In: *Control Systems Technology, IEEE Transactions on* 14.2 (Mar. 2006), pp. 374–383. ISSN: 1063-6536. DOI: 10.1109/TCST.2005.863674.

[33] J.C. Martinez-Rosas and L. Alvarez-Icaza. "Adaptive compensation of dynamic friction in an industrial robot". In: *Control Applications, 2008. CCA 2008. IEEE International Conference on*. Sept. 2008, pp. 1145–1150. DOI: 10.1109/CCA.2008.4629664.

[34] Donald A. McDonald. *Blood Flow in Arteries*. Edward Arnold, 1974.

[35] Deyuan Meng et al. "Adaptive robust motion trajectory tracking control of pneumatic cylinders with LuGre model-based friction compensation". In: *Chinese Journal of Mechanical Engineering* 27.4 (Aug. 2014), pp. 802–815. ISSN: 1000-9345. DOI: 10.3901/CJME.2014.0430.085. URL: http://link.springer.com/10.3901/CJME.2014.0430.085.

[36] William R. Milnor. *Hemodynamics*. Williams & Wilkins, 1982.

[37] H. Olsson et al. "Friction models and friction compensation". In: *European Journal of Control* 4.3 (1998), pp. 176–195. URL: http://www.sciencedirect.com/science/article/pii/S094735809870113X.

[38] Ya-Jun Pan. *MECH4950/6950 Advanced Control Engineering. Part III - Multi-Input-Multi-Output Systems, Section 1: Multivariable Control Methods*. 2013.

[39] T.J. Pedley. *The Fluid Mechanics of Large Blood Vessels*. Cambridge Books Online. Cambridge University Press, 1980. ISBN: 9780511896996.

[40] D B Plewes et al. "An MR compatible flow simulator for intravascular pressure simulation." In: *Medical physics* 22.7 (1995), pp. 1111–1115. ISSN: 00942405. DOI: 10.1118/1.597504.

[41] D. P. Giddens R.A. Cassanova. "Disorder distal to modeled stenoses in a steady and pulsatile flow". In: *Journal of Biomechanics* 11 (1978).

[42] D. Rizos and S. Fassois. "Friction Identification Based Upon the LuGre and Maxwell Slip Models". In: *Control Systems Technology, IEEE Transactions on* 17.1 (Jan. 2009), pp. 153–160. ISSN: 1063-6536. DOI: 10.1109/TCST.2008.921809.

[43] Michael Ruderman and Torsten Bertram. "Two-state dynamic friction model with elasto-plasticity". In: *Mechanical Systems and Signal Processing* 39.1-2 (Aug. 2013), pp. 316–332. ISSN: 08883270. DOI: 10.1016/j.ymssp.2013.03.010. URL: http://linkinghub.elsevier.com/retrieve/pii/S0888327013001106.

[44] Chander Sadasivan et al. "Angiographic quantification of contrast medium washout from cerebral aneurysms after stent placement". In: *American Journal of Neuroradiology* 23.7 (2002), pp. 1214–1221. ISSN: 01956108.

[45] P Segers et al. "Role and relevancy of a cardiovascular simulator". In: *Cardiovascular Engineering* 3 (1998), pp. 48–56.

[46] Steve C Southward, Clark J Radcliffe, and CR MacCluer. "Robust nonlinear stick-slip friction compensation". In: *Journal of Dynamic Systems, Measurement, and Control* 113.4 (1991), pp. 639–645.

[47] Jan Swevers et al. "An integrated friction model structure with improved presliding behavior for accurate friction compensation". In: *Automatic Control, IEEE Transactions on* 45.4 (2000), pp. 675–686.

[48] A.J. Taberner et al. "A Portable Needle-free Jet Injector Based on a Custom High Power-density Voice-coil Actuator". In: *Engineering in Medicine and Biology Society, 2006. EMBS '06. 28th Annual International Conference of the IEEE*. Aug. 2006, pp. 5001–5004. DOI: 10.1109/IEMBS.2006.260243.

[49] Andrew Taberner, N Catherine Hogan, and Ian W Hunter. "Needle-free jet injection using real-time controlled linear Lorentz-force actuators." In: *Medical engineering & physics* 34.9 (Nov. 2012), pp. 1228–35. ISSN: 1873-4030. DOI: 10.1016/j.medengphy.2011.12.010. URL: http://www.ncbi.nlm.nih.gov/pubmed/22245386.

[50] Tegoeh Tjahjowidodo et al. "Friction characterization and compensation in electro-mechanical systems". In: *Journal of Sound and Vibration* 308.3-5 (Dec. 2007), pp. 632–646. ISSN: 0022460X. DOI: 10.1016/j.jsv.2007.03.075. URL: http://linkinghub.elsevier.com/retrieve/pii/S0022460X07002593.

[51] William Tsai and Omer Savas. "Flow pumping system for physiological waveforms". In: *Medical and Biological Engineering and Computing* 48.2 (2010), pp. 197–201. ISSN: 01400118. DOI: 10.1007/s11517-009-0573-6.

[52] P Verdonck et al. "Computer-controlled in vitro model of the human left heart." In: *Medical & biological engineering & computing* 30.6 (1992), pp. 656–659. ISSN: 0140-0118. DOI: 10.1007/BF02446800.

[53] Xingjian Wang and Shaoping Wang. "High Performance Adaptive Control of Mechanical Servo System With LuGre Friction Model: Identification and Compensation". In: *Journal of Dynamic Systems, Measurement, and Control* 134.1 (2012), p. 011021. ISSN: 00220434. DOI: 10.1115/1.4004785. URL: http://dynamicsystems.asmedigitalcollection.asme.org/article.aspx?articleid=1393383.

[54] Jianyong Yao, Zongxia Jiao, and Songshan Han. "Friction compensation for low velocity control of hydraulic flight motion simulator: A simple adaptive robust approach". In: *Chinese Journal of Aeronautics* 26.3 (June 2013), pp. 814–822.

ISSN: 10009361. DOI: 10.1016/j.cja.2013.04.001. URL: http://linkinghub.elsevier.com/retrieve/pii/S1000936113000526.

Appendix A

Drawings

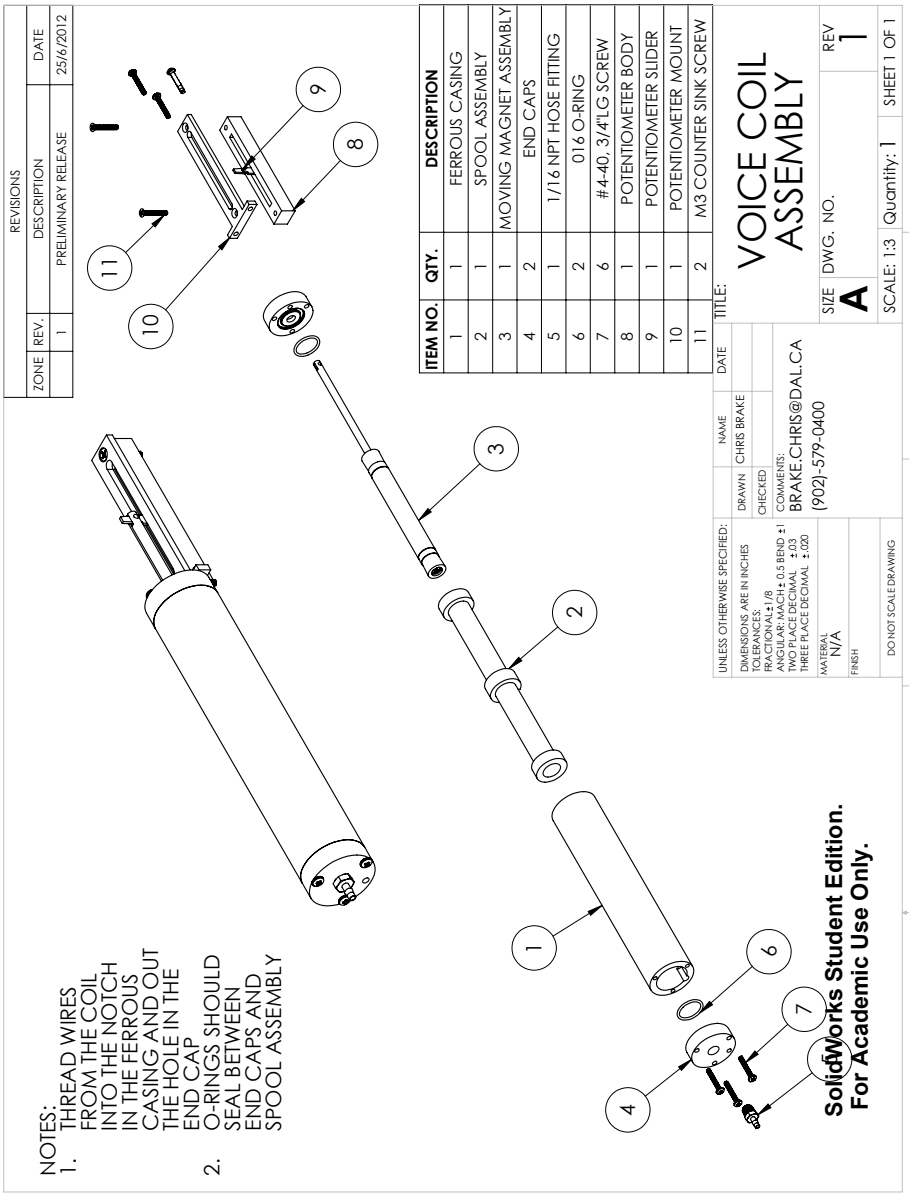

REVISIONS			
ZONE	REV.	DESCRIPTION	DATE
	1	PRELIMINARY RELEASE	25/6/2012

NOTES:
1. SUBSTITUTE SCREW IN PISTON HEAD WITH FEEDBACK ROD
2. APPLY LOCTITE IF NECESSARY

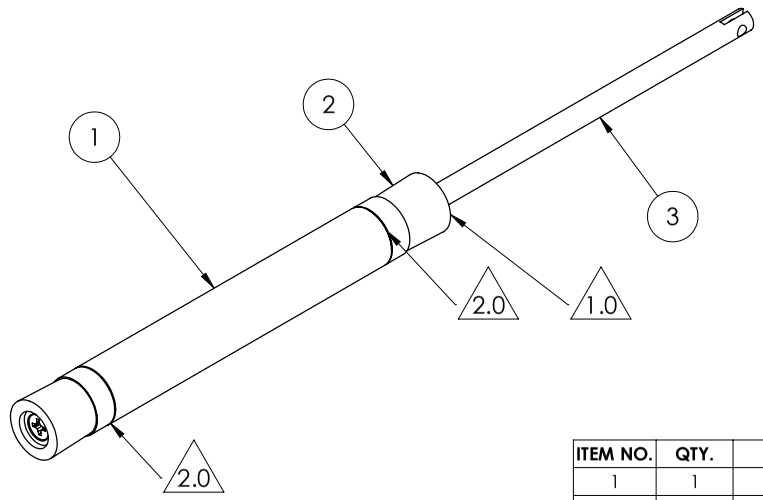

ITEM NO.	QTY.	DESCRIPTION
1	1	D8Z0 MAGNET
2	2	PISTON HEAD ASSEMBLY
3	1	FEEDBACK ROD

UNLESS OTHERWISE SPECIFIED:
DIMENSIONS ARE IN INCHES
TOLERANCES:
FRACTIONAL ±1/8
ANGULAR: MACH ± 0.5 BEND ±1
TWO PLACE DECIMAL ±.03
THREE PLACE DECIMAL ±.020

MATERIAL
N/A

FINISH

DO NOT SCALE DRAWING

	NAME	DATE
DRAWN	CHRIS BRAKE	
CHECKED		

COMMENTS:
BRAKE.CHRIS@DAL.CA
(902)-579-0400

TITLE:
MOVING MAGNET ASSEMBLY

SIZE A | DWG. NO. | REV 1

SCALE: 1:1 | Quantity: 1 | SHEET 1 OF 1

5 4 3 2 1

SolidWorks Student Edition.
For Academic Use Only.

REVISIONS			
ZONE	REV.	DESCRIPTION	DATE
	1	PRELIMINARY RELEASE	25/6/2012

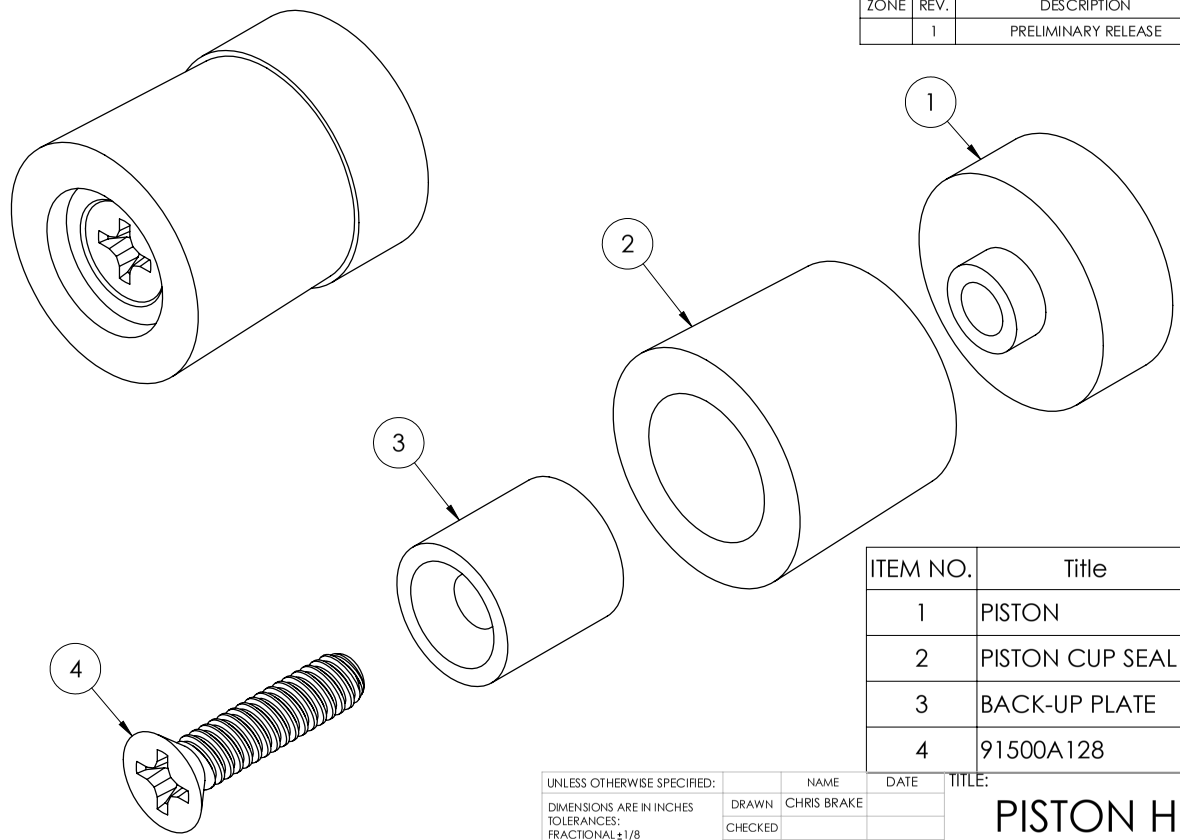

ITEM NO.	Title	QTY.
1	PISTON	1
2	PISTON CUP SEAL	1
3	BACK-UP PLATE	1
4	91500A128	1

SolidWorks Student Edition.
For Academic Use Only.

UNLESS OTHERWISE SPECIFIED:
DIMENSIONS ARE IN INCHES
TOLERANCES:
FRACTIONAL ±1/8
ANGULAR: MACH ± 0.5 BEND ±1
TWO PLACE DECIMAL ±.03
THREE PLACE DECIMAL ±.020

MATERIAL
N/A

FINISH

DO NOT SCALE DRAWING

	NAME	DATE
DRAWN	CHRIS BRAKE	
CHECKED		

COMMENTS:
BRAKE.CHRIS@DAL.CA
(902)-579-0400

TITLE:
PISTON HEAD ASSEMBLY

SIZE **A** | DWG. NO. | REV 1

SCALE: 4:1 | Quantity: | SHEET 1 OF 1

5 4 3 2 1

NOTES:
1. COILS MUST BE WOUND IN OPPOSITE DIRECTIONS
2. USE 22 AWG MAGNET WIRE, WITH 4 LAYERS TO EACH COIL.

REVISIONS			
ZONE	REV.	DESCRIPTION	DATE
	1	PRELIMINARY RELEASE	25/6/2012

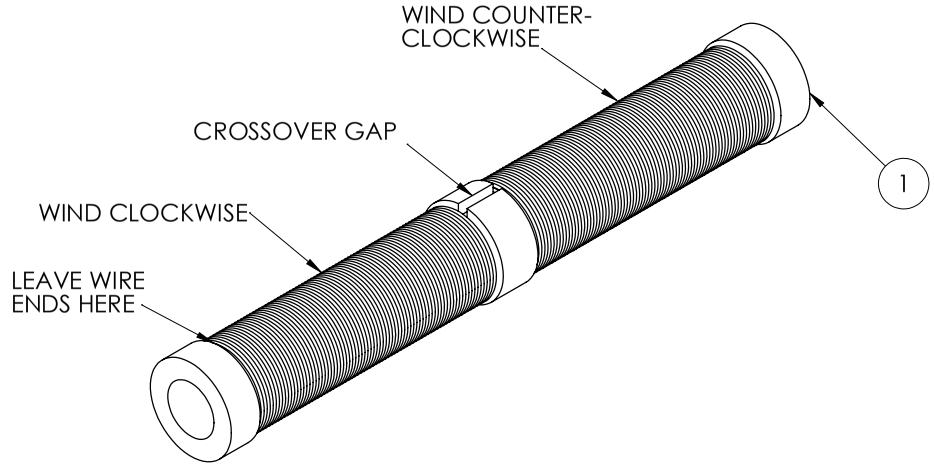

ITEM NO.	title	QTY.
1	CYLINDER SPOOL	1
2	7588K79	2

UNLESS OTHERWISE SPECIFIED:
DIMENSIONS ARE IN INCHES
TOLERANCES:
FRACTIONAL ±1/8
ANGULAR: MACH ± 0.5 BEND ±1
TWO PLACE DECIMAL ±.03
THREE PLACE DECIMAL ±.020

MATERIAL
N/A

FINISH

DO NOT SCALE DRAWING

	NAME	DATE
DRAWN	CHRIS BRAKE	
CHECKED		

COMMENTS:
BRAKE.CHRIS@DAL.CA
(902)-579-0400

TITLE:
SPOOL ASSEMBLY

SIZE A | DWG. NO. | REV 1

SCALE: 1:1 | Quantity: 1 | SHEET 1 OF 1

5 4 3 2 1

SolidWorks Student Edition.
For Academic Use Only.

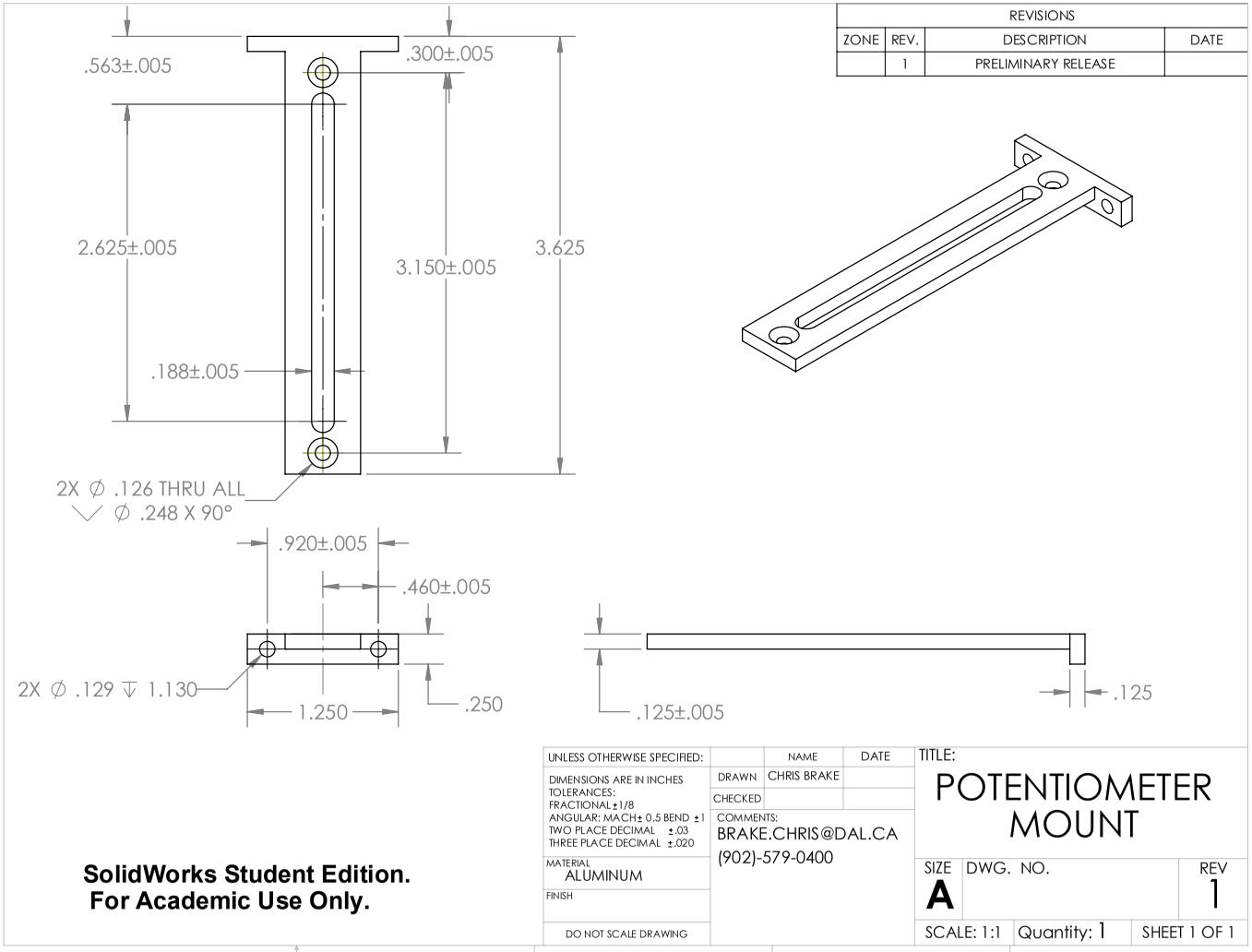
.563±.005
.300±.005
2.625±.005
3.150±.005
3.625
.188±.005
2X ∅ .126 THRU ALL
∅ .248 X 90°
.920±.005
.460±.005
2X ∅ .129 ↧ 1.130
1.250
.250
.125±.005
.125
REVISIONS
ZONE
REV.
DESCRIPTION
DATE
1
PRELIMINARY RELEASE
UNLESS OTHERWISE SPECIFIED:
DIMENSIONS ARE IN INCHES
TOLERANCES:
FRACTIONAL ±1/8
ANGULAR: MACH ± 0.5 BEND ±1
TWO PLACE DECIMAL ±.03
THREE PLACE DECIMAL ±.020
MATERIAL
ALUMINUM
FINISH
DO NOT SCALE DRAWING
NAME
DATE
DRAWN
CHRIS BRAKE
CHECKED
COMMENTS:
BRAKE.CHRIS@DAL.CA
(902)-579-0400
TITLE:
POTENTIOMETER MOUNT
SIZE
A
DWG. NO.
REV
1
SCALE: 1:1
Quantity: 1
SHEET 1 OF 1
SolidWorks Student Edition.
For Academic Use Only.
5
4
3
2
1

REVISIONS			
ZONE	REV.	DESCRIPTION	DATE
	1	PRELIMINARY RELEASE	25/6/2012

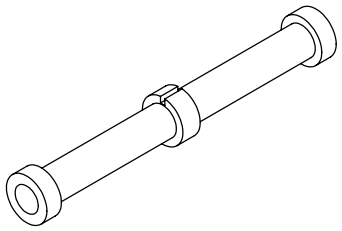

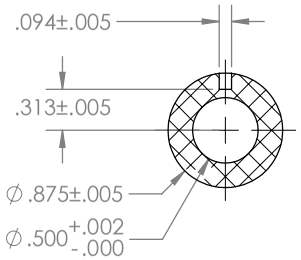

SECTION A-A

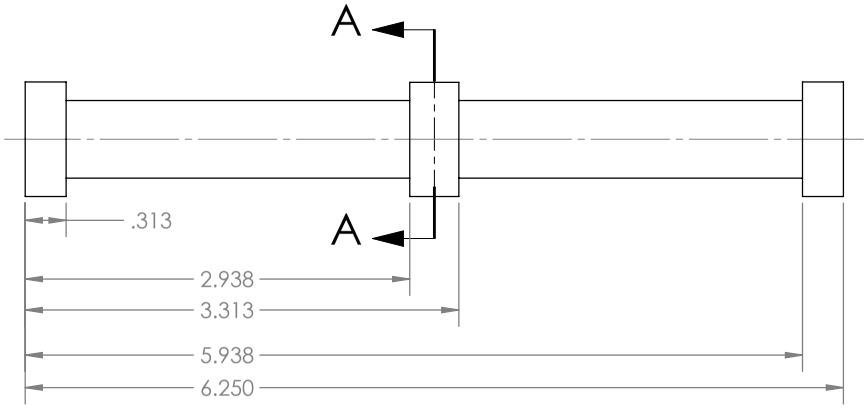

SolidWorks Student Edition.
For Academic Use Only.

UNLESS OTHERWISE SPECIFIED:		NAME	DATE
DIMENSIONS ARE IN INCHES TOLERANCES: FRACTIONAL ±1/8 ANGULAR: MACH ± 0.5 BEND ±1 TWO PLACE DECIMAL ±.03 THREE PLACE DECIMAL ±.020	DRAWN	CHRIS BRAKE	
	CHECKED		
MATERIAL DELRIN	COMMENTS: BRAKE.CHRIS@DAL.CA (902)-579-0400		
FINISH			
DO NOT SCALE DRAWING			

TITLE:

CYLINDER SPOOL

SIZE	DWG. NO.	REV
A		1

SCALE: 1:1	Quantity: 1	SHEET 1 OF 1

5 4 3 2 1

REVISIONS			
ZONE	REV.	DESCRIPTION	DATE
	1	PRELIMINARY RELEASE	25/6/2012

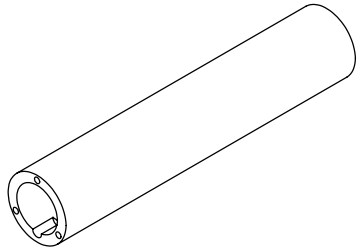

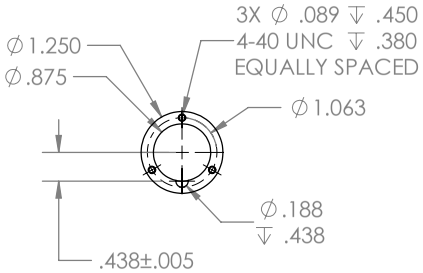

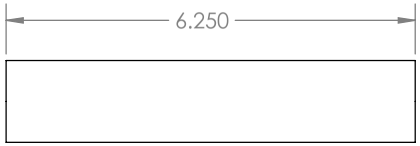

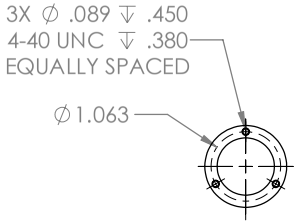

SolidWorks Student Edition.
For Academic Use Only.

UNLESS OTHERWISE SPECIFIED:		NAME	DATE
DIMENSIONS ARE IN INCHES TOLERANCES: FRACTIONAL ±1/8 ANGULAR: MACH ± 0.5 BEND ±1 TWO PLACE DECIMAL ±.03 THREE PLACE DECIMAL ±.020	DRAWN	CHRIS BRAKE	
	CHECKED		
MATERIAL	COMMENTS: BRAKE.CHRIS@DAL.CA (902)-579-0400		
FINISH			
DO NOT SCALE DRAWING			

TITLE:

FERROUS CASING

SIZE	DWG. NO.	REV
A		1
SCALE: 1:2	Quantity: 1	SHEET 1 OF 1

5 4 3 2 1

REVISIONS			
ZONE	REV.	DESCRIPTION	DATE
	1	PRELIMINARY RELEASE	25/6/2012

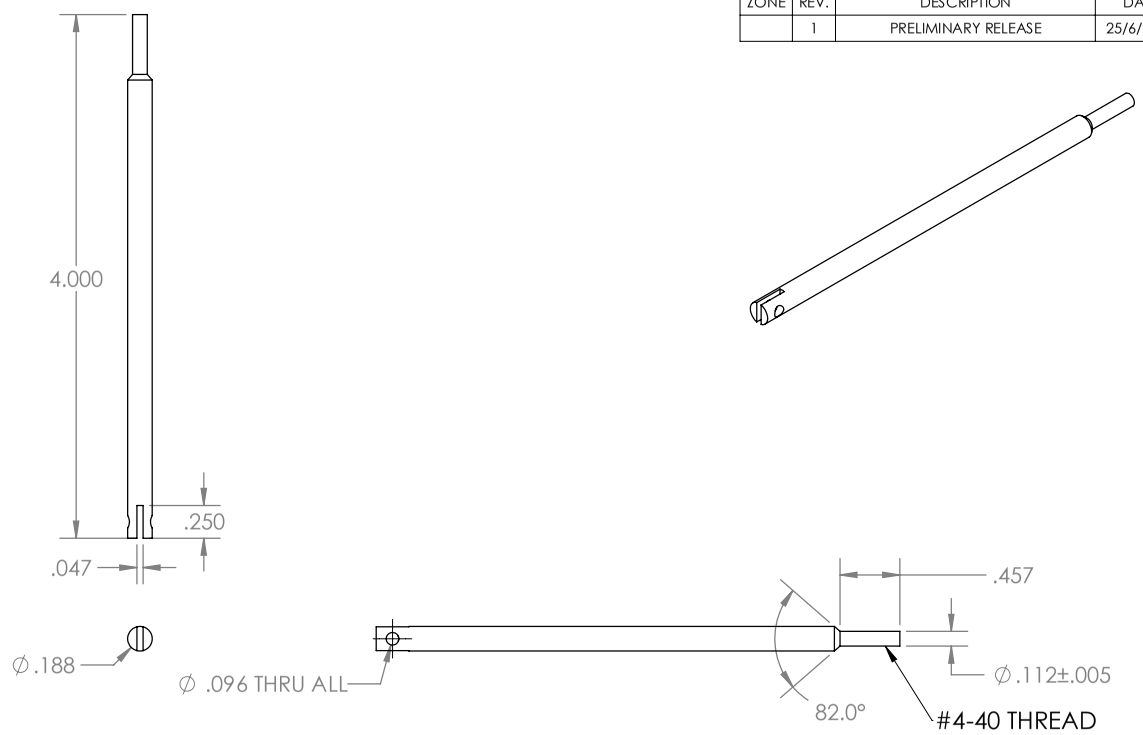

SolidWorks Student Edition.
For Academic Use Only.

UNLESS OTHERWISE SPECIFIED:		NAME	DATE
DIMENSIONS ARE IN INCHES TOLERANCES: FRACTIONAL ±1/8 ANGULAR: MACH ± 0.5 BEND ±1 TWO PLACE DECIMAL ±.03 THREE PLACE DECIMAL ±.020	DRAWN	CHRIS BRAKE	
	CHECKED		
MATERIAL ALUMINUM	COMMENTS: BRAKE.CHRIS@DAL.CA (902)-579-0400		
FINISH			
DO NOT SCALE DRAWING			

TITLE:

FEEDBACK ROD

SIZE	DWG. NO.	REV
A		1
SCALE: 1:1	Quantity: 1	SHEET 1 OF 1

5 4 3 2 1

REVISIONS			
ZONE	REV.	DESCRIPTION	DATE
	1	PRELIMINARY RELEASE	

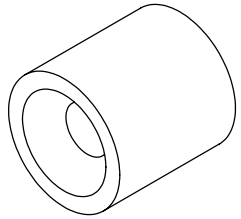

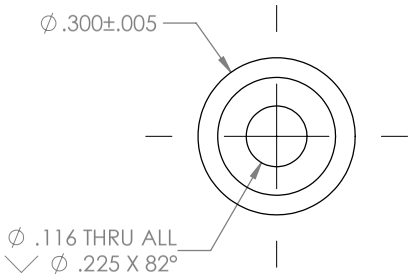

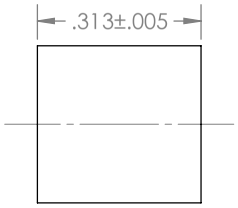

SolidWorks Student Edition.
For Academic Use Only.

UNLESS OTHERWISE SPECIFIED:		NAME	DATE
DIMENSIONS ARE IN INCHES TOLERANCES: FRACTIONAL ±1/8 ANGULAR: MACH ± 0.5 BEND ±1 TWO PLACE DECIMAL ±.03 THREE PLACE DECIMAL ±.020	DRAWN	CHRIS BRAKE	
	CHECKED		
MATERIAL 316 STAINLESS	COMMENTS: BRAKE.CHRIS@DAL.CA (902)-579-0400		
FINISH			
DO NOT SCALE DRAWING			

TITLE:

BACK-UP PLATE

SIZE	DWG. NO.	REV
A		1
SCALE: 4:1	Quantity: 2	SHEET 1 OF 1

5 4 3 2 1

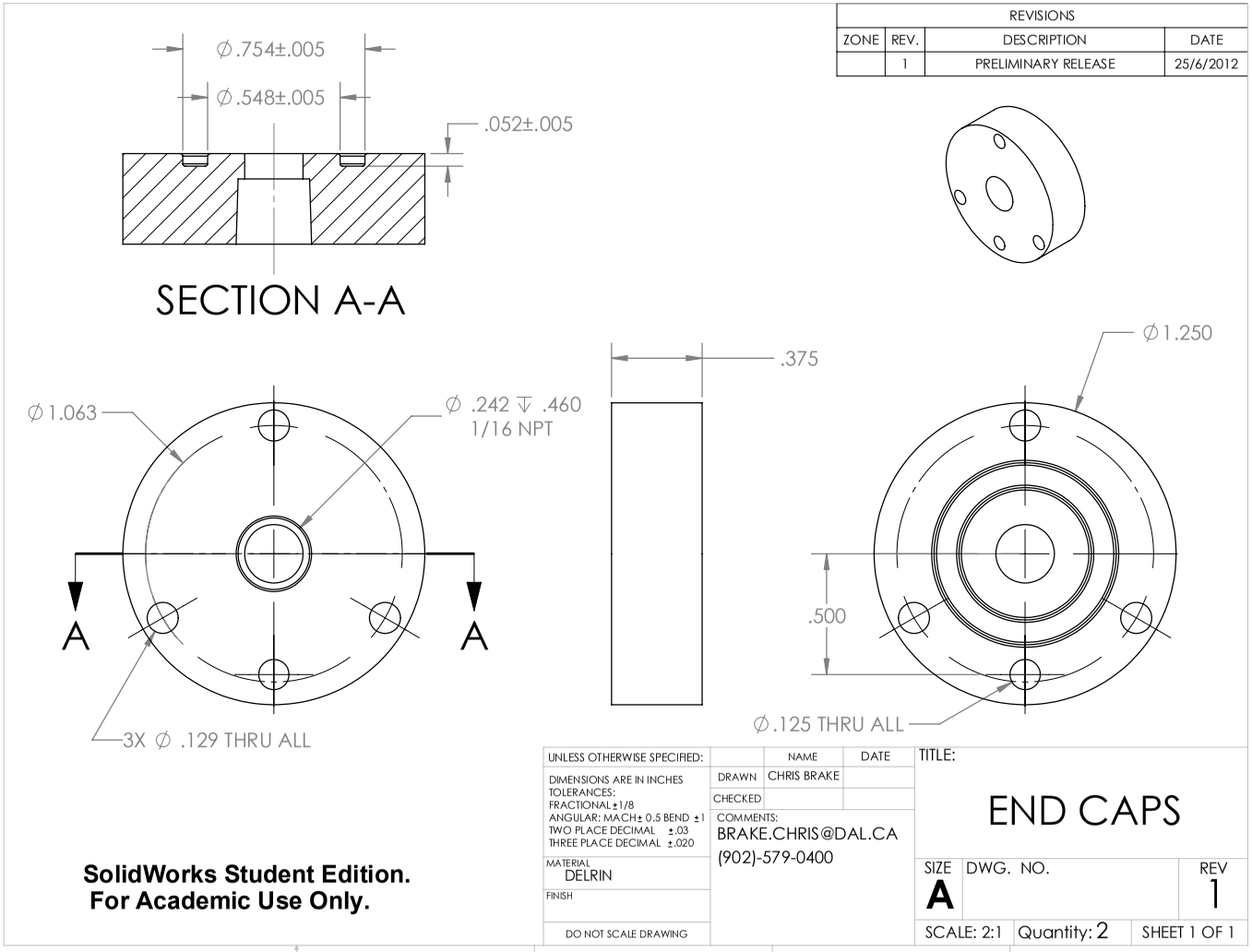
REVISIONS
ZONE | REV. | DESCRIPTION | DATE
1 | PRELIMINARY RELEASE | 25/6/2012
∅.754±.005
∅.548±.005
.052±.005
SECTION A-A
∅1.063
∅ .242 ↧ .460
1/16 NPT
A
A
3X ∅ .129 THRU ALL
.375
∅1.250
.500
∅.125 THRU ALL
UNLESS OTHERWISE SPECIFIED:
DIMENSIONS ARE IN INCHES
TOLERANCES:
FRACTIONAL ±1/8
ANGULAR: MACH ± 0.5 BEND ±1
TWO PLACE DECIMAL ±.03
THREE PLACE DECIMAL ±.020
MATERIAL
DELRIN
FINISH
DO NOT SCALE DRAWING
NAME | DATE
DRAWN | CHRIS BRAKE
CHECKED
COMMENTS:
BRAKE.CHRIS@DAL.CA
(902)-579-0400
TITLE:
END CAPS
SIZE
A
DWG. NO.
REV
1
SCALE: 2:1
Quantity: 2
SHEET 1 OF 1
SolidWorks Student Edition.
For Academic Use Only.
5
4
3
2
1

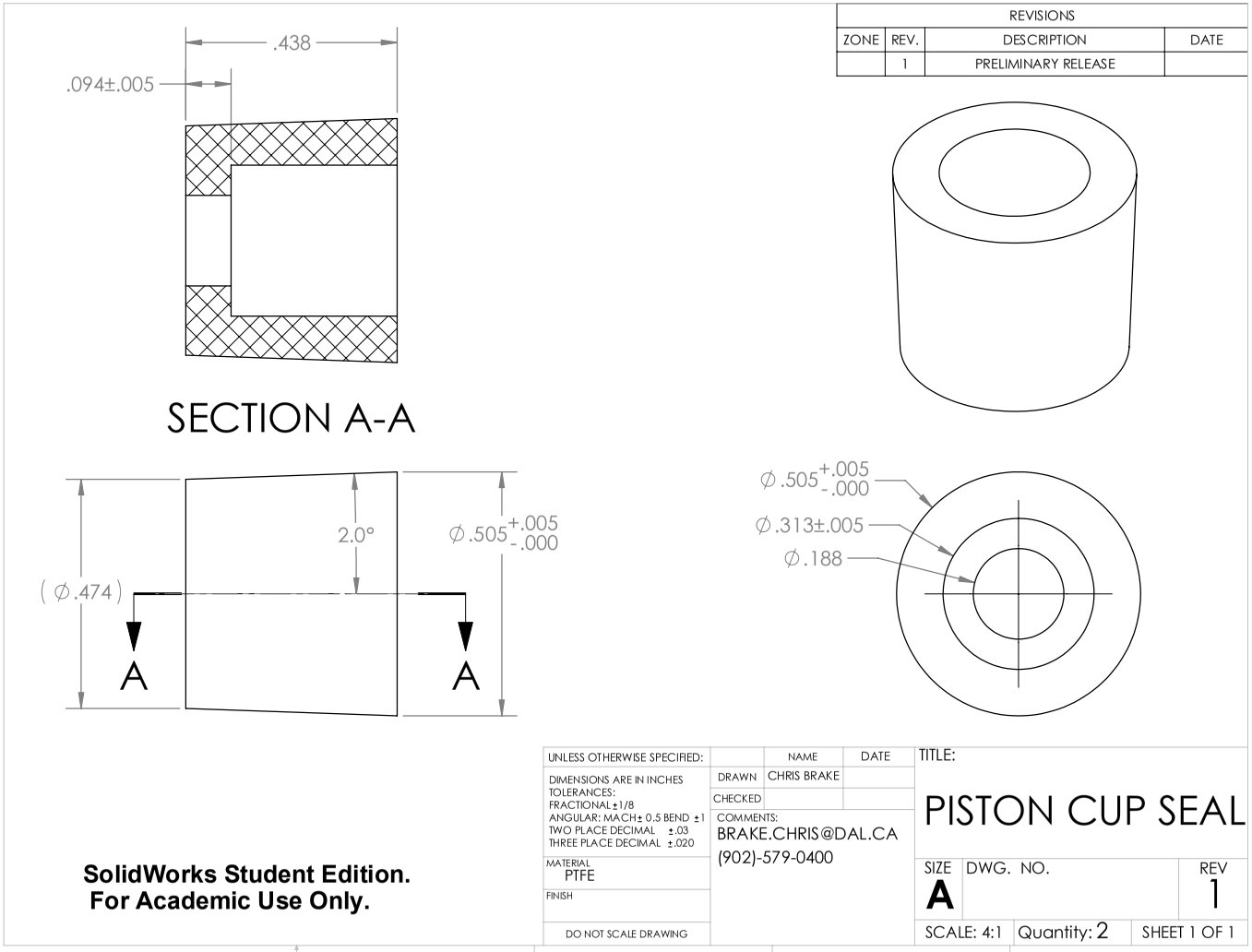
.438
.094±.005
SECTION A-A
2.0°
∅.505 +.005 -.000
(∅.474)
A
A
∅.505 +.005 -.000
∅.313±.005
∅.188
REVISIONS
ZONE | REV. | DESCRIPTION | DATE
1 | PRELIMINARY RELEASE
UNLESS OTHERWISE SPECIFIED:
DIMENSIONS ARE IN INCHES
TOLERANCES:
FRACTIONAL ±1/8
ANGULAR: MACH ± 0.5 BEND ±1
TWO PLACE DECIMAL ±.03
THREE PLACE DECIMAL ±.020
MATERIAL
PTFE
FINISH
DO NOT SCALE DRAWING
NAME | DATE
DRAWN CHRIS BRAKE
CHECKED
COMMENTS:
BRAKE.CHRIS@DAL.CA
(902)-579-0400
TITLE:
PISTON CUP SEAL
SIZE A
DWG. NO.
REV 1
SCALE: 4:1
Quantity: 2
SHEET 1 OF 1
SolidWorks Student Edition.
For Academic Use Only.
5
4
3
2
1

REVISIONS			
ZONE	REV.	DESCRIPTION	DATE
	1	PRELIMINARY RELEASE	24/6/2012

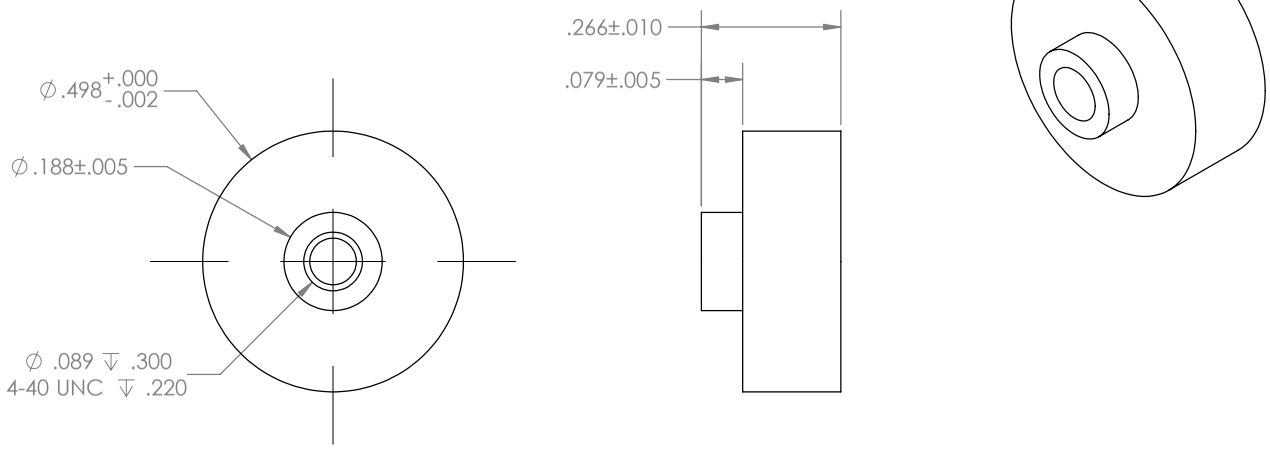

SolidWorks Student Edition.
For Academic Use Only.

UNLESS OTHERWISE SPECIFIED:		NAME	DATE
DIMENSIONS ARE IN INCHES TOLERANCES: FRACTIONAL ±1/8 ANGULAR: MACH ± 0.5 BEND ±1 TWO PLACE DECIMAL ±.03 THREE PLACE DECIMAL ±.020	DRAWN	CHRIS BRAKE	
	CHECKED		
MATERIAL 410 STAINLESS	COMMENTS: BRAKE.CHRIS@DAL.CA (902)-579-0400		
FINISH			
DO NOT SCALE DRAWING			

TITLE:

PISTON

SIZE	DWG. NO.	REV
A		1
SCALE: 4:1	Quantity: 2	SHEET 1 OF 1

5 4 3 2 1

REVISIONS			
ZONE	REV.	DESCRIPTION	DATE
	1	PRELIMINARY RELEASE	

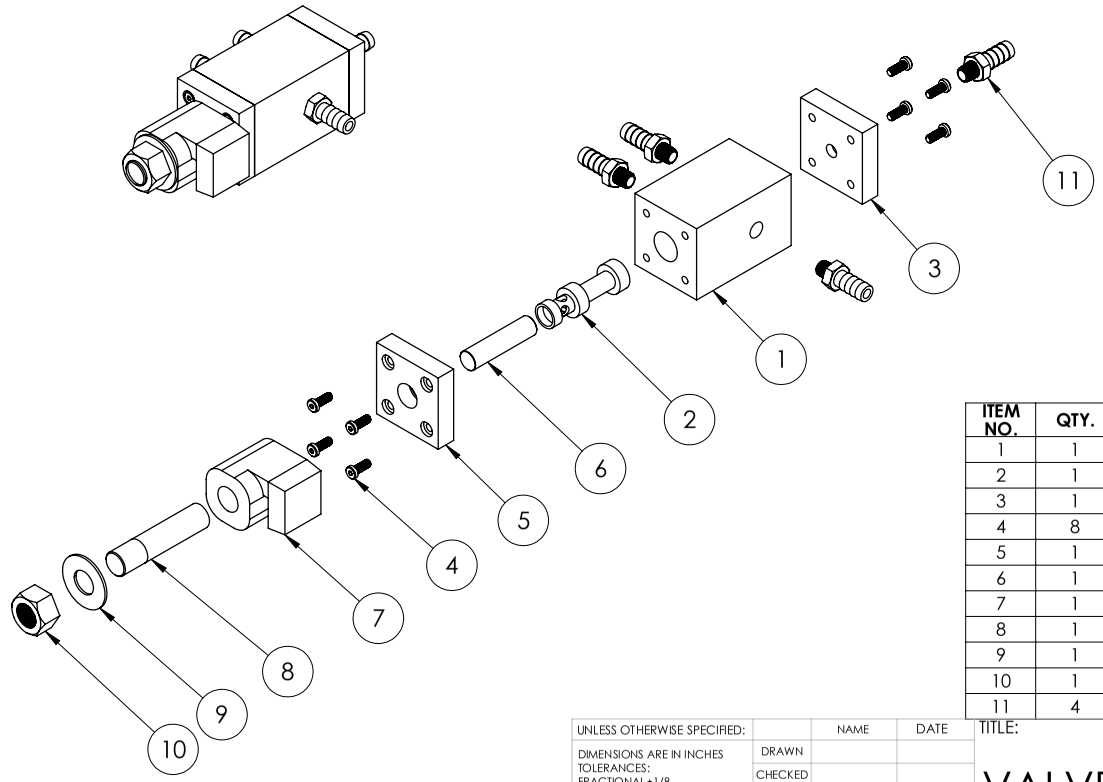

ITEM NO.	QTY.	DESCRIPTION
1	1	VALVE BODY
2	1	SPOOL
3	1	TANK CAP
4	8	#10-32 x 0.5" LHCS
5	1	ACTUATOR CAP
6	1	∅0.5" x 2" MAGNET
7	1	SOLENOID COIL
8	1	COIL COLLAR
9	1	5/8" ID WASHER
10	1	5/8 - 18 NUT
11	4	3/8" TUBE ID x 1/8" NPT

SolidWorks Student Edition.
For Academic Use Only.

UNLESS OTHERWISE SPECIFIED:

DIMENSIONS ARE IN INCHES
TOLERANCES:
FRACTIONAL ±1/8
ANGULAR: MACH ± 0.5 BEND ±1
TWO PLACE DECIMAL ±.03
THREE PLACE DECIMAL ±.020

MATERIAL
SEE BOM

FINISH
N/A

DO NOT SCALE DRAWING

	NAME	DATE
DRAWN		
CHECKED		

COMMENTS:
BRAKE.CHRIS@DAL.CA
(902)-579-0400

TITLE:

VALVE ASSEMBLY

SIZE	DWG. NO.	REV
A	6	1

SCALE: 1:3 | Quantity: 1 | SHEET 1 OF 2

5 4 3 2 1

REVISIONS			
ZONE	REV.	DESCRIPTION	DATE
	1	PRELIMINARY RELEASE	

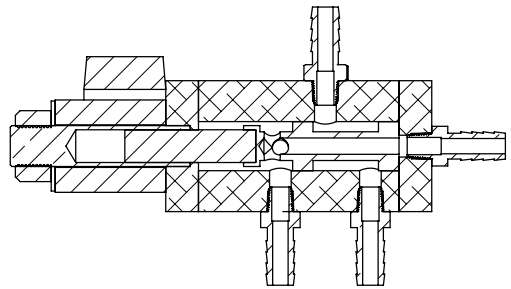

SECTION L-L

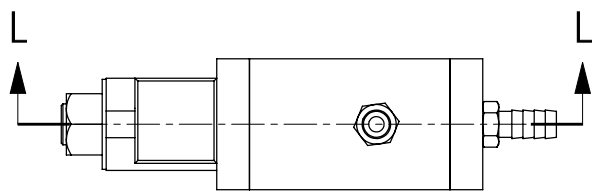

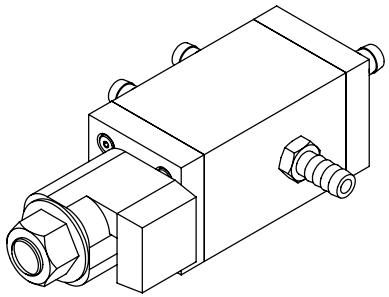

SolidWorks Student Edition.
For Academic Use Only.

UNLESS OTHERWISE SPECIFIED:		NAME	DATE
DIMENSIONS ARE IN INCHES TOLERANCES: FRACTIONAL ±1/8 ANGULAR: MACH ± 0.5 BEND ±1 TWO PLACE DECIMAL ±.03 THREE PLACE DECIMAL ±.020	DRAWN		
	CHECKED		
MATERIAL SEE BOM	COMMENTS: BRAKE.CHRIS@DAL.CA (902)-579-0400		
FINISH N/A			
DO NOT SCALE DRAWING			

TITLE:

VALVE ASSEMBLY

SIZE	DWG. NO.	REV
A	6	1
SCALE: 1:2	Quantity: 1	SHEET 2 OF 2

5 4 3 2 1

REVISIONS			
ZONE	REV.	DESCRIPTION	DATE
	1	PRELIMINARY RELEASE	

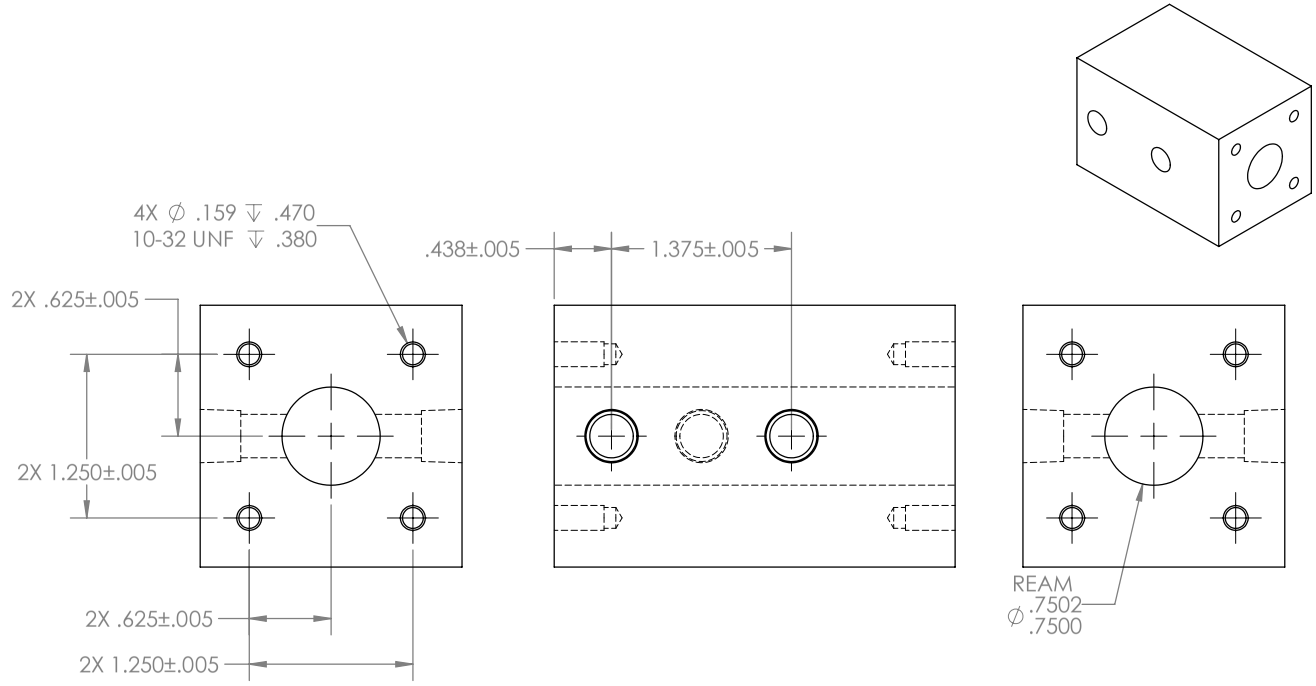

SolidWorks Student Edition.
For Academic Use Only.

UNLESS OTHERWISE SPECIFIED:		NAME	DATE
DIMENSIONS ARE IN INCHES TOLERANCES: FRACTIONAL ±1/8 ANGULAR: MACH ± 0.5 BEND ±1 TWO PLACE DECIMAL ±.03 THREE PLACE DECIMAL ±.020	DRAWN		
	CHECKED		
MATERIAL 1.5" SQUARE BAR	COMMENTS: BRAKE.CHRIS@DAL.CA (902)-579-0400		
FINISH N/A			
DO NOT SCALE DRAWING			

TITLE:

VALVE BODY

SIZE	DWG. NO.	REV
A	1	1
SCALE: 1:1	Quantity: 1	SHEET 1 OF 2

5 4 3 2 1

REVISIONS			
ZONE	REV.	DESCRIPTION	DATE
	1	PRELIMINARY RELEASE	

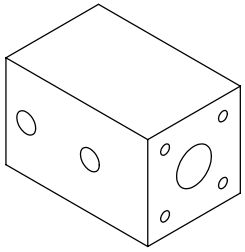

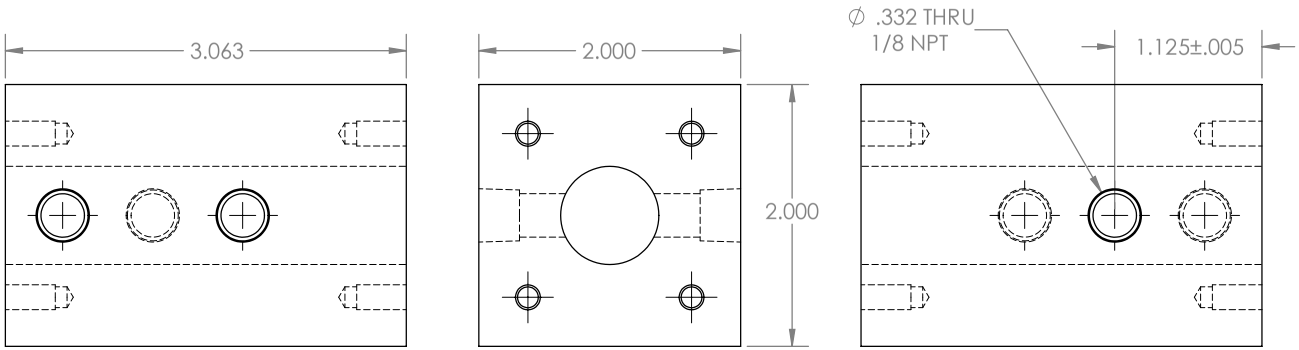

SolidWorks Student Edition.
For Academic Use Only.

UNLESS OTHERWISE SPECIFIED:		NAME	DATE
DIMENSIONS ARE IN INCHES TOLERANCES: FRACTIONAL ±1/8 ANGULAR: MACH ± 0.5 BEND ±1 TWO PLACE DECIMAL ±.03 THREE PLACE DECIMAL ±.020	DRAWN		
	CHECKED		
MATERIAL 1.5" SQUARE BAR	COMMENTS: BRAKE.CHRIS@DAL.CA (902)-579-0400		
FINISH N/A			
DO NOT SCALE DRAWING			

TITLE:

VALVE BODY

SIZE	DWG. NO.	REV
A	1	1
SCALE: 1:1	Quantity: 1	SHEET 2 OF 2

5 4 3 2 1

REVISIONS			
ZONE	REV.	DESCRIPTION	DATE
	1	PRELIMINARY RELEASE	

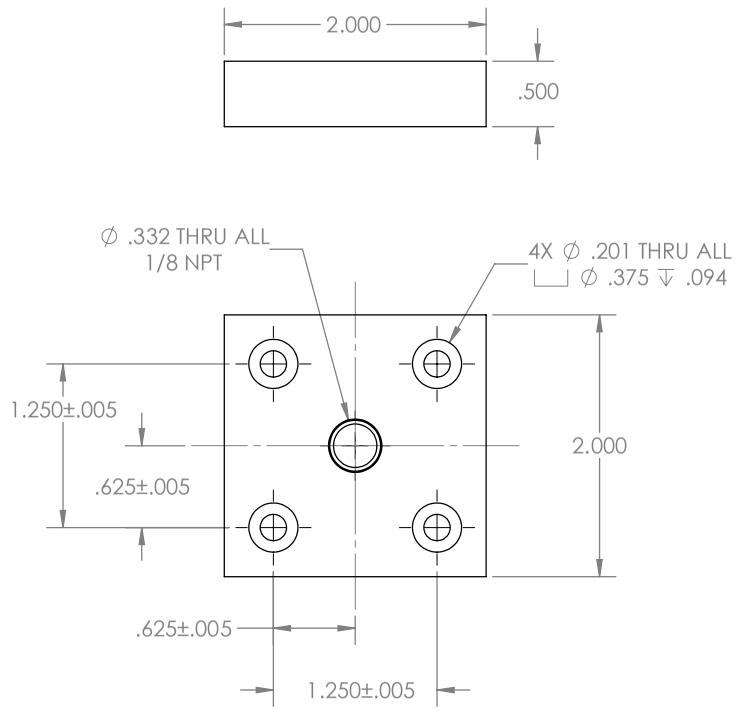

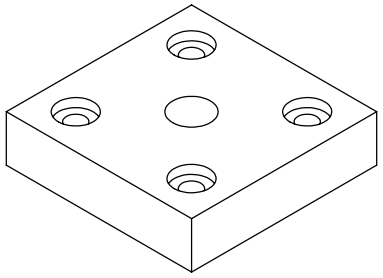

SolidWorks Student Edition.
For Academic Use Only.

UNLESS OTHERWISE SPECIFIED:		NAME	DATE
DIMENSIONS ARE IN INCHES TOLERANCES: FRACTIONAL ±1/8 ANGULAR: MACH ± 0.5 BEND ± 1 TWO PLACE DECIMAL ±.03 THREE PLACE DECIMAL ±.020	DRAWN		
	CHECKED		
MATERIAL 1.5" SQUARE BAR	COMMENTS: BRAKE.CHRIS@DAL.CA (902)-579-0400		
FINISH N/A			
DO NOT SCALE DRAWING			

TITLE:

TANK CAP

SIZE	DWG. NO.	REV
A	2	1
SCALE: 1:1	Quantity: 1	SHEET 1 OF 1

5 4 3 2 1

REVISIONS			
ZONE	REV.	DESCRIPTION	DATE
	1	PRELIMINARY RELEASE	

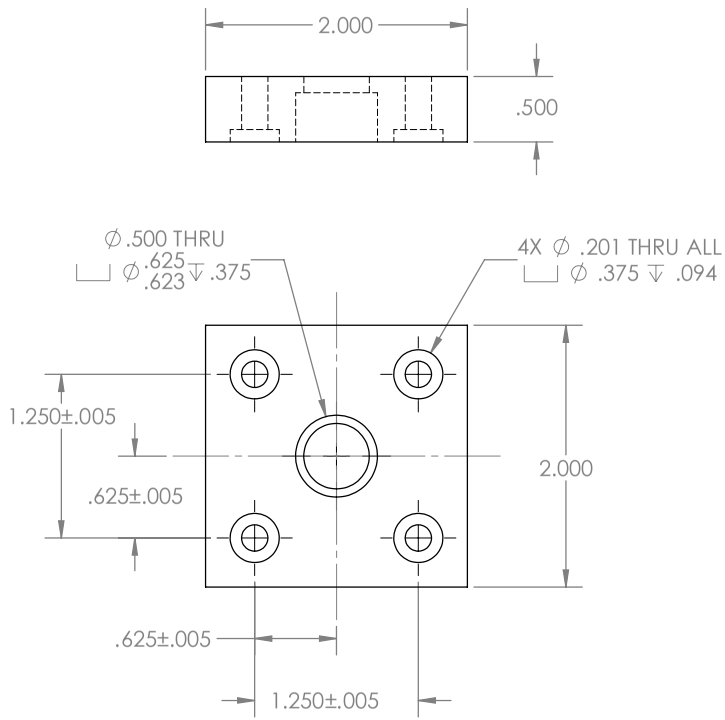

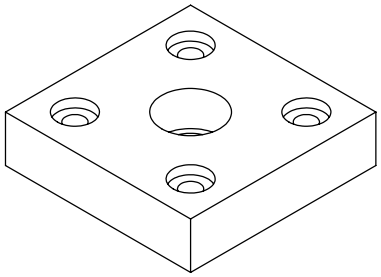

SolidWorks Student Edition.
For Academic Use Only.

UNLESS OTHERWISE SPECIFIED:		NAME	DATE
DIMENSIONS ARE IN INCHES TOLERANCES: FRACTIONAL ±1/8 ANGULAR: MACH ± 0.5 BEND ±1 TWO PLACE DECIMAL ±.03 THREE PLACE DECIMAL ±.020	DRAWN		
	CHECKED		
MATERIAL 1.5" SQUARE BAR	COMMENTS: BRAKE.CHRIS@DAL.CA (902)-579-0400		
FINISH N/A			
DO NOT SCALE DRAWING			

TITLE:

ACTUATOR CAP

SIZE	DWG. NO.	REV
A	3	1
SCALE: 1:1	Quantity: 1	SHEET 1 OF 1

5 4 3 2 1

REVISIONS			
ZONE	REV.	DESCRIPTION	DATE
	1	PRELIMINARY RELEASE	

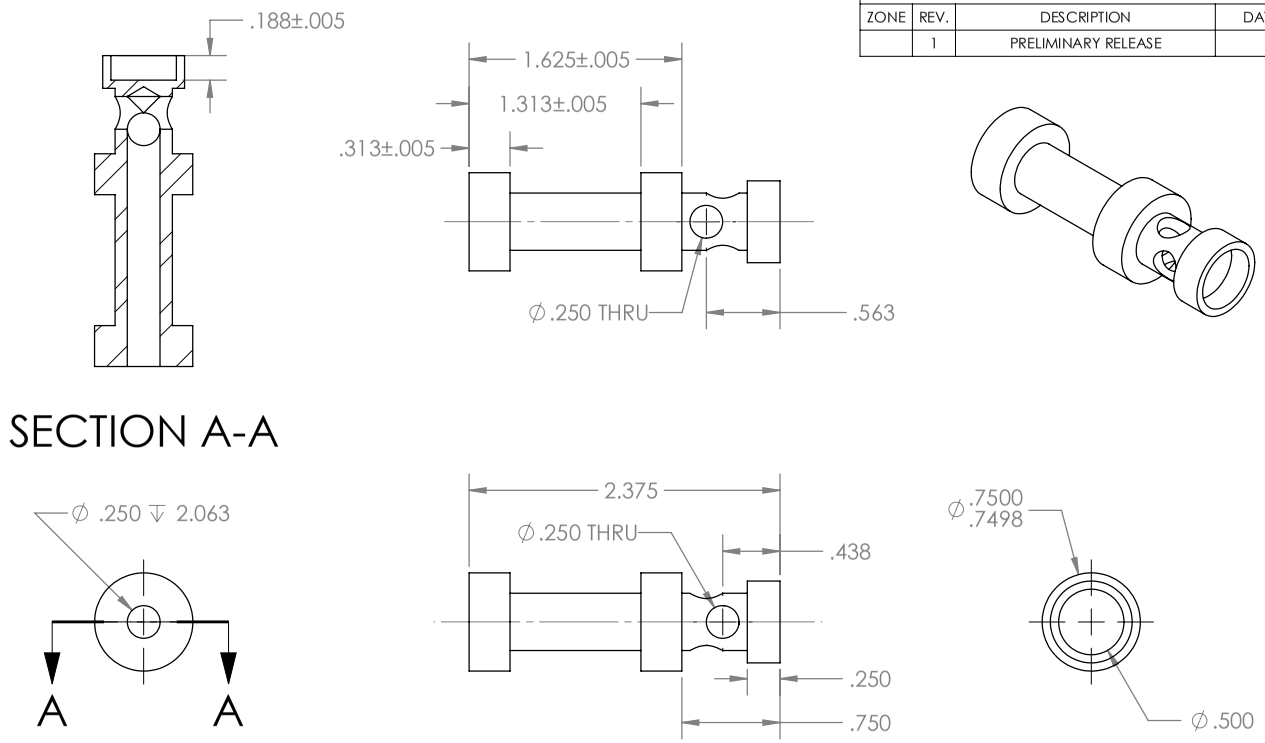

SolidWorks Student Edition.
For Academic Use Only.

UNLESS OTHERWISE SPECIFIED:		NAME	DATE
DIMENSIONS ARE IN INCHES TOLERANCES: FRACTIONAL ±1/8 ANGULAR: MACH ± 0.5 BEND ±1 TWO PLACE DECIMAL ±.03 THREE PLACE DECIMAL ±.020	DRAWN		
	CHECKED		
MATERIAL 440C STAINLESS	COMMENTS: BRAKE.CHRIS@DAL.CA (902)-579-0400		
FINISH N/A			
DO NOT SCALE DRAWING			

TITLE:

SPOOL

SIZE	DWG. NO.	REV
A	5	1
SCALE: 1:1	Quantity: 1	SHEET 1 OF 1

5 4 3 2 1

REVISIONS			
ZONE	REV.	DESCRIPTION	DATE
	1	PRELIMINARY RELEASE	

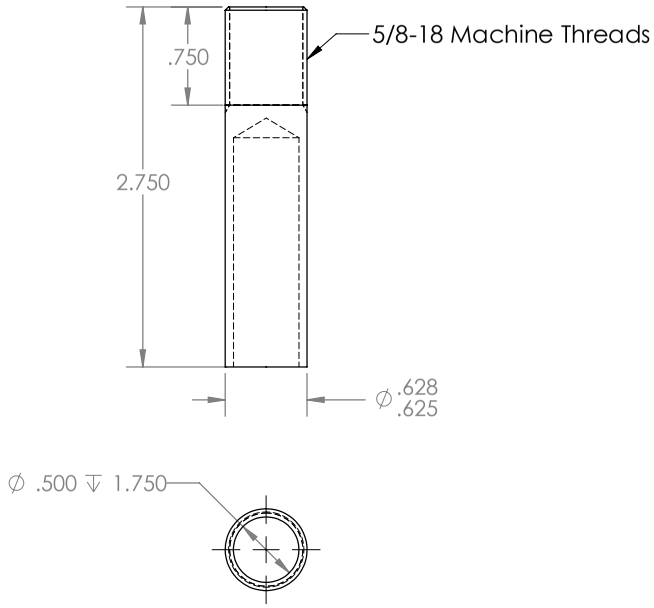

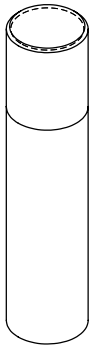

SolidWorks Student Edition.
For Academic Use Only.

UNLESS OTHERWISE SPECIFIED:		NAME	DATE
DIMENSIONS ARE IN INCHES TOLERANCES: FRACTIONAL ±1/8 ANGULAR: MACH ± 0.5 BEND ±1 TWO PLACE DECIMAL ±.03 THREE PLACE DECIMAL ±.020	DRAWN		
	CHECKED		
MATERIAL BRASS	COMMENTS: BRAKE.CHRIS@DAL.CA (902)-579-0400		
FINISH N/A			
DO NOT SCALE DRAWING			

TITLE:

COIL COLLAR

SIZE	DWG. NO.	REV
A	4	1
SCALE: 1:1	Quantity: 1	SHEET 1 OF 1

5 4 3 2 1